

AD-A256 598



2

# Altimeter and Oceanographic In Situ Measurements in the Area of the Greenland-Iceland-Norwegian Sea, 1987-1988

DTIC  
ELECTE  
OCT 28 1992  
S A D

92-28157

\*Original contains color  
plates: All DTIC reproduct-  
ions will be in black and  
white\*

**Pavel Pistek**  
**Ocean Sensing and Prediction Division**  
**Ocean Science Directorate**



Approved for public release; distribution is unlimited. Naval Oceanographic and Atmospheric Research Laboratory, Stennis Space Center, Mississippi 39529-5004.

## Foreword

This report presents the results of the investigation of altimetric measurements in the area of the Greenland-Iceland-Norwegian Sea. This investigation was part of the Navy Space Oceanography Program that had a general objective to use satellite-derived data for interpreting ocean dynamics and thermodynamics.

The program was carried out in cooperation with the NATO SACLANT Undersea Research Centre (SACLANTCEN). In situ oceanographic measurements coincident with satellite data measurements were also collected. They consisted of conductivity-temperature-depth and thermistor chain data collected by the West German ship WFS Planet, airborne expendable bathythermograph data deployed by P-3 aircraft, and some conductivity-temperature-depth data collected by SACLANTCEN. In addition, the infrared satellite images and the historical conductivity-temperature-depth data base, the Generalized Digital Environmental Model, were used. Data were studied and correlated with altimetric measurements to assess the usefulness and the potential of altimetry in this region.

*W B Moseley*

W. B. Moseley  
Technical Director

*L. R. Elliott*

L. R. Elliott, Commander, USN  
Officer in Charge

# Executive Summary

---

A multidisciplinary oceanographic study was performed in the area of the Greenland-Iceland-Norwegian Sea (GIN Sea). To assess the usefulness and the potential of altimetry in this region, the GEOSAT data, the satellite infrared images, and simultaneous in situ measurements of (a) airborne expendable bathythermographs deployed from P-3 aircraft, and (b) ship measurements of conductivity-temperature-depth (CTD) and thermistor chain data along the altimeter tracks were collected. In addition, the historical CTD data base, Generalized Digital Environmental Model (GDEM), was studied and used with altimetry. It was found that the variation in the signal amplitude of altimetric residuals corresponding to mesoscale variability is between 5 and 15 cm. In spite of this small amplitude, the signal is correlated with the oceanographic structure. Dynamic heights computed from CTD cross sections taken along the altimeter ground tracks were used to improve the empirical geoid. The altimetric signal results, namely, across the Norwegian current and the Færoe-Shetland inflow, indicate the possibility of monitoring the inflow by altimeter. In analogy to the CTD method discussed, dynamic height was computed from GDEM data and was used for correcting the altimeter data. This method can be useful in some areas as a first approximation in the improvement of the geoid. In spite of the detection by altimeter of the stronger and larger mesoscale features south of the Iceland-Færoe front, the front itself was not easily detected because of tidal contamination. Statistical results (namely variance) derived from altimetry indicate the larger variability to be near the frontal regions.

Accession For	
NTIS CRA&I	<input checked="" type="checkbox"/>
DTIC TAB	<input type="checkbox"/>
Unannounced	<input type="checkbox"/>
Justification	
By	
Distribution /	
Availability Codes	
Dist	Avail and/or Special
A-1	

## Acknowledgments

---

I am thankful to all participants who processed and cleaned the altimetric data. Special thanks are due to Jurgen Sellschopp, Chief Scientist during Planet cruise for inviting us to participate; D. A. Wiesenburg for collection of CTD data; J. Boyd for collecting AXBT data; Steve Piacsek from SACLANTCEN for GDEM data and help in arrangement of Planet Cruise; P. Minnett from SACLANTCEN for SST data; T. Hopkins from SACLANTCEN for CTD data; D. Johnson from NOARL for help in designing and tracking drifters; H. Perkins from SACLANTCEN for help in collecting CTD data during the Agor 1988 Cruise; J. Dastugue for help in processing the altimeter data; and Nancy McWilliams who typed the draft manuscript.

This work was funded by the Office of Naval Research, Program Element 0601153N, through the NOARL Defense Research Sciences Program.

The mention of commercial products or the use of company names does not in any way imply endorsement by the U.S. Navy or NOARL.

# Contents

---

<b>1.0 Introduction</b>	1
1.1 Background	1
<b>2.0 Data Collection and Treatment</b>	11
2.1 Altimeter	11
2.2 Satellite Images	12
2.3 AXBT Data	12
2.4 CTD Data	13
2.5 Thermistor Chain Data	13
2.6 Surface Drifters	13
<b>3.0 Data Errors</b>	18
3.1 CTD, AXBT, Thermistor Chain	18
3.2 Altimeter	18
<b>4.0 Results and Discussion</b>	23
4.1 SSH and IR Images	23
4.2 Sections Across Atlantic Inflow and Norwegian Atlantic Current	23
4.3 Measurements Across the Iceland-Faeroe Front	28
4.4 Surface Variability from Altimeter Data	30
<b>5.0 Summary and Conclusions</b>	65
<b>6.0 References</b>	69

# Altimeter and Oceanographic In Situ Measurements in the Area of the Greenland-Iceland-Norwegian Sea, 1987-1988

---

## 1.0 Introduction

Determination of frontal areas and their temporal variations globally by using in situ measurements is practically impossible. However, the satellite-borne altimeter may provide the means of tracking frontal and eddy locations globally and in all weather conditions. If this technique is possible, global coverage would be vastly improved and in situ measurement time and cost reduced.

It is well known that altimetric residuals in Gulf Stream or Kuroshio regions have amplitudes in the range of 1 m: large enough to be identified. Several studies were devoted to interpret the signal in terms of oceanic dynamic topography (Cheney and Marsh, 1981; Cheney, 1982; Bernstein et al., 1982; Lybanon et al., 1989; Mitchell, 1989). The majority of oceanic regions have altimetric surface signatures three to five times smaller than the Gulf Stream, and interpretation is more difficult, if not impossible, at our present capability of determining orbital and geophysical errors.

This report is concerned with the interpretation of signatures of GEOSAT's altimetric signals in the Greenland-Iceland-Norwegian (GIN) Sea area. It is an area of small surface height signatures. Johannessen (1984) looked at altimetric variability in the area of the Norwegian North Atlantic Current and Norwegian Coastal Current from several SEASAT colinear tracks. He found evidence of eddy-like features with a maximum amplitude of 20 cm and an extent of 50 km. The Harvard open-ocean model (Robinson et al., 1988), in conjunction with airborne expendable bathythermograph (AXBT) and GEOSAT altimeter differences (between successive 17-day passes), was used in locating the Iceland-Færoe Front. Dobson (1988) also discussed altimeter residuals across this front.

The purpose of this work was to examine altimetric residuals and correlate them with infrared (IR) satellite images and in situ measurements. To show

the steady flows, namely, the inflow of the North Atlantic water into the Norwegian Sea, and to visualize the flow of the Norwegian Atlantic Current in altimetric data, several tracks were calibrated with conductivity-temperature-depth (CTD) measurements. This calibration was compared to the corresponding calibration using the GDEM (Generalized Digital Environmental Model).

While correlations of altimeter measurements with oceanographic measurements in the Norwegian Sea proper were clearly visible, interpreting altimetric residuals in the Iceland-Færoe frontal zone was difficult. The main reason for this disagreement was the introduction of errors into altimetric residuals by geophysical corrections, namely, tidal correction, and part of this work demonstrates the difficulty with corrections.

## 1.1 Background

The GIN Sea area has been the site of many oceanographic measurements over the years. The classic work from this area is *The Norwegian Sea* (Helland-Hansen and Nansen, 1909). The Trangeland series (1973, 1974) gives a historical summary of GIN Sea measurements to about 1973. The new overview of physical oceanography literature for 1972-1985 is given by Hopkins (1988).

The acquisition of large amounts of data has demonstrated very large variability of structures and features, but the qualitative depiction of the Helland-Hansen (1909) surface current chart for the GIN Sea area has been confirmed. Figure 1a shows the main features. The North Atlantic water enters from the southeast and continues northward as the Norwegian Atlantic Current. At the same time, the Polar water enters from the northwest and proceeds southward along the Greenland shelf as the East Greenland Current. These two current systems are separated by cyclonic gyres in the Greenland and Norwegian Seas. These gyres are

defined by the zonal flows along the Greenland-Icelandic-Færoe and Jan Mayen Ridges.

The bottom topography (Fig. 2a) strongly affects the circulation and the distribution of water masses. Both major currents hug the Norwegian and Greenland continental slopes, respectively. In addition to these currents, the Norwegian Coastal Current extends from the shore and onto the Atlantic water, consisting of a wedge of coastal water. Its source is the brackish outflow from the Baltic Sea, as well as runoff from the Norwegian fjords. Figure 1b (Alekseev and Istoshin, 1956) presents a composite of the surface flow structure in greater detail. This composite shows the inflow of North Atlantic water entering the GIN Sea, not only through the Færoe-Shetland channel but also west of Færoe, Iceland, across the Færoe-Iceland ridge, and the portion joining the Irminger current and entering the GIN Sea through the Denmark Strait. It also shows the greater structure in the Norwegian Atlantic Current in the form of embedded cyclonic vortices and the absence of a well-developed Norwegian cyclonic gyre. The IR satellite image in Figure 3a shows the inflow of warm (dark) water with many ramifications and cyclonic eddies and with scales between 50–100 km, progressing in a northeast direction. (Notice the branching at around 65°N, bathymetrically forced around the Voring Plateau in the direction of Mohn Ridge). Corrected Figure 3b depicts the Iceland-Færoe Front. The figure shows the large temperature contrast between the two water masses (4–5°C), and the front is seeded with many vortices, mostly cyclonic, with scales between 30 and 60 km.

These generalized depictions of circulation pose questions concerning the existence of forcing and the cause and stability of splitting of major flows. However, there is no generalized circulation model for the GIN Sea area. Main frontal regions connected with currents are depicted in Figure 4. They were established by investigating the gradients in temperature and salinity fields of CTD data from the GDEM data base. Surface dynamic height topography for the major fronts and eddies corresponds to between 10 and 20 cm. The more detailed, quantitative descriptions in the following sections were based on recent measurements. More emphasis is placed on description of the dynamics of the upper layer because it correlates with altimetric residuals.

### 1.1.1 Færoe Channel

The Færoe Channel is the major entrance of the warm, saline Atlantic waters to the GIN Sea area.

The North Atlantic Current carries water northward along the European continental slope. The upper 1000 m of the water column consists of eastern North Atlantic water. Temperature varies from 5° to 12°C and salinity from 35 to 35.6 (Harvey, 1982), with some admixtures of higher salinity from Mediterranean outflow (Reid, 1979). The Wyville-Thompson Ridge (see Fig. 2b), with its 550-m depth sill, is the first bathymetric impediment in the northward path of the North Atlantic Current. More than half of its volume follows the deeper isobaths westward as the Irminger Current, while the warmer upper layers of this water form the input to the GIN Sea area. Its primary entry route is along the Shetland Slope, where the flow maximum is located approximately over the 500-m isobath. A considerable part of the North Atlantic Current inundates the entire area of the Færoe Bank and the Iceland-Færoe Ridge. After a slight modification, the current enters as a secondary entry, anticyclonically around the northern coast of the Færoe Islands and south of the Iceland-Færoe Front into the GIN Sea area. A schematic of this recirculation is presented in Figure 5. Tait's (1957) data provides the best evidence of the seasonal-to-interannual variability. The wide-range of inflow variability (days to years), as can be seen in Figure 6, depends on the choice of reference level for estimates, based on the dynamic method, local wind forcing, as well as large-scale atmospheric forcing (Meincke and Kvinge, 1978). The presence of quasi-geostrophically balanced eddies (of 30-km scale) that propagate with the mean flow (Dooley et al., 1976; Dooley and Meincke, 1981) enhance this variability. As can be seen in Figure 6, the data points are not evenly distributed throughout the year: the lack of winter data could create the trend.

### 1.1.2 Norwegian Atlantic Current

The Norwegian Atlantic Current transports North Atlantic water northward through the Norwegian Sea into the Greenland Sea. Considerable effort has been spent in collecting data along the transects across the Norwegian Atlantic Current, namely on the Sognefjord and Ocean Weather Station Mike sections, directed to the northwest from 61°N, and 66°N from Norwegian coast, respectively. The main observational problem in terms of describing the Norwegian Atlantic Current is a strongly sheared cross stream with countercurrents, time variable transport, and large undulations at the lower water mass interface (Helland-Hansen, 1934). The large

undulations are also visible in the data of Sognefjord Sections (Saunders and Burns, 1985). Saelen (1959) confirmed these findings. He found that transports for "in" and "out" crossings separated by about 2 days were equally as variable as those calculated for different years. Farther to the north through the other cross section, Kvinge et al. (1968) observed transports of similar variability and magnitude. Helland-Hansen (1934) and later Saelen (1963) related the observed horizontal variability in the flow to the observed large vertical undulations of the water mass interface (35.00 salinity) and suggested that both were caused by elongated cyclonic vortices embedded in the Norwegian Atlantic Current. Dickson (1972) found that these isotherm variations were stationary over the 6-week observational period. Elongated cyclonic eddies embedded into the Norwegian Atlantic Current appear to be characteristic throughout its northward course. Kislyakov (1960) has suggested that the gyres are generated by variations in cross-stream shear, which is generated by barotropic interaction with the bathymetry.

Bathymetric control also affects the branching of the Norwegian Atlantic Current as it passes the Voring Plateau. The westward branch merges with the Jan Mayen Current until it rejoins the more eastward branch of the Norwegian Atlantic Current.

The estimates of volume transports along the course of the Norwegian Atlantic Current do not give simple enlargement, as would be expected to result from continuous entrainment of adjacent waters. On the contrary, the center portions seem to decrease before the increase in the Spitsbergen region.

### 1.1.3 Iceland-Færoe Front

The zonal flow north of Iceland is referred to as the Icelandic Current; its origin is the branch of the Irminger Current that imports Atlantic water into the Iceland Sea through the Denmark Strait. The Icelandic Current flows eastward along the northern continental slope of Iceland until it reaches the easternmost point, Gerpir, where it continues eastward rather than southward. Upon leaving the Iceland coast, it can no longer be considered a coastal boundary current, although it remains bathymetrically steered eastward along the north flank of the Iceland-Færoe Ridge. The Iceland-Færoe Ridge is fully defined by the 500-m depth contour, and about one-third of the ridge is less than 350 m deep. These

depths are too great to cause direct bathymetric steering for the Icelandic current, which is less than 300 m deep. The separation of the Icelandic current has to be caused by large-scale influences: the Icelandic current advects the original Atlantic water anticyclonically around north Iceland. The Atlantic water then undergoes cooling and freshening through advective admixtures of Arctic and Polar waters (see Fig. 7) until approximately Gerpir, where it reencounters original Atlantic water that is lighter by  $\sim 0.2\sigma_t$  units. This density difference is sufficient to reorient the offshore geostrophic flow eastward. North Atlantic waters over the southeastern Icelandic shelf and over the southern portion of the Iceland-Færoe Ridge form a sea-level, high-pressure ridge that extends eastward from Iceland and more or less coincides with the Iceland-Færoe Ridge. Consequently, the lighter North Atlantic water on the south side is forced over Icelandic Current waters. This water mass front progrades to the north; i.e., the front intersects the Iceland-Færoe Ridge at around the northern 500-m depth contour and tilts toward the north. In cross section, the water mass interface is well defined by strong gradients. The data collected in 1975 and 1976 (Dorey, 1978) indicate eastward upper-flow speeds of  $\sim 20$  cm/s.

The surface manifestation of the Iceland-Færoe Front is highly variable in space and time. Figure 8 shows the location of the front. Recent data from AXBT's are now available (Boyd et al., 1987; Boyd, 1988). The surface isotherms spread apart, particularly during summer, due to surface heating and to the mixing associated with large lateral excursions. Surface mappings indicate that the lateral oscillations in the front have periods of days rather than months. This is also substantiated by current meter data, which according to Willebrand and Meincke (1980) have a dominant time scale over the Iceland-Færoe Ridge of 10 days due to frontal baroclinic instabilities. The Iceland-Færoe Front has greater depths and, thus, less lateral variability, as can be seen in Figure 8b. Because the front inclines toward the north, these deeper expressions are found farther south. To the east and north of the Færoes, the front is also inclined toward the west due to the North Atlantic water entering via the Færoe Channel. Near the bottom, two important southward extensions of the frontal position are found (Fig. 8b)—one just east of the Iceland continental shelf break and another at the entrance to the Færoe-Shetland Channel. These

extensions indicate the areas of greater probability of GIN Sea overflow. Ross and Meincke (1979) synthesized all available data and their result is shown in Figure 9. In this figure, the flow over the north and south part of the Iceland-Færoe Ridge follows the general bathymetry to the southeast and to the northwest, respectively. In the near-surface

layer, the northward flow crosses the ridge; near the bottom, the flow over the crest tends to be to the south over the western portion and to the north near the Færoe Islands as a part of recirculation (as described in inflow through Færoe Channel). Deep water formation is described extensively in Hopkins (1988) and Swift (1986).

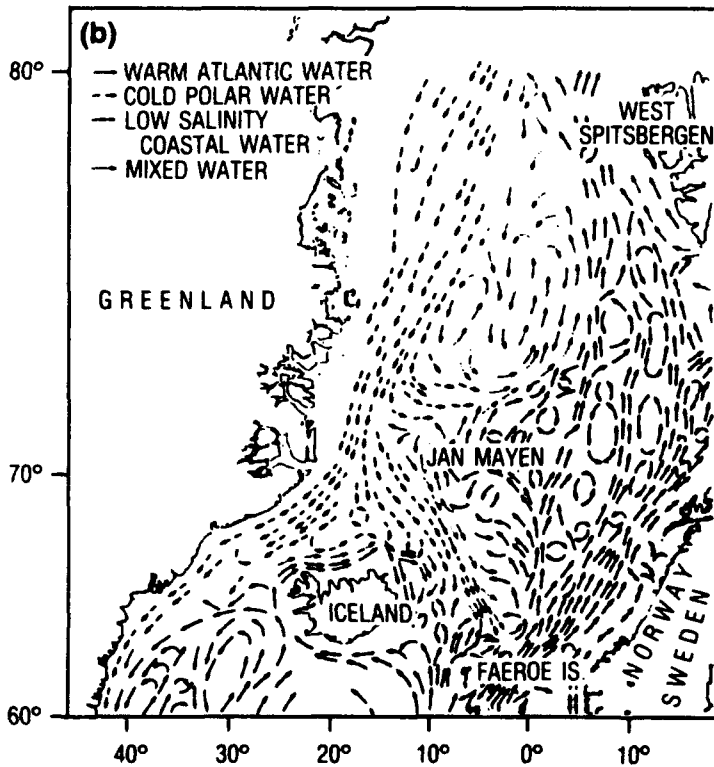
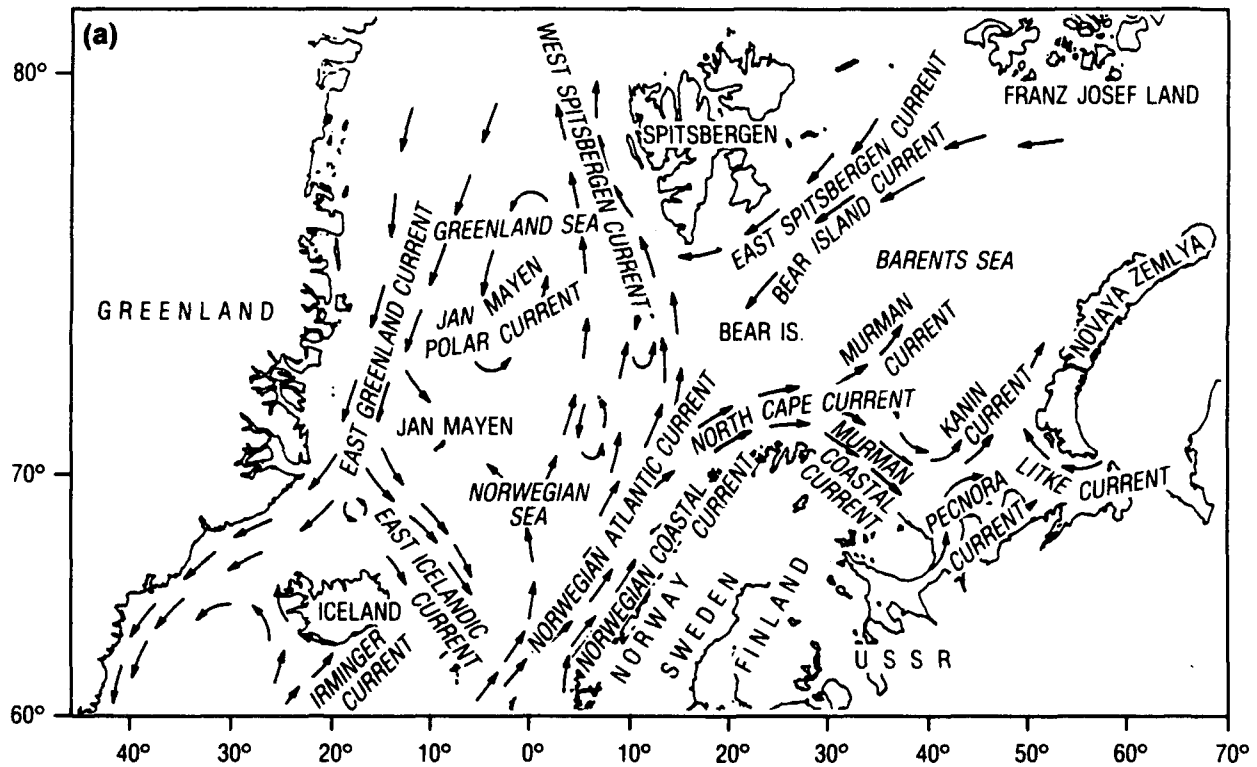


Figure 1. Schematic representations of the surface circulation in the GIN Sea area. (a) From Trangeled (1974), and (b) from Alekseev and Istoshin (1956) and Hermann and Thomsen (1946).

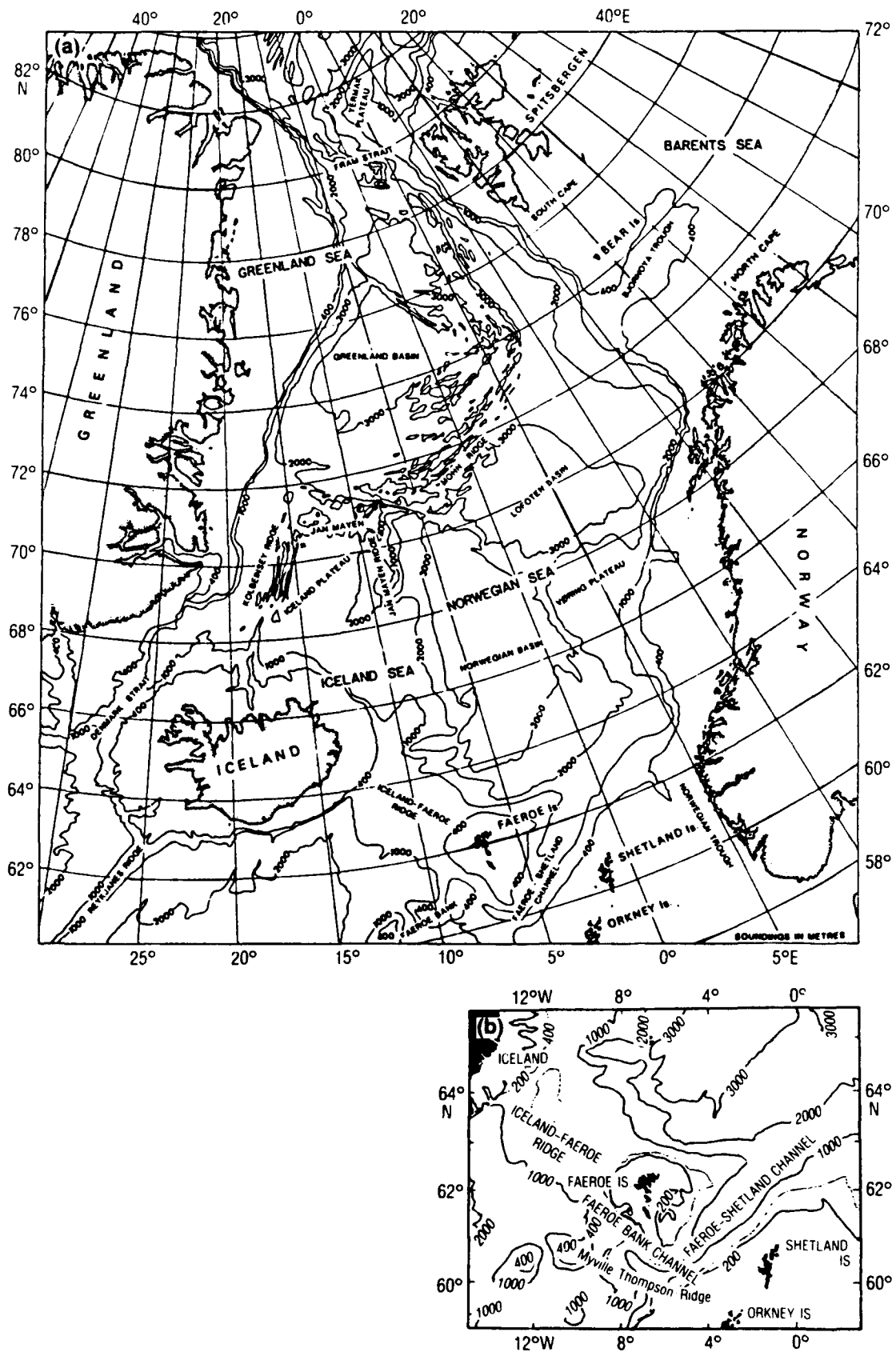


Figure 2. The bathymetry and place names of major features in the GIN Sea area. Depth contours are in meters. (a) Projection is polar-steric, redrawn from Perry, et al. (1980). (b) Southern GIN Sea bathymetry from Ross and Meincke (1979).

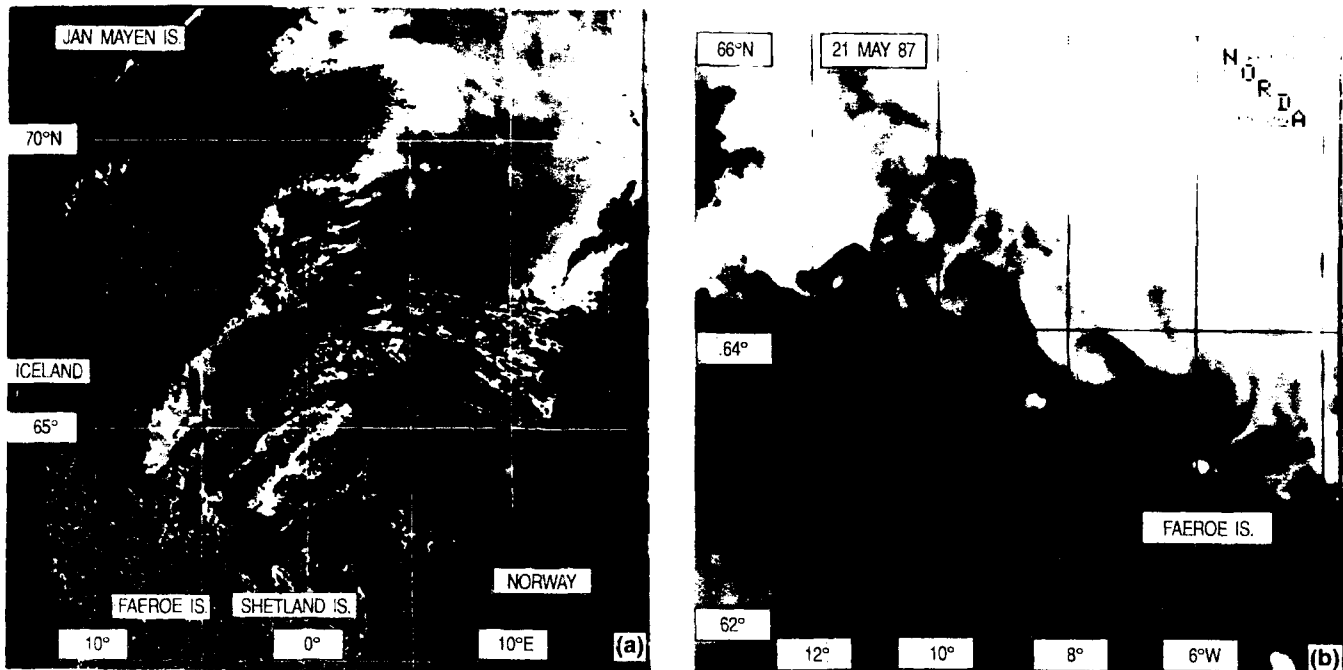


Figure 3. Infrared satellite images from GIN Sea area. Channel #4, NOAA-9: clouds are filtered and show up as a black background. Warmer water is presented by darker shades. (a) Norwegian Atlantic Current and (b) Iceland-Faeroe frontal zone.

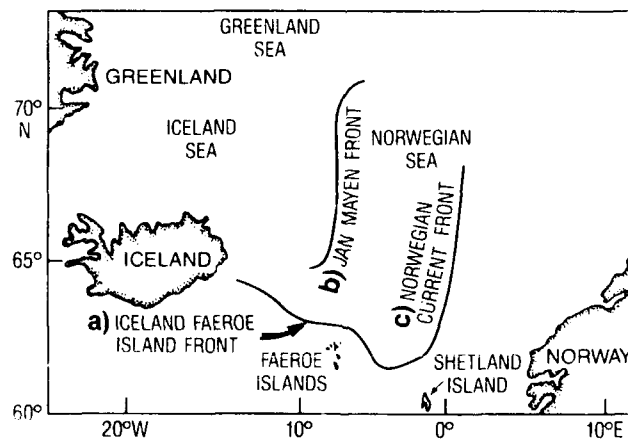


Figure 4. Frontal positions in GIN Sea area from GDEM data.

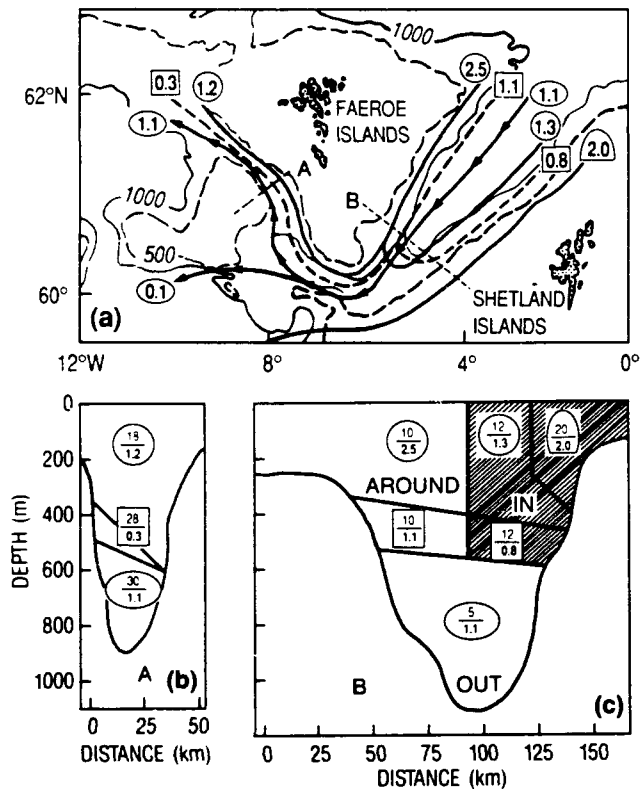


Figure 5. A schematic presentation of the amounts and routes of the various water mass transports within the Færoe Channel. (a) The routes of the transports and locations of transects A and B. The figures indicate the amounts in Sverdrups for the following water masses: circle for Færoe Atlantic water, square for Icelandic Current Intermediate water, ellipse for the upper Norwegian Sea Deep water, and semi-ellipse for the North Atlantic water. (b) Transect A. (c) Transect B. In both (b) and (c) the symbols represent the same water masses as in (a), where the upper number gives the mean speed and the lower number the transport. Both transects (b) and (c) face into the Norwegian Sea (from Dooley and Meincke, 1981).

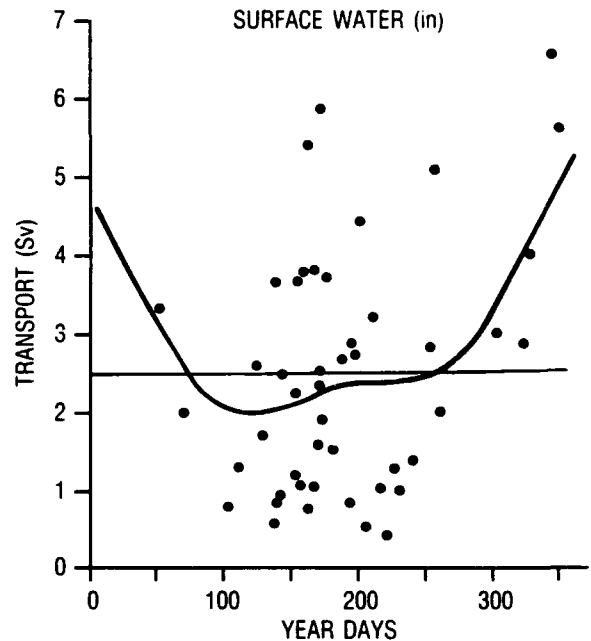


Figure 6. Individual transport estimates from hydrographic transects of the Færoe-Shetland Channel: North Atlantic water inflow data from 1927 to 1958 as calculated by Tait (1957) and Tait and Martin (1961). The heavy line represents an 8th-order polynomial fit, and the light line is the mean of 2.6 Sv.

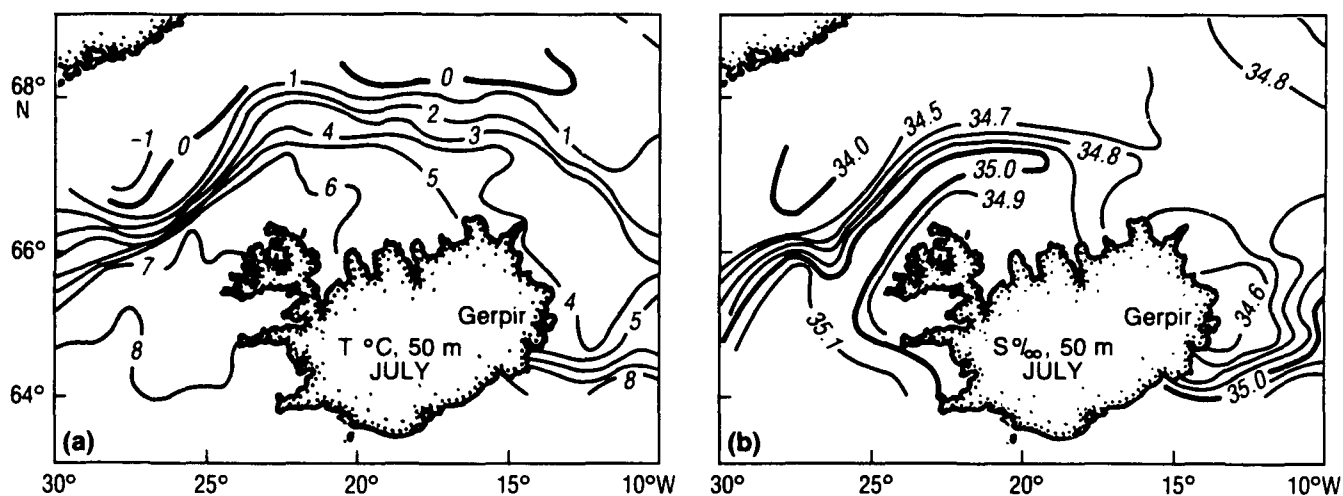


Figure 7. The mean  $T$  (a) and  $S$  (b) distributions at 50-m depth during July from the Service Hydrographique before 1947, from the Bulletin Hydrographique for 1948–1955, and from Icelandic material for 1956–1960 (from Stefansson, 1962).

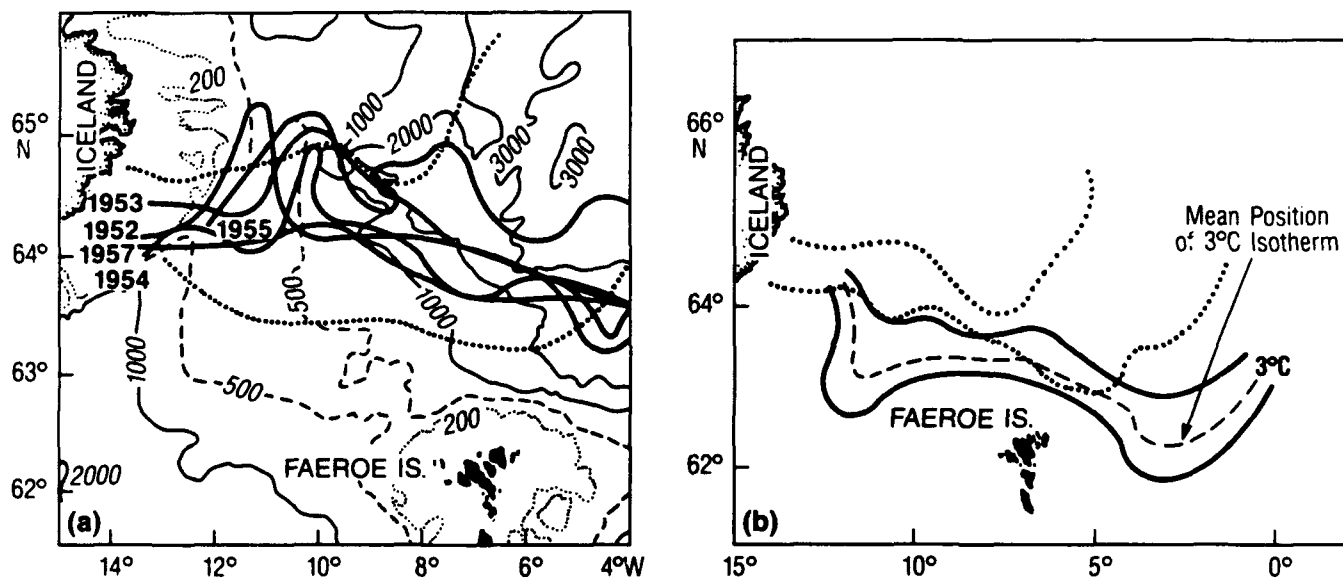
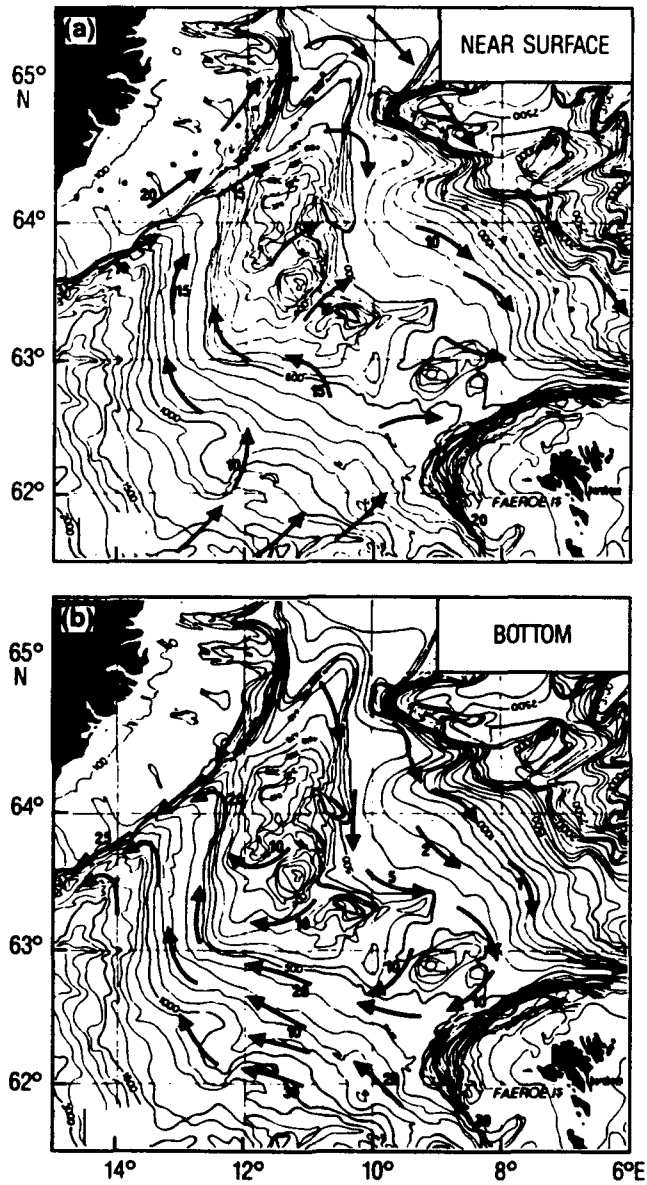


Figure 8. Location of the Arctic Front over the Iceland-Færoe Ridge. (a) Solid lines mark the position of the 35-ppt isohaline at the surface (0 to 25 m) in May and June of the years indicated (from Hansen and Meincke, 1979). Dotted lines indicate the extreme positions of the midgradient isotherm from five surveys taken between July 1971 and October 1972 (from Gotthardt, 1974). (b) Midgradient isotherm envelope for the same five surveys at 300 m (solid), at 100 m (dotted), and at the mean position of the  $3^\circ$  isotherm at 300 m (dashed).



*Figure 9. Schematic representation of the flow over the Iceland-Faeroe Ridge for the (a) surface and (b) bottom layers. (from Meincke, 1983).*

## 2.0 Data Collection and Treatment

### 2.1 Altimeter

The area where the GEOSAT altimetric data were collected is shown in Figure 10a and b. Figure 10a shows the ground tracks of descending satellite paths, and Figure 10b shows the ground tracks of ascending paths in the GIN Sea area. Data were collected during the GEOSAT Exact Repeat Mission (ERM). ERM was designed so that long-term, along-track averaging could give an accurate local mean sea surface and minimize the errors that occur when an imperfectly known marine geoid is subtracted from the altimeter data to produce mesoscale dynamic topography. ERM started on November 8, 1986, and the orbit was adjusted to maintain this pattern laterally within less than 1 km. Thus, the ground track is a network that repeats every 244 revolutions (17.05 days), with a spacing of about 45 km in the GIN Sea area.

Altimeter data were received by the Johns Hopkins Applied Physics Laboratory (APL) ground station. APL produced NOARL Data Records (NDRs) and transmitted them to NOARL. Sampling rate for these data was 10 per second. Data were processed at NOARL. Primary processing consisted of data quality checks, removal of satellite height by extracting the orbital distance (to establish the sea level), averaging 10 data points (to the sampling interval of 1 second), and removing geophysical corrections (ocean tides and electromagnetic [EM] bias). Tide was calculated from the Schwiderski-Szeto (1981) model; accuracy was 10 cm over open ocean. The EM bias, an apparent shift in sea-surface elevation caused by a difference in reflection strength from the troughs and crests of ocean waves, can be modeled adequately as a range error that is proportional to significant wave height. The altimeter's electronic tracker is responsible for a similar bias; combined correction factor of 5% of significant wave height was used (Born et al., 1982). More details of primary processing are given in Lybanon et al. (1989).

Secondary processing consisted of linearly approximating all repeat sea level profiles into the set of fixed locations along the tracks (chosen arbitrarily as a set from the first passes) called "bins," and obtaining the sea surface residuals (*SSH*) that provide information on ocean dynamics. *SSH* can be represented by the following equation:

$$\begin{aligned}
 h_r - h_o - E &= SSH + h_g \\
 E &= E(\text{tide}) + E(\text{EM}) + E(\text{tropo}) \\
 &\quad + E(\text{orbit}), \quad (1)
 \end{aligned}$$

where  $h_r$  is a range measurement given by the altimeter,  $h_o$  is the orbital distance, and  $h_g$  is geoid height (where  $h_o$  and  $h_g$  are referenced to reference ellipsoid).  $E(\text{tide})$ ,  $E(\text{EM})$ ,  $E(\text{tropo})$ , and  $E(\text{orbit})$  represent corrections due to tide, EM bias, tropospheric water vapor, and orbital error, respectively. While  $h_r$  and  $h_o$  are given by measurements,  $h_g$  is a large value relative to *SSH*. Figure 11 presents an example of this problem. Figure 11a represents the sea-level data (without *tide* and *EM*) for 13 repeat orbits along track D21 (see Fig. 10); Figure 11b is their ensemble average, and Figure 11c is the estimate of *SSH* for one particular path. The large differences in signal amplitude (11a and 11c) are clear; the geoid estimate changes by 15 m, while *SSH* variations are  $\pm 10$  cm. Precise knowledge of the geoid is needed to retrieve the oceanographic information in the GIN Sea area. Available geoid estimates do not have this precision. Three methods of geoid estimation were used, and the results are compared in this report.

The first method: The long-term temporal mean of altimeter-derived sea level approximates the marine geoid. Method can be expressed as

$$\frac{1}{N} \sum_i (h_r - h_o - E)_i = h_g \quad (2)$$

where  $N$  is the number of profiles used in averaging and  $h_g$  is the mean that approximates the geoid. ERM's repeat orbit provides the opportunity to use the along-track ensemble means as a reference surface for the *SSH* computation. Each profile used in averaging was first shifted by subtracting its mean value, where its mean value was created only from points that were defined in all profiles. This value was important because when data gaps are present (because of rain, etc.), averaging creates artificial steps (because orbital error is  $\pm 300$  cm) in ensemble average. *SSH*'s were estimated by the difference between the instantaneous profile and the ensemble mean. Last, the simple linear detrending of *SSH* was adequate to reduce the residual orbit error, a good approximation for the relatively short tracks (1500 km or less) through the GIN Sea area. *SSH* obtained by this method will be annotated in the text as *SSH<sub>M</sub>*.

However, that mean also includes the time-independent part of dynamic topography. The presence of this contaminant significantly interferes with interpretation of *SSH* residuals. Figure 12 illustrates this problem. The dashed line in Figure 12a

shows an idealized part of the time-independent dynamic topography across the frontal zone. The three solid lines are the instantaneous frontal positions as they would appear if they could be calculated without error. The mean is "smeared" because of meandering while the altimeter data incorporated into mean were being collected. Figures 12b, 12c, and 12d show the result of differencing the instantaneous and mean profiles, as in the subtraction of the "contaminated" reference surface from sea level. In general, both the resulting profile shape and, to smaller extent, its position are affected.

It is impossible to separate the time-independent part of the dynamic topography from the altimetry without additional independent information. The construction of so-called "synthetic geoids" by removing the mean oceanography contamination is a topic of considerable current interest. Kilgus (1989) reports on several synthetic geoid methods, all of which introduce additional information to achieve the separation. Tapley et al. (1988) describe a different approach, which uses altimeter data, tracking data, and surface gravity data to solve simultaneously for the sea surface topography, the earth's gravity field, the satellite's orbit, and other parameters.

The second method: Even if the main purpose of altimetry is to derive surface topography and to interpret ocean dynamics, this role can also be reversed. To use oceanographic measurements, namely CTD data, compute dynamic topography from CTD's collected along altimeter ground tracks in simultaneous measurements with altimeter and obtain geoid by a simple calculation:

$$(h_r - h_o - E) - DH = h_g, \quad (3)$$

where  $DH$  is dynamic height computed from oceanographic data, and  $h_g$  is the geoid estimate. This method gives good results only if the corresponding dynamic height represents well the dynamic surface, if the baroclinic component is dominant, and if the reference level is well established and the orbital error is small (small tilt). The advantage is that only one altimeter track and one set of CTD data along this track can estimate geoid. This method is useful in calibrating some of the altimeter tracks across the important oceanic current systems to monitor their fluxes. Results of this method are examined in this report. Similarly, if temperature-salinity (T-S) relationship in the particular oceanic area is well behaved, it is adequate to measure only

temperature (for example, by AXBTs), estimate the salinity from T-S dependence, and then proceed as above. This method has been used successfully by Mitchell et al. (1989) in the Gulf Stream area.  $SSH$  obtained by this method will be annotated in the text as  $SSH_c$ .

The third method: Historical CTD data from GDEM can also be used to improve the reference surface. As these data represent the average properties, the dynamic height computed from them also represent the average for a particular period. Taken along the altimeter track, dynamic height can be subtracted from the altimeter-created reference surface for the same period (for example, summer data) to obtain the geoid estimate. This method can be expressed as follows:

$$\frac{1}{N} \sum_i (h_r - h_o - E)_i - \text{GDEM} = h_g, \quad (4)$$

where  $\frac{1}{N}$  represents ensemble average (the same as method 1), GDEM is the dynamic height computed along a satellite ground track from a GDEM data set, and  $h_g$  is the geoid estimate. Error in this estimation is introduced by the problems of the dynamic method in computing the dynamic height, barotropic component in the current, and the nonsimultaneity of altimeter and CTD data sets. In addition, the  $SSH$  has the orbital error.  $SSH$  obtained by this method will be annotated in the text as  $SSH_{\text{GDEM}}$ . The results of this method are also presented in this report.

Altimetric data were processed for the period of 1 year, but more than 30% descending and 15–20% ascending passes are missing due to altimeter malfunctions. Data are missing mostly during the fall and winter periods.

## 2.2 Satellite Images

AVHRR from the NOAA-9 and NOAA-10 satellites were collected and processed at NOARL. Collected images had 1-km resolution. Channel 4 and gray-shaded temperature differences were used instead of the color coding because oceanic features are easier to identify.

## 2.3 AXBT Data

AXBTs were deployed from the Naval Research Laboratory's P-3 aircraft underflying the GEOSAT altimeter track across the Norwegian Atlantic Current on 1 June 1987 (Fig. 13a).

The frequency-modulated signals from the three aircraft sonobuoy receivers (channels 12, 14, 16) were received, amplified, filtered, and digitized at 10 Hz (about every 15 cm in depth). The airborne data acquisition system is described in Holland et al. (1982), Brundage et al. (1985), and Boyd et al. (1986). Later processing consisted of filtering (a 21-point median filter to remove noise in profiles), conversion to temperature and depth (Boyd, 1987), decimation to a 1-m resolution. A final 9-point median filter was applied to complete the smoothing process (to eliminate enhanced noise at depth near the end of the profile when atmospheric conditions cause ducting of the transmitted signal (Boyd, 1986). Navigation accuracy was estimated to be about 7 km. The vertical temperature profile extended to 400 m with a 0.2°C accuracy. AXBT data used for comparison with the altimeter across the Iceland-Færoe Front are described in Boyd (1988).

## 2.4 CTD Data

Two cruises participated in collecting the data simultaneously with altimeter measurements. Figure 13a shows the positions of CTD casts conducted aboard the Wehrforschungsschiff *Planet* operated by the Bundeswehr Research Establishment for Acoustics and Geophysics, Kiel, Federal Republic of Germany. Jurgen Sellschopp was Chief Scientist during the cruise, which was designated NORDMEER 87 and lasted from 1 to 19 June 1987. Figure 13b indicates CTD positions taken during the U.S. Navy Agor cruise organized by NOARL 3 to 16 October 1988.

Preliminary results of CTD data from the first cruise are described in Wiesenburg et al. (1987). CTD measurements in both cruises were taken by the Neil Brown MARK IIIB System. Systems were calibrated and operationally checked by the Sensor Calibration Laboratory of the U.S. Naval Oceanographic Office (NAVOCEANO). A post cruise instrument check was also conducted by NAVOCEANO to insure that the units had remained in calibration during the cruise. Data were recorded on a Digi-Data, Inc., 9-track tape recorder and later processed on the Digital Equipment Corporation VAX computer. Different parameters were calculated based on the algorithms in UNESCO Report 44 (UNESCO, 1983). Data were finally decimated to 1-m values. Loran positioning accuracy was  $\pm 1.5$  km. The depth of casts was either 1000 m or 50 m above bottom, if shallower.

## 2.5 Thermistor Chain Data

These data were taken by Selshop (1987) during the NORDMEER 87 cruise. The thermistor chain extended to about 150 m depth, with 60 thermistors evenly distributed. Thermistors with an accuracy better than 0.05°C were embedded in blocks, resulting in a time constant of about 40 seconds. Towing speed was constant, between 6 and 7 knots, and temperature profiles were sampled every 12 seconds. Location of the section compatible with altimeter data is shown in Figure 13a between points A and B.

## 2.6 Surface Drifters

Six surface drifters were deployed in the area of the Iceland-Færoe Front to visualize the circulation. Figure 13b shows the deployment positions. The first three drifters were deployed during the NOARL cruise; and the rest were deployed 14 days later by the *Alliance* during the SACLANT Undersea Research Centre cruise. Drifters were constructed at NOARL (see Fig. 14 for schematic). A plastic tube, 15 cm in diameter and 1-m long, housed the Service Argos transmitter, the antenna, and two 12V (10 AHR) batteries. The simple dipole antenna was fixed along the tube, together with other components, by polyurethane foam that hardened 1 day after injection. The end-cups were then glued to the tube, ensuring enough buoyancy that about one-third of the tube was above water level in a horizontal position.

A drogue was made from the two perpendicularly-mounted, canvas-covered sails. The heavy canvas pieces were sewn on two crosses made of iron tubes. To keep the structure from horizontal collapse, nylon ropes were tightly stretched around. The drogue was connected to the surface drifter by a nylon cord. Along this line there were buoyancy floats. Distribution of buoyancy was such that several floats were positioned near the drogue, partly to compensate for its large negative buoyancy. The rest of the floats were attached closer to the surface drifter in such number that there was total positive buoyancy for the whole drogue. With the transmit interval of 60.2 seconds, projected duration was 3.5 months.

Argos positions and their timing were obtained through telephone line. The data obtained were then averaged for each day in position, and receiving time and resulting data were linearly interpolated to midday positions. The average daily velocities were computed from interpolated data.

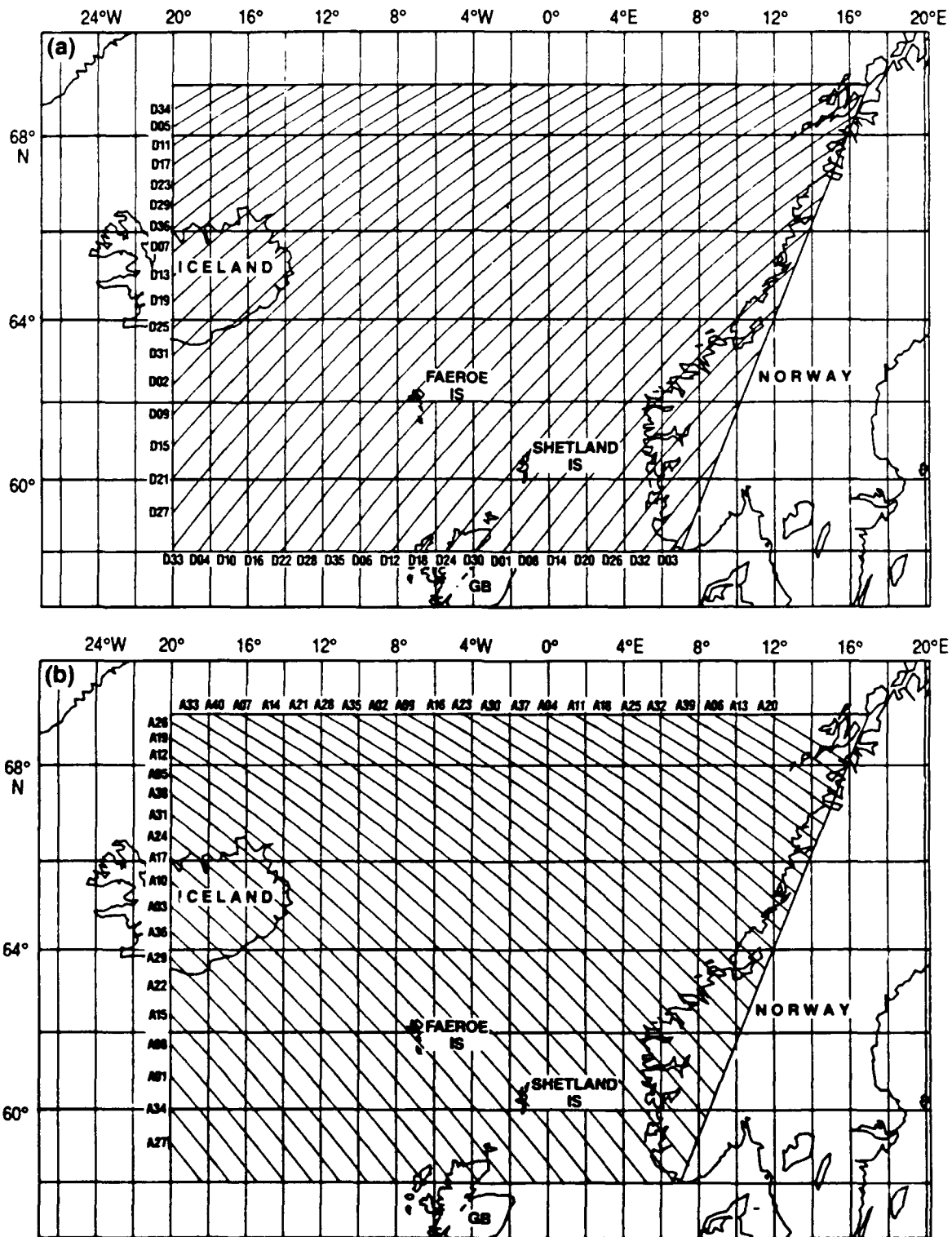


Figure 10. Area where GEOSAT altimeter data were collected during the Exact Repeat Mission; (a) ground tracks of descending passes and (b) ground tracks of ascending passes.

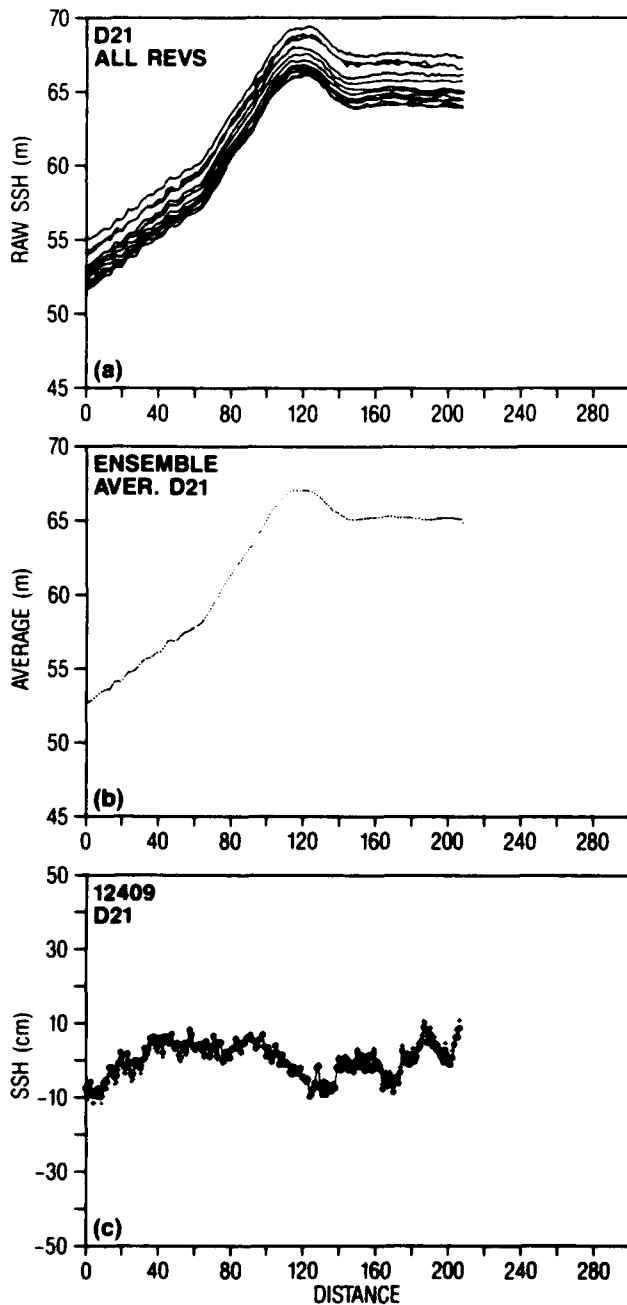


Figure 11. Example of altimetric signal along track D21 (see Fig. 4) DIST is in along-track samples from 69°N southward. Each dot represents a 1-second average separated by 6.5 km: (a) sea level data, corrected off tide and EM bias for 13 repeat revolutions; (b) ensemble average of data; (c) estimate of SSH for REV 12409 as a difference of the particular sea level and ensemble average.

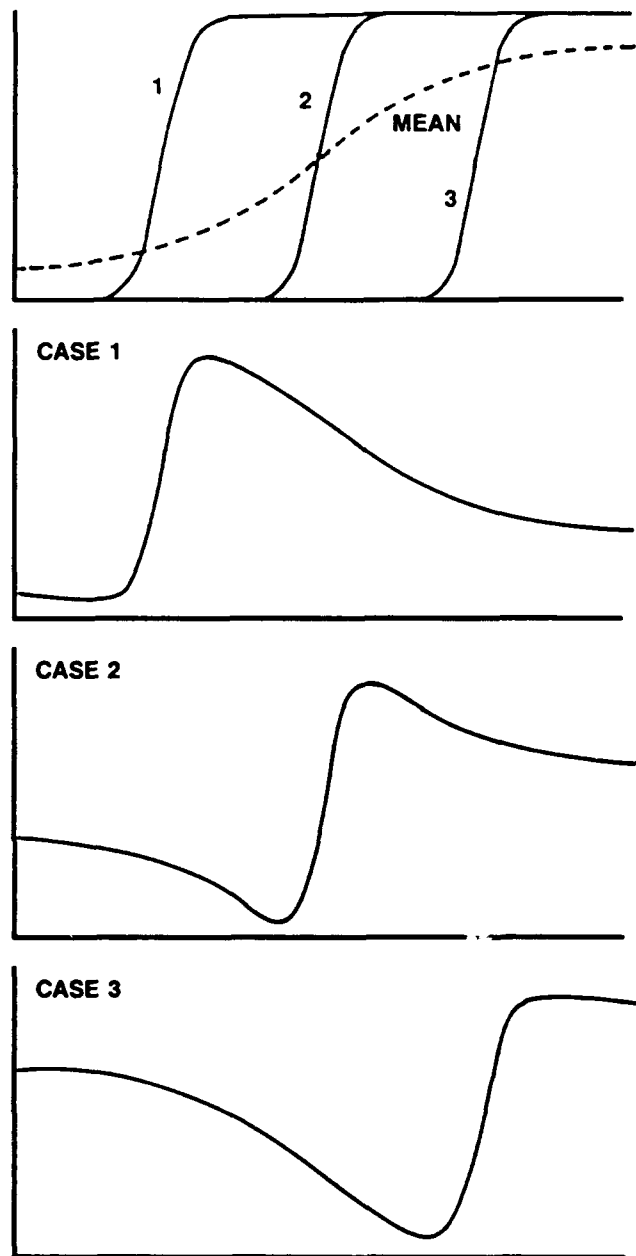


Figure 12. Effect of mean oceanography in reference surface upon SSH residuals (from Lybanon et al., 1989): (a) mean frontal profile and 3 instantaneous frontal profiles; (b), (c), and (d) differences of instantaneous profiles 1, 2, 3 and mean frontal profile, respectively.

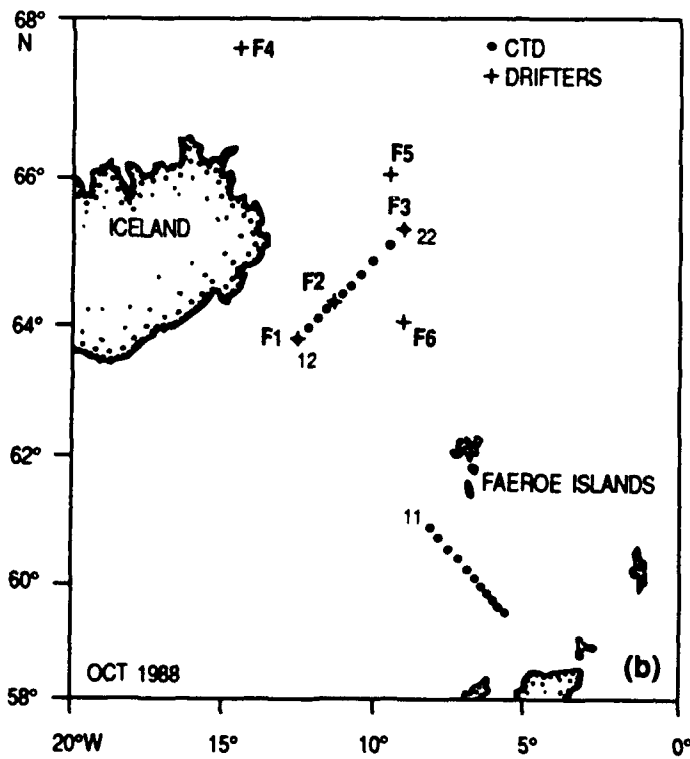
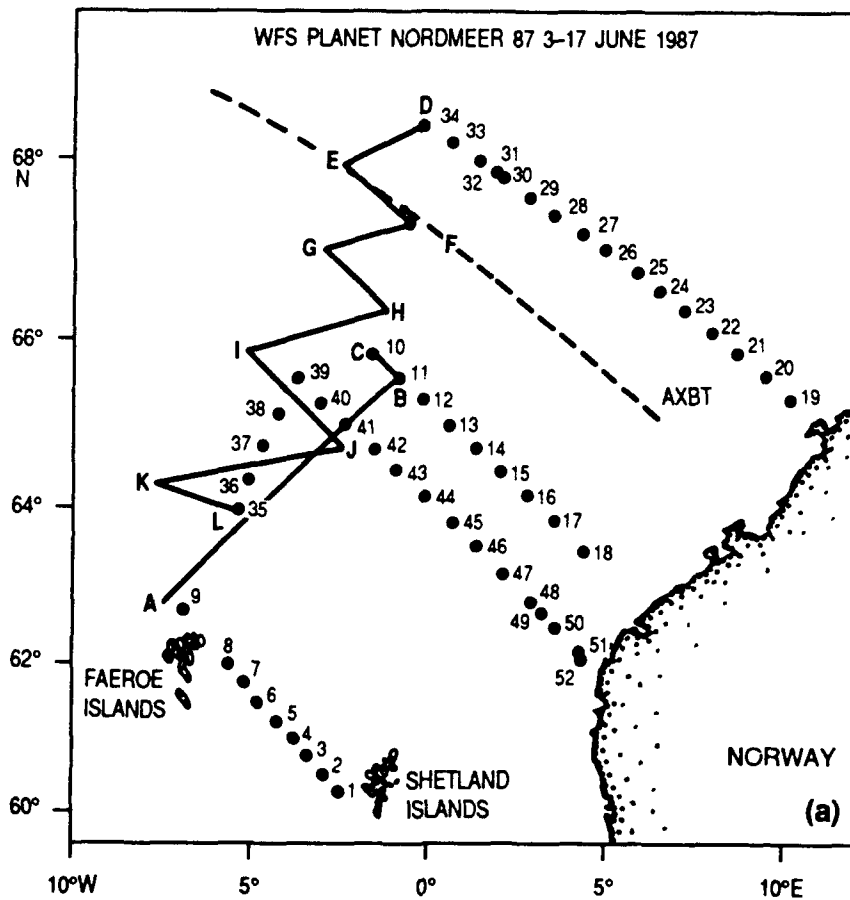


Figure 13. Charts of oceanographic measurements. (a) CTD and thermistor chain positions during Planet cruise in June 1987 and the path of AXBT flight from 1 June 1987. (b) CTD positions and positions of drifters' deployments during the Agor cruise in October 1988.

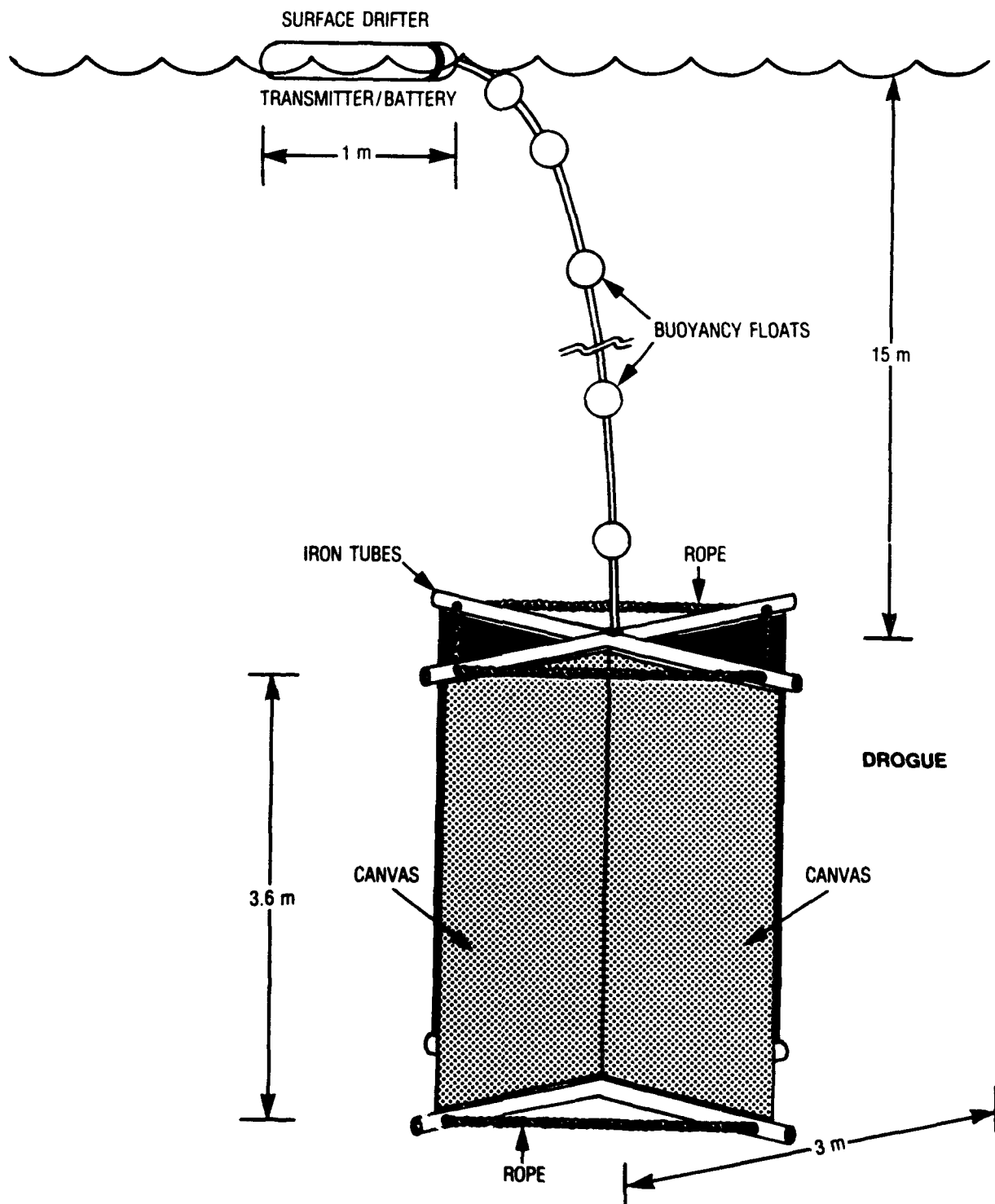


Figure 14. Schematic of surface drifters.

### 3.0 Data Errors

#### 3.1 CTD, AXBT, Thermistor Chain

The accuracy and the resolution of AXBT, CTD, and thermistor chain measurements easily indicated mesoscale features in the GIN Sea area because the temperature and salinity contrasts of these features are large. The CTD calibrations before and after the cruises insured that the sensors worked properly. Surface topography computed from CTD data is based on the dynamic method and is therefore subject to errors in the choice of reference level. In addition, any sea-level change related to barotropic signal, which is important for the shallower stations, is not accounted for in CTD analysis.

Accuracy of the drop positions for the AXBT were less than 7 km. For CTD's and the thermistor chain, positions were less than 5 km (compared with GPS).

The sampling interval for the AXBT cross section was about 13 km, AXBT's over the Iceland-Færoe Ridge about 35 km and more. Separation between the CTD stations in the NORDMEER 87 experiment was 35–45 km, in the 1988 (NOARL) cruise the separation was variable between 6 and 25 km. Thermistor chain sampled about every 60 m.

Some CTD cross sections lasted 2 days, and some were taken in delay to the altimeter overflight.

The large separations between some AXBT and CTD stations does not permit the full horizontal resolution of mesoscale eddies and fronts. The nonsimultaneity between altimeter and other measurements may cause the change of the oceanographic features under the satellite track, due to convection or dynamical changes, because the time scales for the significant variation in the GIN Sea area can be as short as 1–4 days.

#### 3.2 Altimeter

The radar altimeter measures the distance from its antenna's electrical center to the instantaneous sea surface as average over the footprint. This footprint is a function of significant wave height; for flat sea its diameter is 1.7 km; for 10-m waves it extends to 5.6 km. Ten data points (every 0.1 s) are averaged giving 1-second values corresponding to about 6.5-km-long segments of averaging along the satellite's nadir track. The lateral error in the ERM ground tracks is 1 km. All ground tracks that are  $\pm 1$  km apart are projected on this fixed track. Estimated error in *SSH*, corresponding to this projection, was derived from the largest geoid slopes in GIN Sea area and is less than 2 cm.

Precision of the GEOSAT range measurement is estimated to be 3.5 cm (MacArthur et al., 1987). The detailed error budget for the GEOSAT mission, based on postlaunch estimates of the gravity, drag, solar pressure, station coordinates, and instrument noise uncertainties, and the list of assumptions on which it is based, is given in Lybanon and Crout (1987).

##### 3.2.1 Orbital Error

An important source of error is the uncertainty in the orbit determination. Orbits were determined by the Navy Astronautical Group with a radial position uncertainty of 3 m. Simple detrending was adequate to reduce the residual orbit error to centimeter level for the relatively short tracks (less than 1500 km) through the GIN Sea area. This linear fit removes also other long-range (>1000 km) geophysical errors present in the altimeter data. Some geophysical errors are in the mesoscale range or have significant energy at mesoscale wavelengths, namely ocean tides, electromagnetic bias, and wet troposphere pathlength correction.

##### 3.2.2 Wet Tropospheric Correction

Data collected by the special sensor microwave/imager (SSM/I) radiometer, which was launched aboard the DMSP satellite in June 1987, are used in calculation of the wet troposphere pathlength correction. Algorithms for this computation were developed by Hollinger (1980) based on linear combinations of the brightness temperatures measured by several channels of the SSM/I radiometer. The range correction is given by

$$h_w = 6.43W, \quad (5)$$

where  $W$  is the total precipitable water. Preliminary study of SSM/I data in the GIN Sea area for the 3-month period (July–September 1987) indicates the importance of this correction. The “tongues” of wet and dry air, which accompany the low-pressure disturbances, cause variations that correspond to the altimetric range correction between 5 and 15 cm in mesoscale wavelengths ( $\sim 100$  km). The effect of this correction is more important for the data along the descending altimetric tracks because the bands of the wet and dry atmosphere often seem to be perpendicular to the direction of moving atmospheric fronts (north-east) that coincide with descending tracks, causing the largest gradients in the correction amplitudes. In contrast, wet correction has the small gradients in long wavelengths for the ascending altimetric ground tracks.

Near simultaneity between the SSM/I and altimeter data is the important constraint in applying the wet tropospheric correction to altimetric data. It was observed that atmospheric fronts move with speeds as high as 35 km/h over the GIN Sea area; therefore, the time difference of 2 hours between collection of altimeter and SSM/I data leads to highly inaccurate altimetry corrections. No wet tropospheric correction was used for the GIN Sea project.

### 3.2.3 Electromagnetic Bias (EM)

The primary effect is directly proportional to wave height and causes a range error of about 2% of the significant wave height at the frequency of the GEOSAT altimeter. The tracker itself is responsible for a similar bias; the combined effect used in our data is 5% of the significant wave height. Figure 15 illustrates the amplitudes of EM and its effect on *SSH*. The three columns represent the three different passes of altimeter along the D27 altimeter ground track. They are distinguished by their revolution number. The first row displays altimeter off-nadir angle along the path (latitude). The very high off-nadir angle for REV19772 stopped to be recorded above 1.3°. The second row shows the amplitude variation for the signals obtained as 2% and 5% of significant wave height. In addition to the low-frequency variations, the high-frequency "noise" is significant (>5 cm) for the large significant wave heights (>5 m). The third and fourth rows show the EM corrected (5%) and uncorrected *SSH<sub>M</sub>* data, respectively. It is clear that EM correction does not improve the high-frequency noise in *SSH* data. The *SSH<sub>M</sub>* data taken during the high sea state (large significant wave heights) are noisy (variations >10 cm) and were not incorporated into sets for computing the ensemble averages.

### 3.2.4 Tidal Error

Tides are accounted for by the Schwiderski-Szeto (1981) model, which has an accuracy of 10 cm or better over the open ocean. Schwiderski (1986) described the tidal problems in the GIN Sea area. Semidiurnal partial tides ( $M_2$  is dominant) have three amphidromes in the southern part of GIN Sea area, one of which is located close to the Iceland-Færoe Front. The dominant diurnal ( $K_1$ ) tide has two amphidromes in the GIN Sea area. The same is valid for  $P_1$ , while  $O_1$  and  $Q_1$  depict no amphidrome in the GIN Sea area. In coastal waters and areas of rough bottom reliefs, lesser accuracy must be assumed. The  $1^\circ \times 1^\circ$  graded grid system fails to allow a sufficient resolution of quickly varying tidal heights, particularly for the  $M_2$  tide between Iceland,

the Færoe Islands, and the Shetland Islands. Figure 16 shows *SSH<sub>M</sub>* data (tide removed) along ascending track A38, which passes across the Færoe-Shetland Channel and the Iceland-Færoe Ridge.

Tidal error is visible across the Færoe-Shetland Channel and is very pronounced in the Iceland-Færoe area, where the amplitude is about 15 cm in the 200-km range. All ascending tracks that pass across this area have severe tidal problems in mesoscale range. Figure 17 illustrates tidal error across the Iceland-Færoe area along descending ground track D33. Even if the tidal error is present in the longer wavelength, it masks the Iceland-Færoe Front. The maximum of tidal error in Figure 17 is at  $64.5^\circ\text{N}$ , with a magnitude of about 8 cm. At that point, Figure 18 displays the four dominant tidal components (from Schwiderski-Szeto model) in the time window of  $\pm 12$  hours from the time that corresponds to each altimetric pass shown in Figure 17. Amplitudes for the semidiurnal tidal components are small (namely  $S_2$ ) because of the proximity to amphidromic point ( $63.5^\circ\text{N}$ ,  $8^\circ\text{W}$ ). It is clear in Figure 17 that variation in tidal error is a product of the beat frequency between  $M_2$  and  $S_2$ , with periodicity of 14.77 days. This variation is clearly present in all *SSH* data (tide removed) taken across the southern part of the GIN Sea area.

Figure 19 shows tidal error introduced into the data by bilinear (or other) approximation. The  $1^\circ \times 1^\circ$  graded system of Schwiderski data are too coarse to allow a sufficient resolution of quickly varying tidal heights. Data in Figure 19 represent descending passes along track D10. The first column shows the bilinearly approximated Schwiderski tidal data as points and "smoothed" data as a line. The second column displays the *SSH* data without the Schwiderski tide as points, and with tide present as a line. The third column shows *SSH* data with tide, as points, and *SSH* without the smoothed tide as a line. (Tilt and bias are always removed.)

The bilinear approximation causes the spurious signal between  $63.0^\circ\text{N}$  and  $64.2^\circ\text{N}$ . This signal occurred in descending passes crossing the Iceland-Færoe Ridge, in an area where the Iceland-Færoe Front is also present. Introduced error is in mesoscale range, which makes it difficult to determine the position of the Iceland-Færoe Front. Any smoothing of tidal curves may diminish the large tidal error but cannot solve the problem. Only the gridwise refined tidal model for this area can improve the data. The correlation of frontal position and the gross bathymetry creates two problems: (1) tidal amplification and (2) geoid error. This is in addition to dynamic topographic effects over the area.

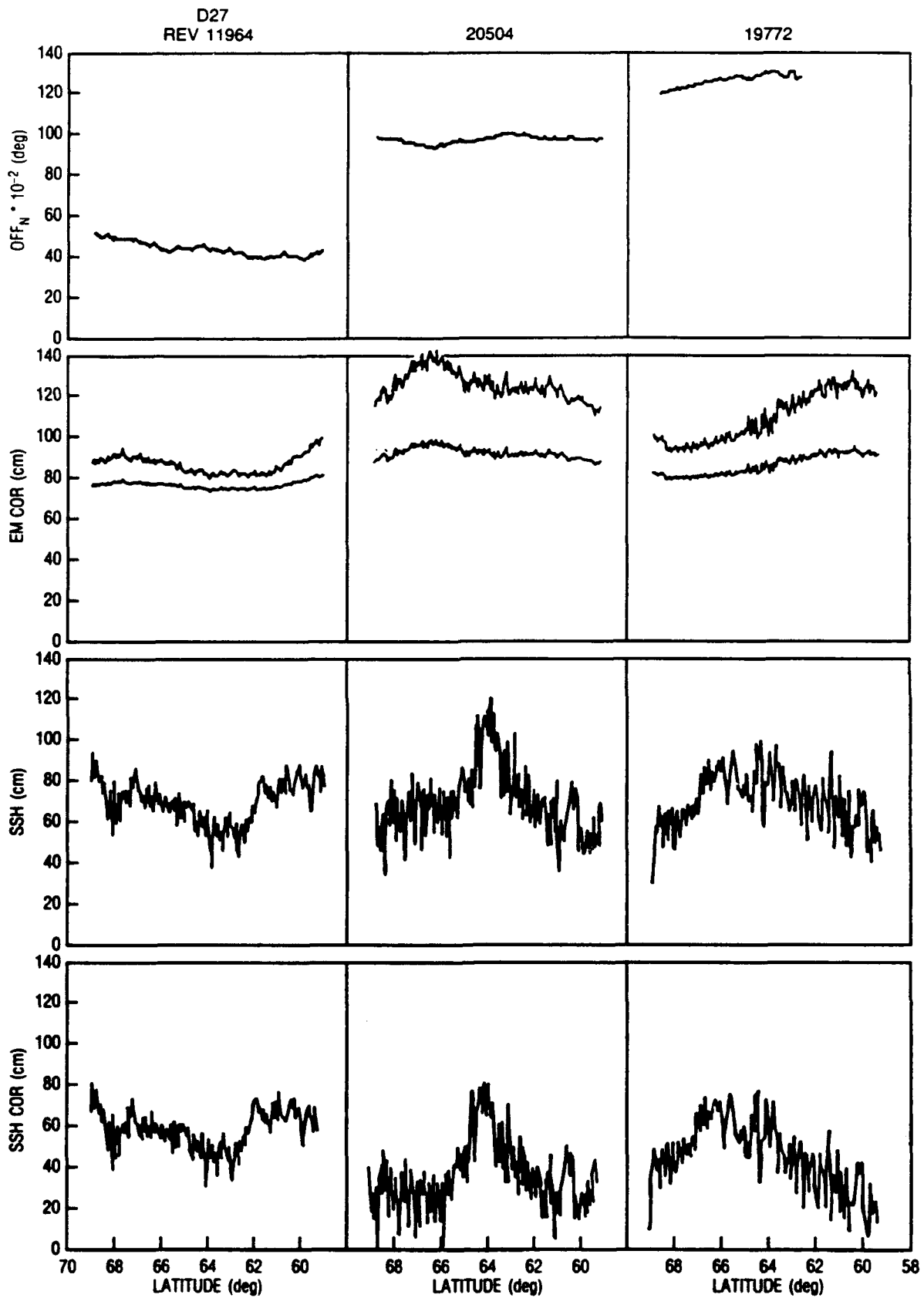


Figure 15. EM correction and its effect on  $SSH_M$ . The three columns represent three passes of altimeter along D27. (a) Off-nadir angle (in  $10^{-2}$  deg.), (b) EM correction (2% and 5% of significant wave height), (c) EM corrected (5%), and (d) uncorrected  $SSH_M$  data.

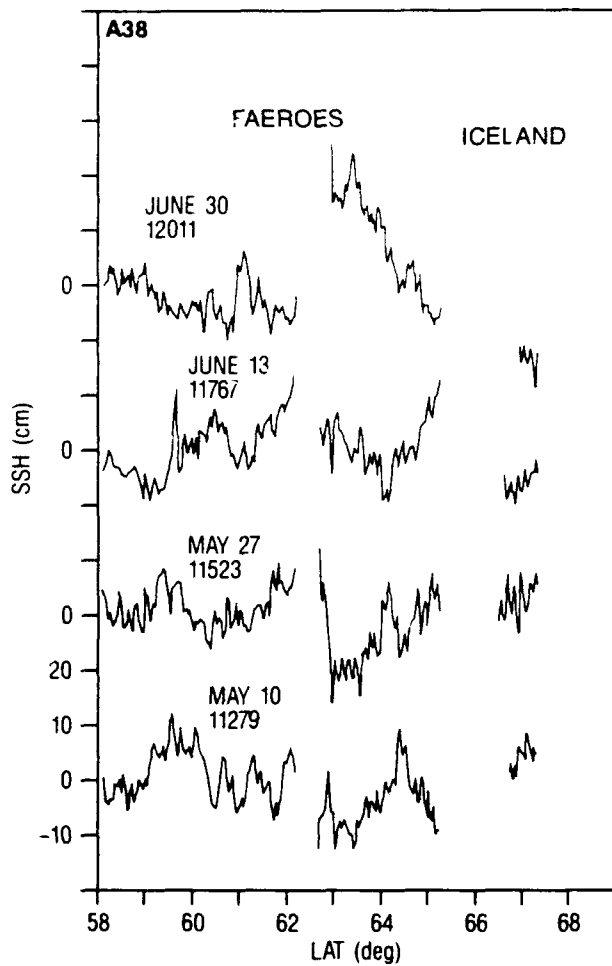


Figure 16. Several  $SSH_M$ 's along ascending track A38 showing tidal residual error across Iceland-Færoe Ridge area and Færoe-Shetland Channel.

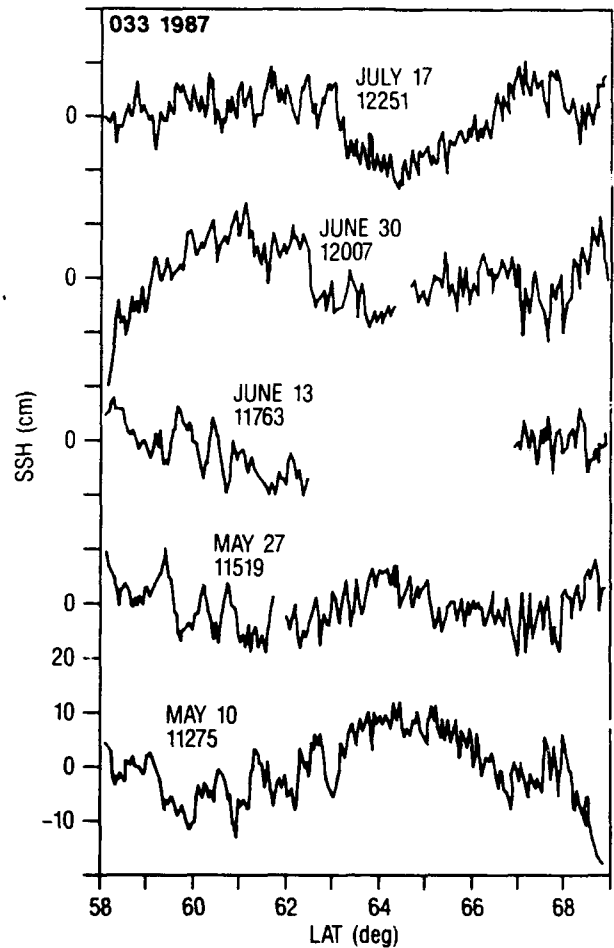


Figure 17. Several  $SSH$ 's along descending track D33 displaying tidal error across Iceland-Færoe Ridge.

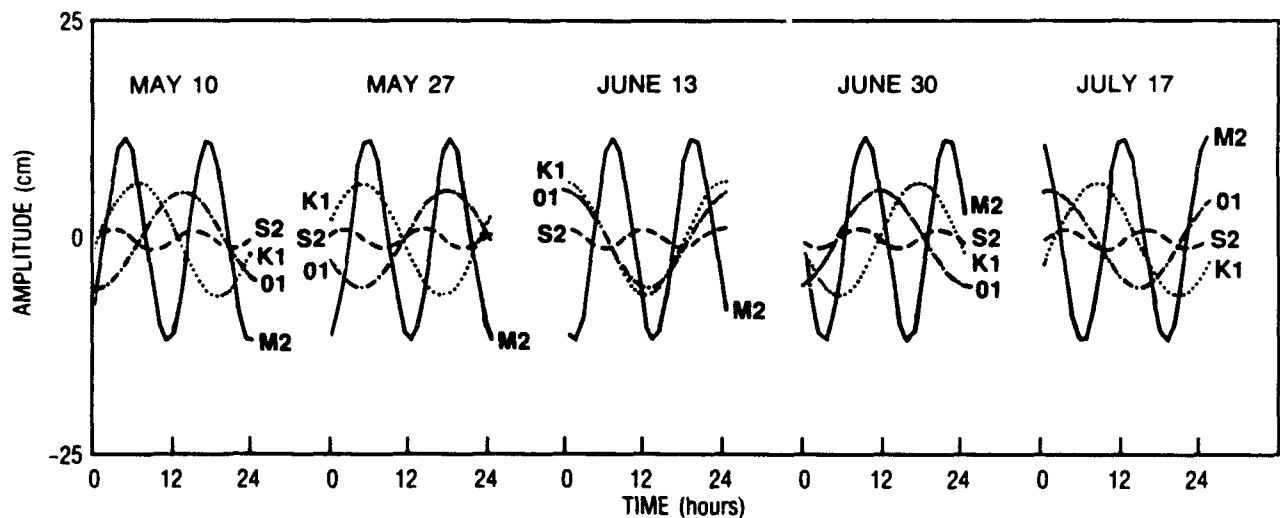


Figure 18. Illustration of four dominant tidal components (from Schwiderski model) at  $64.5^{\circ}N$ ,  $8.5^{\circ}W$  (at the maximum of tidal error in Fig. 17). The time window is  $\pm 12$  hours from the altimeter passes. Data are shown in Figure 17.

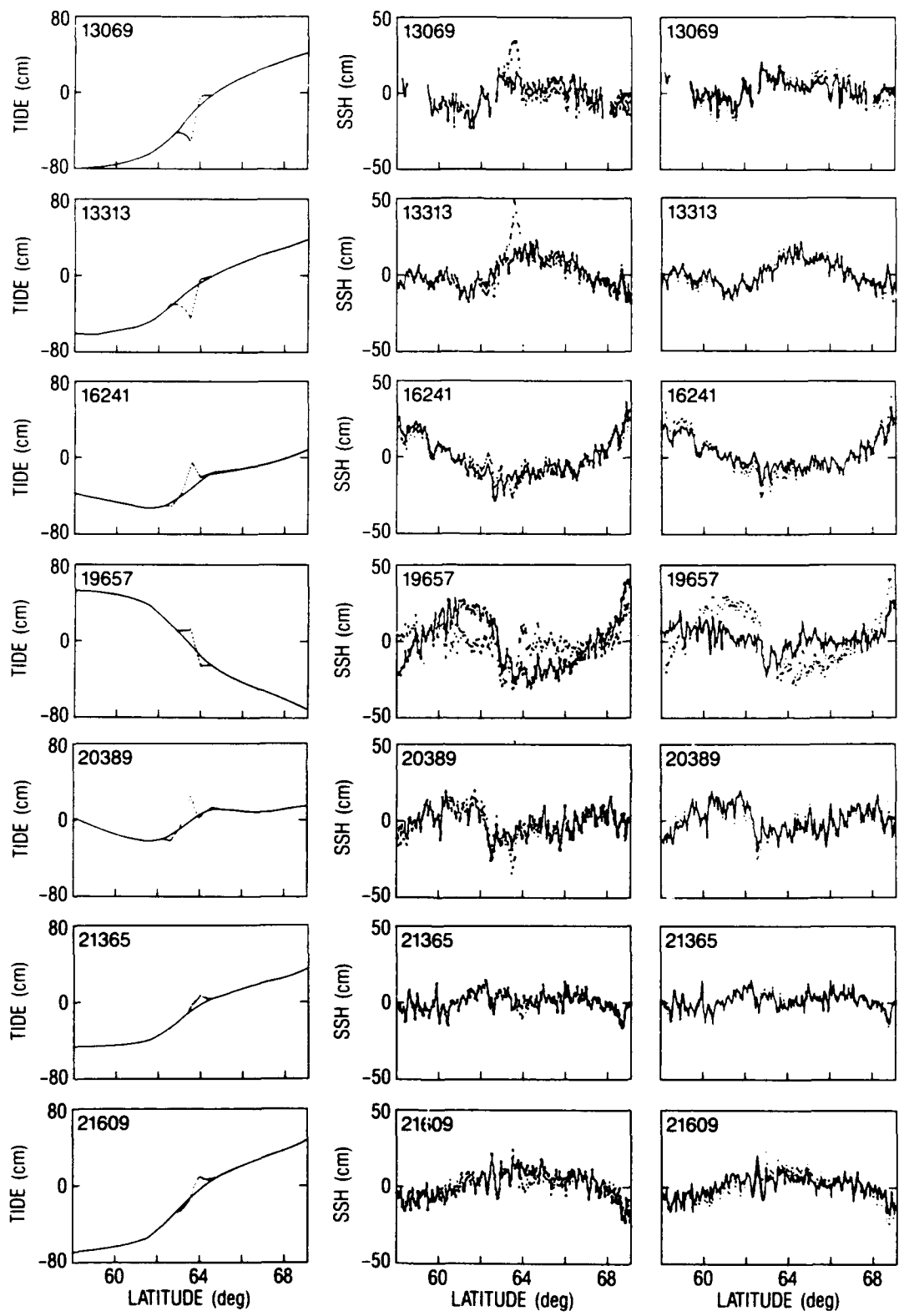


Figure 19. Tidal error in mesoscale range introduced by bilinear approximation of  $1^\circ \times 1^\circ$  graded grid to descending tracks D10. As an example 7 tracks are displayed. (a) Schwiderski tides as points, and the spline approximated version as a line. (b) SSH data with removed Schwiderski tide as points and SSH with tide not removed as a line. (c) SSH with tide not removed as points and SSH with the spline approximated version of tide removed as a line.

## 4.0 Results and Discussion

Altimetric interpretations for the GIN Sea project were strongly oriented to the ground truth measurements. *SSH* residuals were small, often close to the range of uncertainty in the geophysical corrections. In such a case, in situ measurements are the necessary and indispensable part of understanding and interpreting altimetry.

### 4.1 SSH and IR Images

The GIN Sea area is usually covered by clouds. It is difficult to have a clear IR image and, simultaneously, the altimeter data over it. IR images show large spatial variability in the surface temperature field associated with meanders and eddies, many of them in the scale of 25 to 35 km. Several figures (Figs. 20–25) show the *SSH* residuals superimposed on IR images. *SSH* residuals were obtained as a difference between the instantaneous and mean profiles, so they do not contain information about the steady components of the flow. The exception is in Figure 23, track A21, which contains this information. There may be a difference of several days between the IR image and the *SSH* overlay. Assuming about 10 cm/s as characteristic speed along fronts (mean surface currents), it translates to possibly 8 to 10 km/day lateral shift between features.

Figure 20 shows two altimeter tracks with *SSH<sub>M</sub>* across the Norwegian Atlantic Current. It is apparent that some IR features correlate with altimeter signal (for example, the warm feature in the central part of A04), but the other parts do not correlate well even if the time difference between IR and altimeter is taken into account. This is commonly the situation.

Figure 21 also shows two altimeter paths situated to the south of previous paths. Altimeter data along A09 represent data taken 3 days later than IR imagery. The northward shift of 30 km in the IR image could possibly match the altimeter. *SSH<sub>M</sub>* along A35 came 2 days earlier than IR image. Data are filtered by Fourier filter; only variations of the scales larger than 30 km are left. Interpretation of the altimeter signal and correlation with IR have the same problems as already discussed.

Figure 22 displays the IR image from May 27 and the altimetry along A35 (the same as above, only unfiltered) and A04. A35 passes 1 day earlier and A04 3 days later than IR image. Correlation with the features is good, A35 with the warm flow around 5°E and A04 with cyclonic eddy around 7.5°E. In interpreting the altimetry, it should be

remembered that fronts can appear to be like cold or warm eddies (see Fig. 12).

Figure 23, with the IR image from 21 May and altimeter tracks A02 and A21, shows good correlation of IR features with A21. Altimeter signal was obtained by the second method, taking into account dynamic height from the CTD cross section taken during the altimeter pass 17 days later. It contains information about the mean flux, which is visible as general sloping (from 1°E to 3.5°E) superimposed on the eddy field. Altimetry shows two cold eddies of 55 and 40 km diameter. One eddy is visible in the IR image, just on the edge of a cloudy area. The warm anticyclonic eddy around 3°E is also correlated with altimetry.

Figure 24, with the IR image from 21 May and two altimetry tracks D16 and D21, is from the Iceland-Færoe region. D21 passed on the same day as the IR image and D16 2 days earlier. The IR image and the altimeter data show that the area is seeded with cyclonic eddies that are 45 to 50 km in diameter. It is obvious that at the northern side of the front, altimetric residuals have small amplitude variations. The cyclonic eddy, centered at 11.5°W on D21 with an amplitude of about 10 cm, is well correlated with the IR feature. D16 shows a strong anticyclonic eddy centered at about 6°W, followed by two cyclonic eddies. Likewise, the IR image is in good agreement with the altimeter.

Figure 25 presents the IR image from 29 May 1987 and altimeter track A12, which passed 3 days later. The anticyclonic eddy in the middle of the track is the same eddy visible in Figure 24, only now well delineated from the frontal region, which is situated in a southwesterly direction from the cyclonic eddy. The sloping of the *SSH<sub>M</sub>* signal to the west of the eddy may indicate the presence of the Iceland-Færoe Front.

### 4.2 Sections Across Atlantic Inflow and Norwegian Atlantic Current

Figure 26a shows altimetric ground tracks involved in in situ measurements, and Figure 26b displays bathymetry, positions of cross sections, and locations of the AXBT and CTD casts.

#### 4.2.1 AXBT Cross Section

Figure 27 summarizes the results of the altimeter and AXBT measurements. Figure 27a represents the temperature cross section taken simultaneously with AXBT data. It clearly shows that the main branch of the Norwegian Atlantic Current is centered

around 6°E and that a more diluted branch deviates from the main one around the Voring Plateau, centered at 2°W. Several warm and cold core eddy-like structures extending to a depth of at least 300 m are visible, some of them with a tilted vertical axis. Figure 27b represents altimeter data. The dotted line shows the low-pass filtered data with a cut-off wavelength of about 30 km.  $SSH_M$  data represent the difference from the ensemble average (created from 14 passes), which means that the steady features do not show up. This can explain why there is no pronounced rise in  $SSH_M$  west of the main inflow (around 5°E). Figure 27c represents the curves of surface temperature and the averaged temperatures for the columns of water between 0–40 m and 200–350 m, respectively. Visual inspection between temperature cross section and altimeter reveals high correlation between them. The deeper layers are clearly better correlated, as shown in Figure 27c. The average temperature between 200 and 350 m is better correlated with the altimeter than the surface or upper-layer temperatures. This result is also obtained by computing the cross correlation as seen in Table 1.

This large correlation of altimetry with the deep structure indicates that the deep structure has a dominant effect on the dynamics of the whole column from the surface to at least 350 m. This also is an indication that low mode (1st) baroclinic dynamics dominate. The eddies are probably “fresh” instabilities of the front. Corresponding sea surface temperature (SST) was obtained by calibration of NOAA 10 satellite data along the A09 altimeter ground track. The  $SSH_M$  along this track is shown in Figure 28. The cross correlation between these two data sets is shown in Figure 29. Visual inspection of SST and  $SSH_M$  indicates that some features are well aligned. SST data were taken 3 days earlier than  $SSH_M$ , which may account for some relative shifts between data sets. The cross correlation between data is small, and an 8-point shift to the

Table 1. Cross correlation between altimeter and temperature data for AXBT cross section.

Data	Cross Correlation
Altimeter/temperature surface	0.21
Altimeter/temperature 0- 40 m	0.16
Altimeter/temperature 0-150 m	0.02
Altimeter/temperature 0-300 m	0.13
Altimeter/temperature 200-350 m	0.58

left for  $SSH_M$  to obtain the better fit, would likely improve the matching of features on the right side of graphs but not on the left side. It is possible that the lateral convection of features is not uniform. The low cross correlation between  $SSH$  and SST was also observed for other comparisons. The reason is that the water masses of different temperatures are entrenched into eddies and fronts and can confuse their SST expression. In addition, the absolute temperature structure is compared with  $SSH_M$ , which represents only the deviation from the mean.

#### 4.2.2 Cross Section 0

This cross section was taken across the Færoe-Shetland Channel (see Fig. 26). Figure 30 shows the cross sections of several variables. The section was taken on 3–4 June 1987. Dynamic calculation of geostrophic velocity, with the level of no motion chosen at 500 m, shows very small currents flowing northward on the Shetland side and, perhaps, the presence of the weak recirculation flow (as discussed in Background section) to the west of it (Fig. 31). The time of the closest altimetric pass was along ground track A05 on 30 May (4 days before the CTD cross section). Figure 32 shows the position of A05 relative to the CTD cross section. Figure 33 shows  $SSH_M$  taken along A05 on 30 May and cross sections of variables for the surface layer (0–150 m) along transect 0. The altimeter track was parallel, but about 40 km to the north of section 0 and to compare the cross section with it, the  $SSH_M$  was projected onto section 0, as indicated in Figure 32.  $SSH_M$  indicates the presence of the weak recirculation (sloping between the CTD station 5 and 6) and, perhaps, the cyclonic eddy to the west of it. Figure 34 shows  $SSH$ 's for several satellite passes along A05. Figure 34a represents  $SSH_M$ 's obtained by differencing the instantaneous pass and the ensemble average. Figure 34b represents  $SSH_C$ 's obtained by differencing the instantaneous profile and the profile from 30 May (dynamic height obtained from the CTD cross section associated with this day was constant). Essentially, the instantaneous altimetric profile from May 30 served as a geoid. Ensemble average was created from only five profiles. The reason is that the tidal error does not often change from one pass to the other (see section 3.2.4), but the error would be detrimental if many profiles were averaged. The same is true about the results in Figure 34b;  $SSH_C$ 's adjacent to May 30 are less contaminated by tidal error. The remarkable similarity between the  $SSH$ 's in Figures 34a and 34b signifies the absence of a steady current. Likewise,

the agreement of eddy structures in both figures for the corresponding profiles indicates that the 30 May profile, taken as a geoid, was not contaminated by strong eddies (as also indicated by the CTD cross section) and that the eddy structure, namely, in 3 July, is real.  $SSH$  from 16 June indicates the strong inflow of the North Atlantic water has an estimated geostrophic velocity of 17.5 cm/s. A crude estimate of transport gives 4.6 Sv. The estimate is based on the assumption of the same velocity of current between 61.6°N and the shelf break (positions on A05 track), to 500 m depth (or bottom, where less deep) and linear decay of the velocity from the surface, 17.5 cm/s to 0.0 cm/s at 500 m.

In a strict sense, altimeter profiles yield only the surface geostrophic current velocity. Information on the current structure of the underlying water can be extracted only with simultaneous hydrographic data, with a dynamic upper-layer ocean model, or by "calibration fit," where the altimeter profile is compared with the set of profiles for which the current structures were determined from the hydrographic data (Kao and Cheney, 1982). Altimeter data from the other passes do not show strong inflow, indicating that the variability in inflow is considerable and the "no current" condition is not exceptional.

Figure 35 compares dynamic height obtained from CTD casts (Fig. 35a) and altimeter residuals (Fig. 35b).  $SSH_M$  was computed as a difference between instantaneous profile and ensemble mean. The time lag between the CTD cross section and the altimeter is 5 days. Dynamic heights in the CTD section indicate the weak inflow to the west of Shetland shelf. Altimeter residuals show the stronger inflow in the same area due, perhaps, to the 5-day delay in altimeter data. As in the above example, the estimated geostrophic velocity is about 17 cm/s. Even if this estimate was not obtained from the absolute topography, it may give the correct result due to the reasons already described. As in the previous case, the altimeter data along A12 have tidal error problems and to obtain the reliable results, the tidal correction has to be improved.

#### 4.2.3 Cross Section 1

This cross section was taken across the Norwegian Atlantic Current. Its location and the positions of the CTD casts are shown in Figure 26. This cross section is coincident with the position of Sognefjord Sections described and plotted for the period of 1900–1970 by Saunders and Burns (1985). The CTD

section was taken simultaneously with the altimeter data along ground track A21. Figure 36 shows the cross sections of several oceanographic variables obtained from the CTD data. The cross sections show remarkably smooth inflow of Atlantic water on the east side of the cross section without oscillations of isolines to the west, which are usually present. In the dynamic calculation the reference level was chosen at 900 m, but the isopycnals of potential sigma indicate that it is not yet compensated.

Corresponding geostrophic velocity is displayed in Figure 37. It shows the northward current to be more than 10 cm/s for the main inflow and indicates (from CTD cast 18) the presence of a contracurrent to the west of it. Figure 38 displays  $SSH$  taken along A21 during the oceanographic measurements, as well as cross sections of oceanographic variables for the surface layer (0–150 m depth). There is variation of the altimeter signal in scales smaller than 40 km and, except for the variation corresponding to the warm-core feature near CTD cast 15, they cannot be resolved by CTD grid.  $SSH_M$  does not show the large signal visible in the dynamic height plot, as it represents only the difference from the mean. To evaluate the usefulness of the historical CTD data base for the improvement of the reference surface, GDEM +  $SSH_M$  and CTD data were compared.

Figure 39 shows plots of GDEM, GDEM +  $SSH_M$ , and the dynamic height obtained from CTD's of cross section 1, all computed along the ground track A21. The dynamic height computed from GDEM summer data and added to  $SSH_M$  residuals shows a much smaller slope than CTD cross section 1. Figure 40c, where GDEM +  $SSH_M = SSH_{GDEM}$  are shown for several consecutive passes, also indicates smaller slope of each profile than the absolute topography in Figure 40b. The GDEM data set possibly does not have enough representative measurements in this particular area to create a reliable average. Figure 40a represents  $SSH_M$  residuals for several altimeter profiles obtained as a difference of particular pass and the mean. Figure 40b shows the absolute topography obtained by subtracting the CTD dynamic heights from the June 6 altimeter profile and differentiating this instant geoid with the appropriate profiles (described earlier). The dynamic topography obtained from the CTD cross section does not fully resolve smaller eddies (<40 km), and this poor resolution partly degrades the other profiles, as visible in May 3 and March 30 data.

Table 2. Estimates of average surface velocity from  $SSH_C$  data for the cross section 1.

Profile	Width (km)	Velocity (cm/s)
June 23	130	10.3
June 6 (CTD)	195	6.4
May 20	125	12.0
May 3	137	8.2
March 30	100	15.0

While  $SSH_M$  obtained from the mean does not show inflow of Atlantic water, the absolute topography ( $SSH_C$ ) shows its presence in every profile. An example is the profile A21 from May 20 in an IR image, Figure 23. The estimates of the average surface geostrophic velocities and the width of inflow are given in Table 2.

#### 4.2.4 Cross Section 2

Cross section 2 was taken across the Norwegian Atlantic Current as indicated in Figure 26. The CTD section was taken simultaneously with the altimeter data along ground track A30. Figure 41 shows the cross sections of several oceanographic variables obtained from the CTD data. Dynamic height, as well as potential temperature and salinity cross sections, show considerable horizontal variability of the isoline depth, indicating the presence of the entrenched eddies described in section 1.1. The main inflow of Atlantic water is guided by the continental slope, but a portion of it appears near CTD stations 29–30, indicating the branch that continues around the Voring Plateau. It is apparent that the Atlantic water mass is present over the Holtenbank area, east of the main inflow. The surface, however, is overlaid by the fresher water that belongs to the Norwegian Coastal Current. The geostrophic current cross section obtained from CTDs is shown in Figure 42. It indicates a complicated flow pattern. It is interesting to notice the southward flow near CTD stations 33 and 34 where the presence of Atlantic water (salinity 35.00) extends to 450 m.

Figure 43 shows  $SSH$  with its low-pass filtered version taken during the oceanographic measurement and the cross sections of potential temperature, salinity, and potential sigma for the surface layer (0–150 m). The Norwegian Coastal Current water is visible at the right side of the cross sections. It is

Table 3. Cross correlation between altimeter  $SSH$  and the oceanographic variables for cross section 2.

Depth	Temperature	Salinity	Dynamic Height
Surface	0.523	0.396	0.025
0–40 m	0.022	0.494	-0.615
0–200 m	0.532	0.566	0.152
200–330 m	0.581	0.699	0.464
350–600 m	0.154	0.214	0.083

present in the surface layer only a few tens of meters thick.  $SSH_M$  represents the sole variation from the mean. Its peaks are visually well correlated with the main warm surface features.

Figure 44 shows dynamic height computed along the CTD cross section and  $SSH_M$  and its low-pass filtered version. Figure 45 is the cross correlation between the dynamic height and the filtered version of  $SSH_M$ . The cross correlation here is small. The result of the cross correlation between  $SSH_M$  and oceanic integrated variables for different depths is given in Table 3.

Results indicate good cross correlation with the structure between 200 and 330 m. This result agrees with AXBT data discussed earlier. Figure 46 shows plots of GDEM, GDEM +  $SSH_M$ , and the dynamic height obtained from CTD's of cross section 2, all computed along ground track A30. The slope of GDEM +  $SSH$  data underestimates the CTD's. Likewise, Figure 47c, where the GDEM +  $SSH_M = SSH_{GDEM}$  are shown for several consecutive passes, indicates that the slope of each profile is smaller than the profiles representing the absolute topography (obtained from CTD) in Figure 47b.

The profiles of Figure 47a represent  $SSH_M$ 's obtained as a difference of a particular pass and the mean. The set of profiles in Figure 47b shows the absolute topography obtained by subtracting the CTD dynamic heights from the altimeter profile of June 10 and differentiating this instant geoid with appropriate profiles (described earlier). The important feature in these profiles is the sloping of the curves. It indicates the presence of the steady component of the Norwegian Atlantic Current. The slopes in the profiles are larger than the slope of the CTD dynamic height. The reason could be the presence of orbital error (in the form of tilt) in the June 10 altimeter data. The average velocities and the width of the flow are in Table 4.

Table 4. Estimates of average surface velocity from  $SSH_C$  data for cross section 2.

Profile	Width (km)	Velocity (cm/s)
May 7	160	8.7
May 24	200	8.9
June 10 (CTD)	265	4.7
June 27	239	7.5
July 14	214	8.8

#### 4.2.5 Cross Section 3

Cross section 3 was also taken across the Norwegian Atlantic Current in (Fig. 26). This section was taken about 90 km south of and parallel to cross section 1 and 10 days later (16 and 17 June 87). It was taken simultaneously with the altimeter data along ground track A07. Figure 48 shows the dynamic height and several cross sections of oceanographic variables obtained from the CTD's. In spite of the time and space proximity to cross section 1, features in cross section 3 are different. The main core of Atlantic water is near and westward of the Norwegian Continental Slope. Considerable variation in the isoline depths and the corresponding eddy-like structure in the geostrophic currents is demonstrated in Figure 49.

Figure 50 shows the filtered version of  $SSH_M$  taken during the oceanographic measurement, and the cross sections of potential temperature, salinity, and potential sigma for the surface layer (0–150 m). The presence of the Norwegian Coastal Current water is detectable almost 300 km from the coast. It creates a slab only 20–30 m thick near the surface; the slab is detectable by lower salinity, and overlays the North Atlantic water.  $SSH_M$  indicates the presence of cold eddies (Fig. 50c) with the scale 35–45 km and a 10-cm amplitude. The CTD section does not have enough resolution to detect the eddies. Visual inspection indicates that many features in  $SSH_M$  are matched by the structure displayed in cross sections.

Figure 51 shows the dynamic height computed from CTD casts and corresponding  $SSH_M$ . As before, CTD separations were too large to resolve the eddies smaller than 50 km in diameter. The cross correlation between the filtered  $SSH_M$  and dynamic height is very small (Fig. 52). Figure 53 shows cross correlations between filtered  $SSH_M$  and potential temperature and salinity in different depths, respectively. Results from this figure indicate that

the upper layer (<200 m) in the cross section is better correlated with  $SSH$  than the deeper strata. This result is different from the results obtained in the AXBT cross section and cross section 2, where the deeper oceanic structure (200–300 m) was better correlated with  $SSH_M$ . Again, it is important to realize that the cross correlations of  $SSH_M$  with the parameters of ocean structure have only limited validity.  $SSH_M$ 's represent the differences from the mean, while parameters used in the cross correlation are not the residual fields (differences from the means) but the absolute structures. If the oceanic features would average out in the mean (for example, the field of eddies), then the cross correlation, obtained as described, would have proper meaning. In our cases, the part of structure does not average out, namely the part which corresponds to Norwegian Atlantic Current. Corresponding  $SSH_M$ 's would indicate only the changes in position and amplitude of this front (Fig. 12) and cause the decorrelation.

Figure 54 shows plots of GDEM,  $GDEM + SSH_M$ , and the dynamic height obtained from the CTD's of cross section 3, all computed along ground track A07. The slope of  $GDEM + SSH_M$  data corresponds to the slope of the dynamic height obtained from CTD's. Likewise, Figure 55c, where the  $GDEM + SSH_M$  are shown for several passes, indicates that the slope of each profile is comparable to the profiles representing the absolute topography (obtained from CTD) in Figure 55b. The profiles on Figure 55a represent  $SSH_M$ 's obtained as a difference of a particular profile and the mean. The mean was created from 14 profiles. Profiles in Figure 55b show the absolute topography obtained by subtracting the CTD dynamic heights from the altimeter profile (June 17) and differentiating this instant geoid with appropriate profiles (described earlier).

$SSH$  profiles, as well as the CTD dynamic height and the profiles of oceanographic parameters, display large variability in their structures along this ground track. It is caused by proximity of this cross section to the area where inflow of the Norwegian Coastal Current from the Baltic Sea, the Norwegian Atlantic Current, and waters from the Icelandic Current meet.

#### 4.2.6 Cross Section 4

Cross section 4 is taken across the inflow of the North Atlantic Current. Its location is shown in Figure 26. It started near the shelf of Scotland,

crossed the Wyville Thompson Ridge, and finished on the Færoe Bank. This section was taken 1.5 days later than altimeter data along ground track A17. The orbit of the altimeter for the passes along this ground track were calibrated by two transponders operated by Rutherford Appellton Laboratory. The orbit determination for altimeter data was determined by the Navy Astronautics Group.

Figure 56 shows the cross section of potential temperature and salinity. The warm, saline Atlantic water is centered along the British continental slope and extends to a depth of 550 m, which corresponds to the depth of the Wyville Thompson Ridge. The lower layer shows the outflow from the GIN Sea area, which is also concentrated along the British continental slope.

Figure 57 shows the  $SSH_M$  and the salinity cross section.  $SSH_M$  represents the deviation from the mean, but assuming that its structure corresponds to that described in Figure 12, case 2 or 3, the surface geostrophic velocity is estimated to be 20.8 cm/s and the width of flow about 56 km.

### 4.3 Measurements Across the Iceland-Færoe Front

There is a considerable problem with the Schwiderski-Szeto tidal model in the Iceland-Færoe Front area. Tidal variation is large in small spatial scales, and a  $1^\circ \times 1^\circ$  tidal model is too coarse for proper approximation along altimeter tracks. Errors due to the tidal inadequacy are discussed section 3.2.4. Important short wavelength error (<100 km) along the descending altimeter tracks due to bilinear (or other) approximation is located between  $62.5^\circ\text{N}$  to  $64^\circ\text{N}$ , and interferes with the frontal position. Likewise, the ascending altimeter passes have large tidal error ( $\sim 15$  cm) because of the track's proximity to shallow-water areas (Færoes, Iceland) and approximations.

Tidal error displays the 15-day periodicity; therefore, there is an advantage to using the difference between successive altimetric profiles for determining the frontal translation, as the tidal error tends to be eliminated.

The fine resolution model of the North-East Atlantic generated by Proudman Laboratory in the UK is presently available but was not tested and used in this work.

#### 4.3.1 Thermistor Chain

Figure 58 shows the position of the thermistor chain tow, which was towed from point A to B

starting 4 June and ending 6 June 1987. Figure 59 shows the cross section of temperature along A to B obtained from the thermistor chain. Isotherms are marked every  $0.5^\circ\text{C}$  and the isotherms corresponding to  $7^\circ$  and  $5^\circ\text{C}$  are marked by the thicker lines. A rich lateral structure in isotherms demonstrates the mixing processes between the North Atlantic and Icelandic Current water masses. The arrows above thermal structure point to warm structures: 1 indicates the main frontal region; 2, anticyclonic eddy; and the others correspond to smaller features (25–30 km). These main features could be identified on the IR image taken 6 days earlier (Fig. 60). The thermistor chain was towed along the line marked D16. In agreement with thermistor chain data, the main frontal position is  $63.2^\circ\text{N}$  and the center of the warm eddy is at  $63.6^\circ\text{N}$ . Altimeter data were collected along the thermistor chain pass on 5 June. Altimeter residuals obtained as a difference from the mean are displayed in Figure 59 under the thermal structure.  $SSH$  indicates the gentle slope to the left of the main thermal front (1), but this is an area of tidal problem, so the result is biased by tide. The altimetric signal corresponding to the warm eddy is missing (precipitation in that area), but the eddy signature was recorded on the ascending pass (A12) on 2 June (Fig. 60). The ascending pass intersects the eddy, and a clear signal of about 15 cm was detected. The eddy moved eastward about 1.7 cm/s (25 km/17 days), as indicated by the altimeter pass and IR image in Figure 24. The other thermal features of Figure 59 are rather small and do not have the convincing expression in  $SSH$ . The stronger structure 6, however, has a corresponding altimeter signal greater than 5 cm.

#### 4.3.2 CTD Cross Section

Figure 58 shows the location of CTD casts. This section was taken in October 1988. Positions of CTDs were chosen along descending altimeter ground track D21. Altimeter data were not obtained because the GEOSAT malfunctioned. The cross section of potential temperature and salinity is displayed in Figure 61. Both variables indicate a very sharp boundary in the frontal area, extending from the surface almost to the bottom of the cross section. The IR image taken 10 days before the CTD measurements is displayed in Figure 62. It indicates that the CTD transect crossed the tongue of warmer water usually present in IR images near  $65^\circ\text{N}$ ,  $10^\circ\text{W}$ . The temperature cross section of Figure 61 indicates its presence as an intrusion of warmer water near CTD station 20. It also indicates that the water

Table 5. Operational chart for surface drifters.

Drifter	No.	Start	End	Days in Operation
F1	8080	14 Oct 88	4 Feb 89	112
F2	8082	14 Oct 88	24 Jan 89	102
F3	8079	15 Oct 88	24 Nov 88	40
F4	8084	6 Nov 88	23 Feb 89	108
F5	8081	15 Nov 88	30 Jan 89	76
F6	8083	16 Nov 88	20 Nov 88	4

present in the tongue is already considerably modified Atlantic water and that it is limited to the layer less than 100 m deep, near the surface.

#### 4.3.3 Surface Drifters

Figure 58 shows the deployment locations of six surface drifters. Table 5 gives the deployment time and the time of transmission termination for each drifter. Drifter F6 transmitted its position for only 4 days and is not discussed in the analysis.

Figure 63 shows the tracks of all drifters constructed from raw data. Their general movement in the southeastern direction is in agreement with the circulation pattern in the Iceland-Færoe Front. The departure of the two northernmost drifters in a northeastern direction is in agreement with the idea of the sea surface tilt being up in the southward and eastward directions, connected with the Iceland-Færoe Front and the Norwegian Atlantic Current. Some of the floats were caught in eddies, and one was caught in the recirculation current around Færoe Island.

Figures 64-68 show the tracks of individual drifters, the north and east component of velocities, and the vector diagram of velocity along the path as a function of year-days. The points on the individual tracks represent the midday position, and every multiple of 10 days is marked by a larger dot and the year-day. Velocities were calculated from the daily positions. The speed of drifters is usually small, but during the time when they are caught in the flow, it may reach 50 cm/s. Drifter F5 (8081) was not tracked for several days and the missing positions and speeds were obtained by linear interpolation.

Several figures compare the results obtained from drifters, IR images, CTD's, and altimeter. Figure 69 presents the composite IR image from 8 and 9 November 1988, with the superimposed tracks of drifters. The yellow parts of the tracks represent the paths of the drifters in the period centered around the reception time of the IR image (from 1 to 16 November). Drifter F1 follows the tongue,

outlined by temperature contrast. The speed is in excess of 20 cm/s. Drifter F2 is caught in a cyclonic eddy, and F3 moves along the northern boundary of the Iceland-Færoe Front with a speed of about 15 cm/s.

Figure 70 shows the IR composite from 29 and 30 December 1988, with the superimposed tracks of drifters. The yellow parts of the tracks represent the path of the drifters in the period centered around the reception time of the IR image (from 22 December to 6 January 1989). Drifter F4 outlines the darker boundary of the Icelandic Current as it turns in the northeastern direction and moves slowly (~3 cm/s) along the weak front toward the Norwegian Atlantic Current. Similarly, the F5 moves in the same direction as F4 but much faster (20 cm/s). There were only a few days when the Argos position of F5 in its northeastward movement was determined, and the tracks are only the linear approximations between the known locations. Clouds and mist preclude identifying the features along the F2 track. F2 moved into the Færoe-Shetland Channel and became caught in the recirculation current, with a speed as high as 60 cm/s.

Figure 71 also presents an IR image, composed of 3 days, and the tracks of drifters. The yellow portion represents the path of the drifters during the period centered around the reception time of the IR image (from 8 January to 24 January 1989). Drifters F4 and F5 move eastward, as discussed in Figure 70. Drifter F2, caught in a cyclonic eddy about 30 km in diameter, drifted southward with the eddy (5-6 cm/s). The IR image is too cloudy to identify the features in its southeastern area.

Figure 72 shows tracks of drifters overlaid on the dynamic height topography obtained from CTD's. The colored portion of the tracks (from 5 to 30 November) overlays the period of CTD measurements. CTD measurements were taken 10-21 November 1988 by T. Hopkins of SACLANTCEN (T. Hopkins, 1988). Drifter F1 moves 20 cm/s around the tongue depicted in dynamic height. F2 was caught in a cyclonic eddy, which is not resolved by CTD's. F3 moved 15 cm/s along the northern boundary of the front, and F5 was stagnant during that period. There is general agreement between the dynamic topography and the motion of drifters during the period of CTD measurements. The noncoincident parts of drifters' tracks indicate frontal displacements at other times.

Figure 73 presents the overlay of the three descending altimeter tracks. The  $SSH_M$  is displayed, along with the dynamic topography obtained from

the CTD's (discussed in the description of Fig. 72). Only a few descending passes were made from October 1988 to February 1989 due to improper functioning of the GEOSAT altimeter. The altimeter set, which overlays the dynamic topography, was more than 3 weeks delayed. The front shifted during that period, but the main features may persist. The altimeter data indicate the shift of the tongue to the east (track D27) of about 50 km, as also visible in IR images from December and January (Figs. 70 and 71). The same interpretation is valid for the trough south of the main front. The altimeter signal along track D15 shows a mild sloping in the area of the Icelandic Current, and an indication of a strong flow of Atlantic water as a continuation of a meander detected by CTD data (also visible in the previous IR images). Data along track D10 indicate the large slope north of the Færoe Islands and the presence of the warm eddy north of it (also seen in IR images). The amplitude of the altimeter signal is about 1.5 times larger than the values of dynamic topography. It would indicate the presence of a barotropic component, as also derived from the Harvard numerical model for this area (Robinson et al., 1988). The spline function was used to smooth the tidal data before applying the tidal correction to the altimeter, but the tidal error was still present and caused uncertainty in interpretation. An additional difficulty in interpretation of altimeter data in this area originated in the presence of the time-independent component related to the front.

The same set of altimeter data is overlaid on the drifter tracks in Figure 74. The red portion of tracks corresponds to the period (from 5 to 25 December 1988) that overlapped the time of the altimeter passes. F2 moved around the warm eddy, as indicated by altimetry on track D10.

The same set of altimeter data is superimposed on an IR image from 29 and 30 December in Figure 75. The IR image was taken 10 days later than the altimetry, and some features are shifted in the IR image relative to the altimeter signal. Namely, the warm eddy to the right in Figure 75 moved southeastward relative to the position determined by the altimeter. The large meander, displayed in earlier figures, moved eastward (in Fig. 75 covered by clouds), but altimeter data along the middle track depict its position well.

Figure 76 shows the dynamic height topography superimposed on the IR image. This IR image was taken in the beginning of the CTD measurements

from 8 to 9 November. It is the smooth version of IR variations. Spatial distribution of CTD's does not resolve the smaller (<40 km) variation along the front that was detected by IR images (namely, the anticyclonic eddy near 64°N, 7°W), and perhaps meander should be sharper in its southwestern part. Also, the cyclonic eddy present west of the Færoe Islands and detected by drifter F2 and by the altimeter was not resolved by the CTD measurements.

Another attempt to use the altimeter in detection of the Iceland-Færoe Front is presented in Figure 77. The dynamic heights (reference level 400 m) were computed from AXBT data collected on 23 April 1988 (Boyd, 1988) assuming the known temperature-salinity relationship. The separation between AXBT drops was about 40 km. Altimeter residuals, obtained as differences from the mean, were collected on 13, 16, 19, 22, 24, and 27 April 1988 along ground tracks D27, D33, D04, D10, D15, and D21, respectively.  $SSH_M$ 's are plotted along the tracks in Figure 77. The spatial resolution of the AXBT survey is coarse and the resulting front is spread. Except for track D15, all others pass over the area several days earlier or later. The  $SSH$  signals vary, but only the sloping part of  $SSH_M$  (between 64.5°N and 64°N) on D27 and on D10 (between 63.5°N to 63.2°N) can be identified with the front and D27 (near 63.5°N) with the cold eddy. The tidal error south of 64°N causes spurious signals in  $SSH$ 's and makes the interpretation uncertain.

#### 4.4 Surface Variability from Altimeter Data

Variance for each point on the tracks was computed from repeated passes covering 1 year. Because the late fall and winter  $SSH_M$ 's are missing (malfunctioning of GEOSAT altimeter), 14–15 repeat tracks were used. Figures 78 and 79 show the variability of the sea surface in meters, obtained as a square root of mean variance, for ascending and descending tracks, respectively.

Ascending tracks show the large variability along the Iceland-Færoe Front, the Færoe-Shetland Channel, and in an area corresponding to the location of the Norwegian Atlantic Current and the Norwegian Coastal Current. The large variance near the Færoe-Shetland Islands and near Iceland is caused partly by tidal error in the data. Data in ascending tracks started about 50–100 km from the Norwegian Coast. Due to a problem with the automatic tracker in GEOSAT, they missed the main part of the

Norwegian Coastal Current, which is rich in energetic mesoscale eddies. This lapse accounts for the low variability near the Norwegian Coast. Variability obtained from the descending passes in Figure 79 shows a similar result—an active Iceland-Færoe Front area and part of the Norwegian Atlantic Current in the north and a quiet Norwegian Sea. Again, as with the ascending passes, the large variability along

the Iceland-Færoe Front is partly contaminated by tidal error. It is interesting to notice the southern extension of the low variability field near Iceland (near 65°N) and the large variability around 64°N, 10°W. These features correspond to areas where IR images also indicated smaller and greater activity, respectively. The quietest area, with the smallest variability, is located northeast of Iceland.

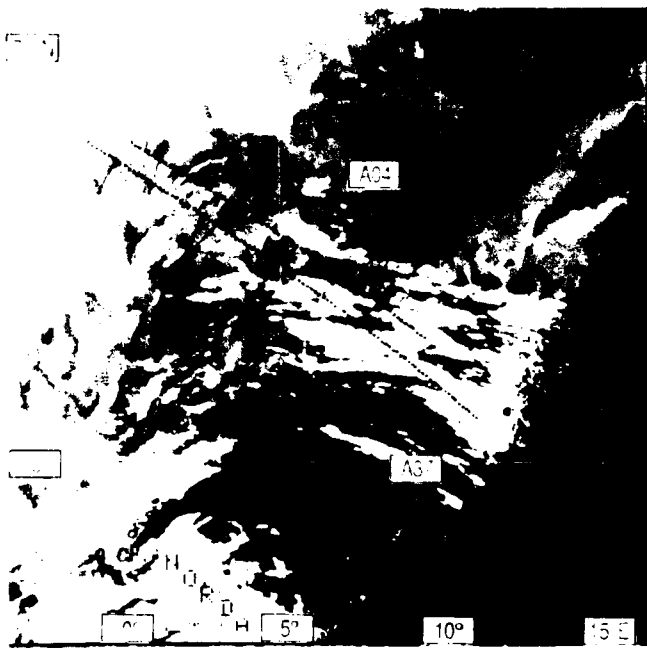


Figure 20. Altimeter  $SSH_M$  residuals overlaid on IR image from 28 May 1987.  $SSH_M$ : A37-Rev 11522, 27 May 1987, A04-Rev 11565, 30 May 1987. Altimeter tracks cross the Norwegian Atlantic Current. Amplitude variation of  $SSH_M$  is less than  $\pm 10$  cm.

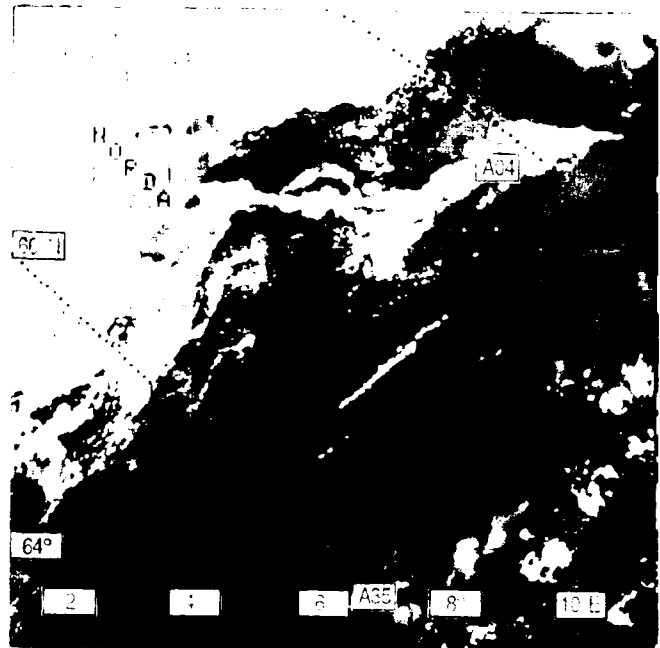


Figure 22.  $SSH_M$  residuals overlaid on IR image from 27 May 1987.  $SSH_M$ : A35-Rev 11508, 26 May 87, A04-Rev 11565, 30 May 1987. Altimeter tracks cross the Norwegian Atlantic Current.

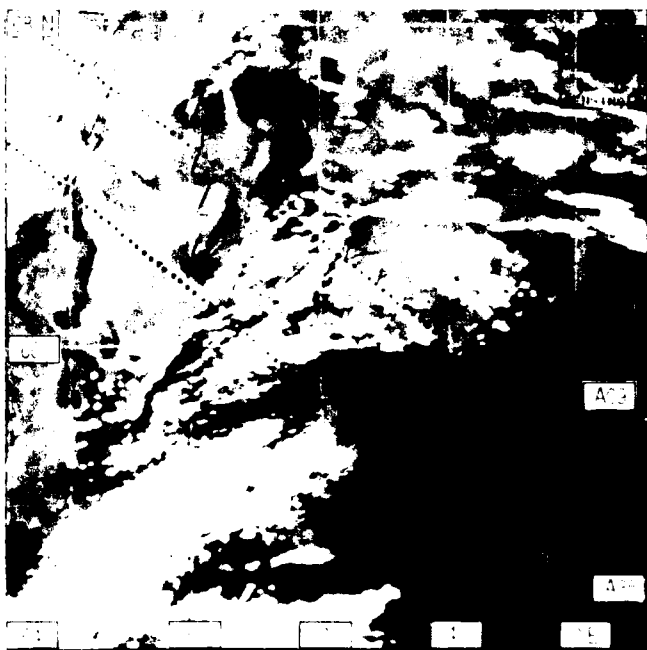


Figure 21.  $SSH_M$  residuals overlaid on IR image from 28 May 1987.  $SSH_M$ : A09 Rev 11594, 1 June 1987, A35-Rev 11508, 26 May 87. Altimeter tracks cross the Norwegian Atlantic Current. Track A35 represents filtered data.

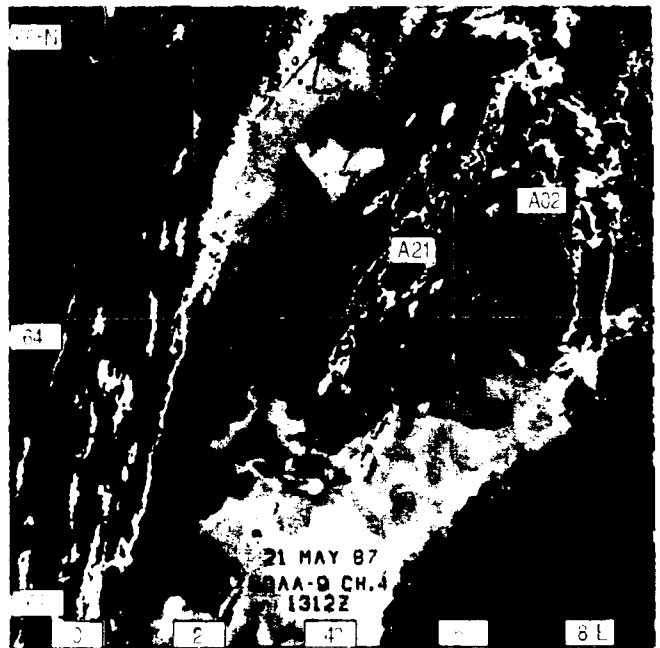


Figure 23.  $SSH$  residuals overlaid on IR image from 21 May 1987.  $SSH_C$ : A21-Rev 11422, 20 May 1987.  $SSH_M$ : A02-Rev 11551, 29 May 1987. Altimeter tracks cross the Norwegian Atlantic Current.  $SSH_C$  in A21 contains also the steady component of current (from CTD's).

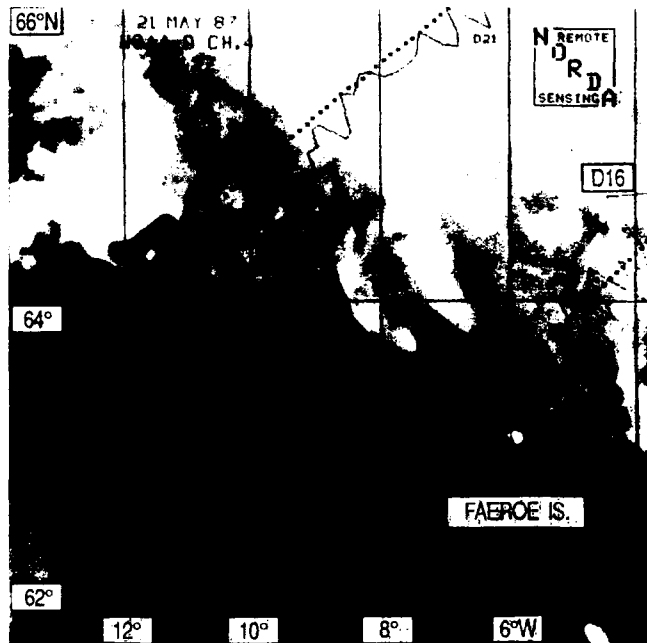


Figure 24.  $SSH_M$  residuals overlaid on IR image from 21 May 1987.  $SSH_M$ : D21-Rev 11433, 21 May 1987. D16-Rev 11404, 19 May 1987. Altimeter tracks cross the Iceland-Færoe Front.

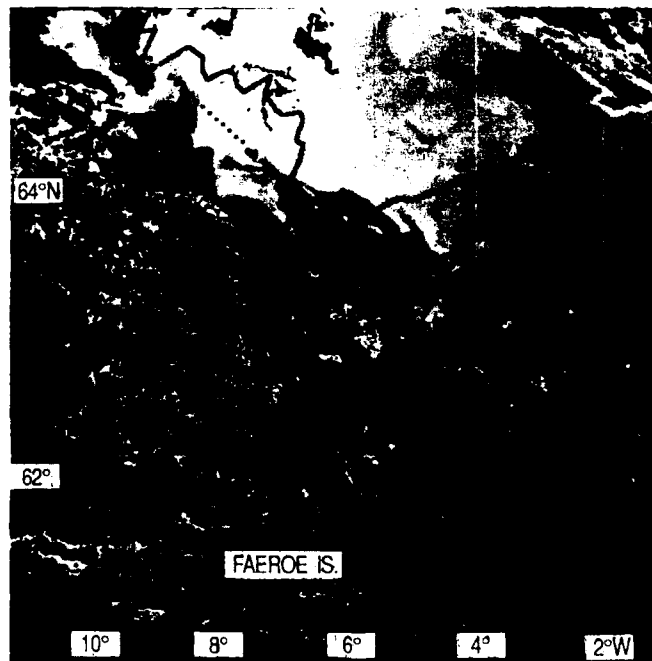


Figure 25.  $SSH_M$  residuals overlaid on IR image from 29 May 1987.  $SSH_M$ : A1 2-Rev 11609, 2 June 1987. Altimeter track passes quasi-parallel to Iceland-Færoe frontal zone.

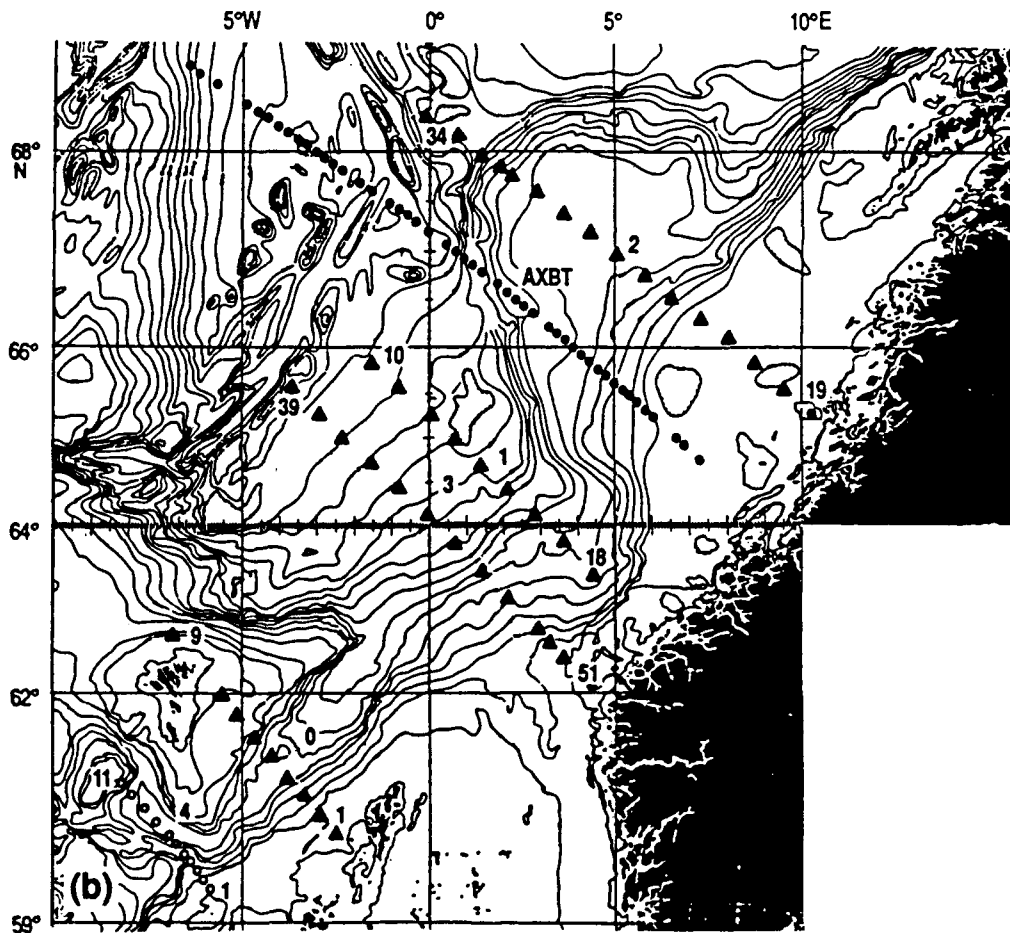
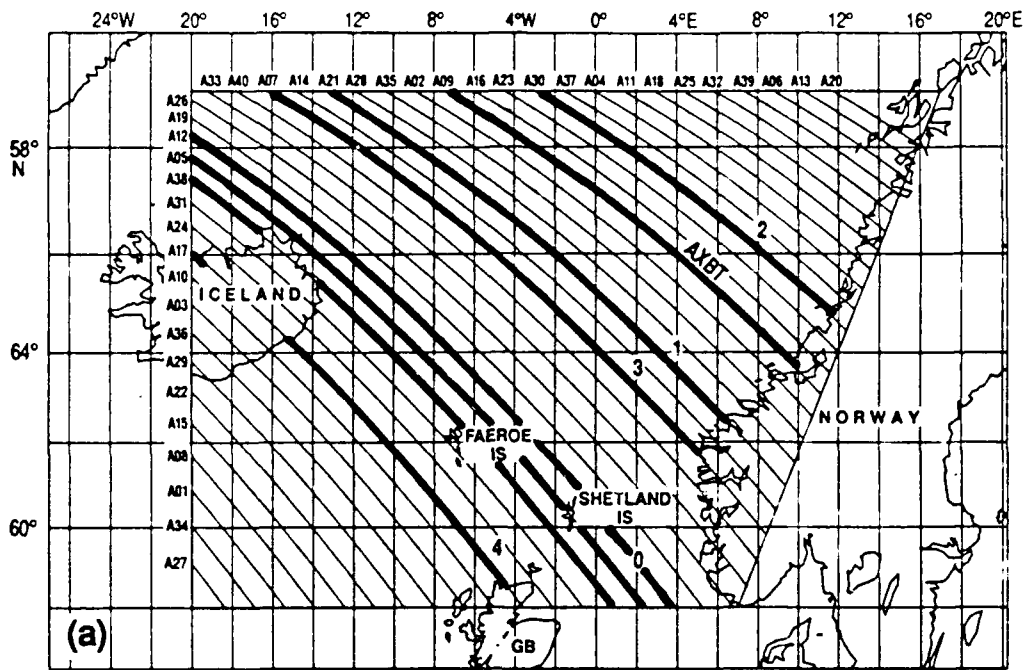


Figure 26. Schematic chart of sections across Atlantic inflow and Atlantic Norwegian Current. (a) Altimetry ground tracks along which altimetric data were collected simultaneously with in situ measurements. (b) Bathymetric chart with positions of AXBT's and CTD casts. Numbers mark individual cross sections. AXBT identifies the position of AXBT cross section. Depth is in meters.

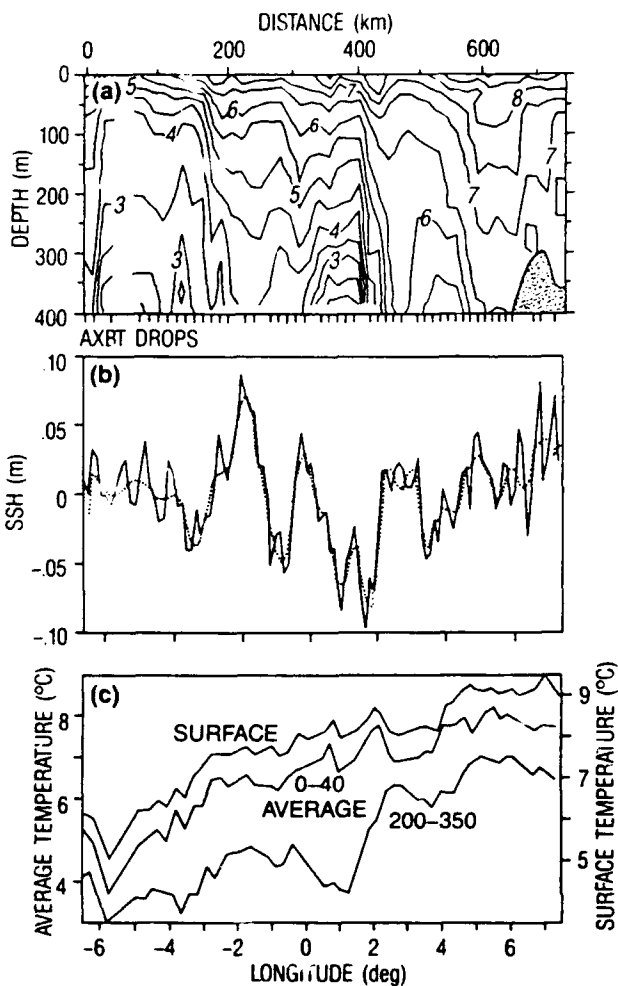


Figure 27. AXBT cross section and  $SSH_M$ . (a) Temperature cross section from AXBT along ground track A09, taken on 1 June 1987. (b) Altimeter residuals taken simultaneously with AXBT data. The dotted line is the Fourier filtered version of  $SSH_M$  (cutoff about 30 km). (c) Curves for the surface temperature and the averaged temperatures for the columns of water between 0 to 40 m and 200 to 350 m, respectively.

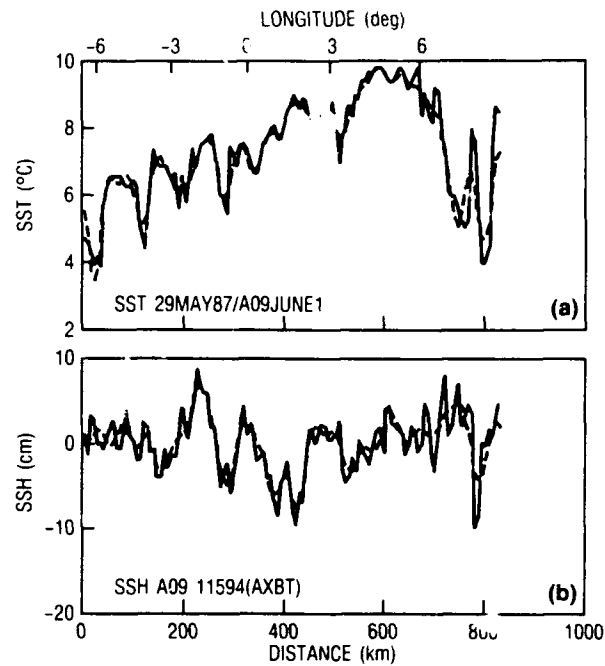


Figure 28. SST obtained from IR data and  $SSH_M$  along the same ground track. (a) SST obtained 29 May 1987 and (b)  $SSH_M$  collected 1 June 1987. The dotted line is the Fourier filtered version of  $SSH_M$ .

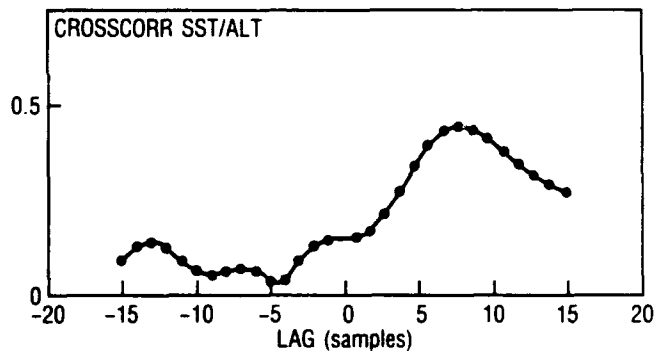


Figure 29. Cross correlation between  $SSH_M$  and SST data. Units of lag are given by altimeter sampling (1-second data, about 6.50 km). Maximum for the lag = 8 means the shift of altimeter data relative to SST, 8 samples to the left. (in Fig. 28).

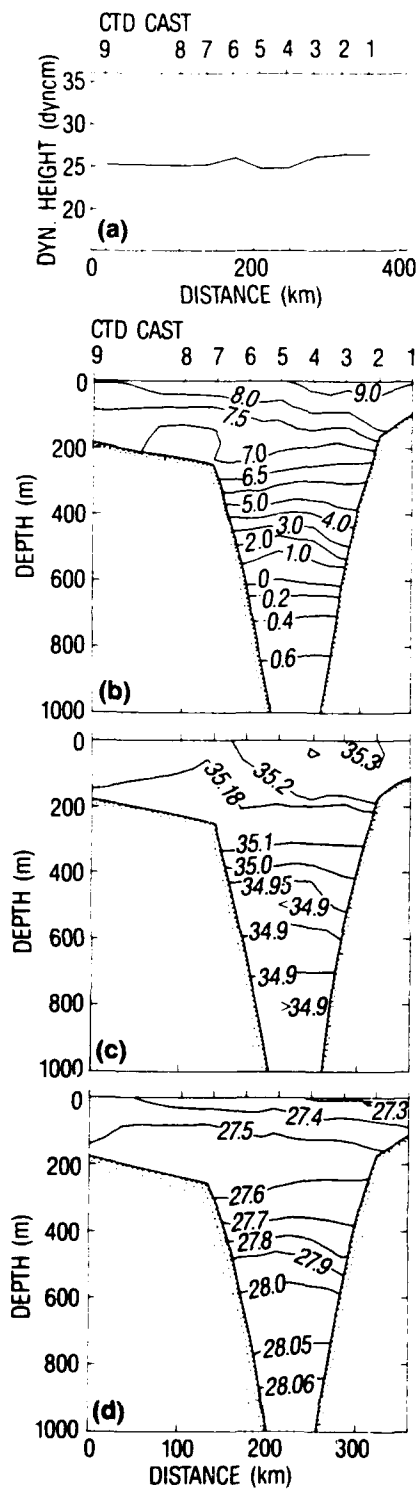


Figure 30. Cross section 0, across Færoe-Shetland Channel. Variables are (a) dynamic height, (b) potential temperature, (c) salinity, and (d) potential sigma. Section taken 3-4 June 1987.

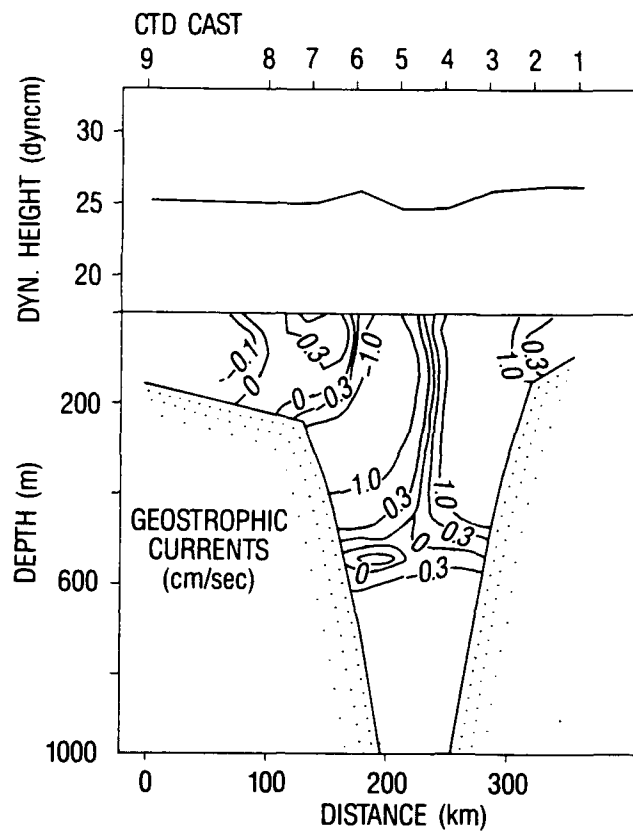


Figure 31. Cross section 0, across Færoe-Shetland Channel. Variables are dynamic height and geostrophic current, respectively. Positive velocity indicate northward direction.

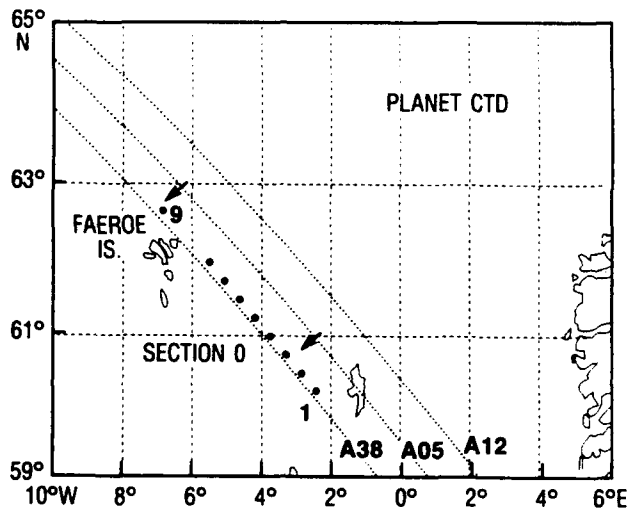


Figure 32. Position of A05 ground track and CTD cross section 0. Dots indicate positions of CTD casts.

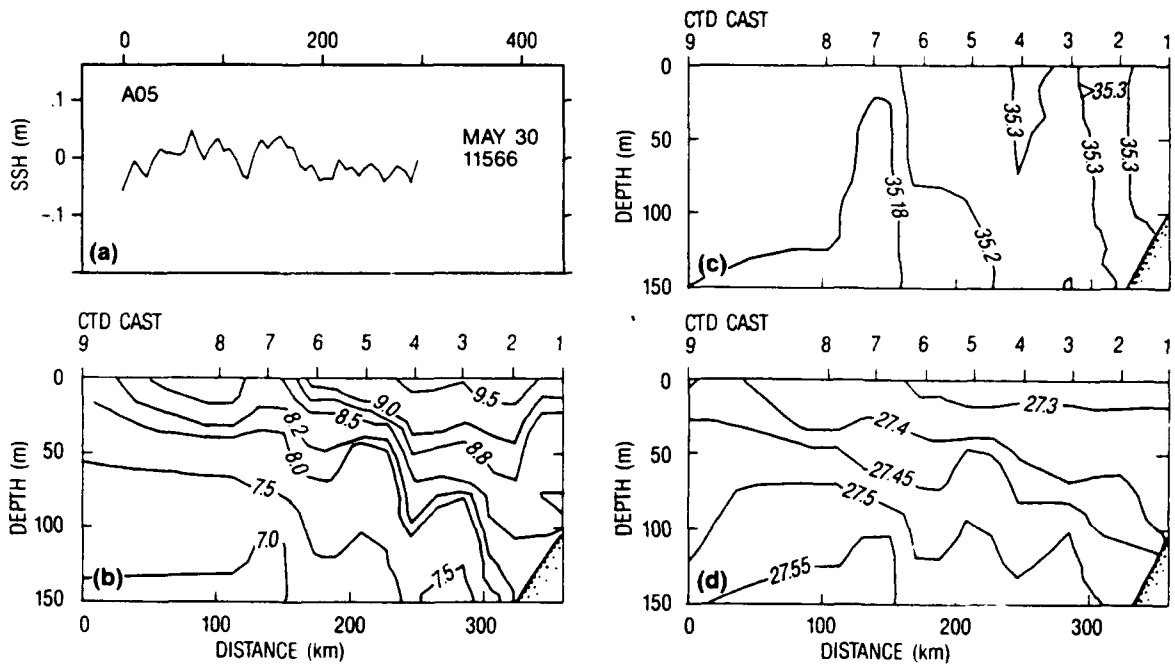


Figure 33. Cross section 0, surface layer (0–150 m) across Færoe-Shetland Channel. Variables are (a)  $SSH_M$ , (b) potential temperature, (c) salinity, and (d) potential sigma, respectively.  $SSH_M$  was taken along ground track A05 on 30 May 87. The ground track was parallel to cross section 0, but separated about 40 km north of it (see Fig. 32).

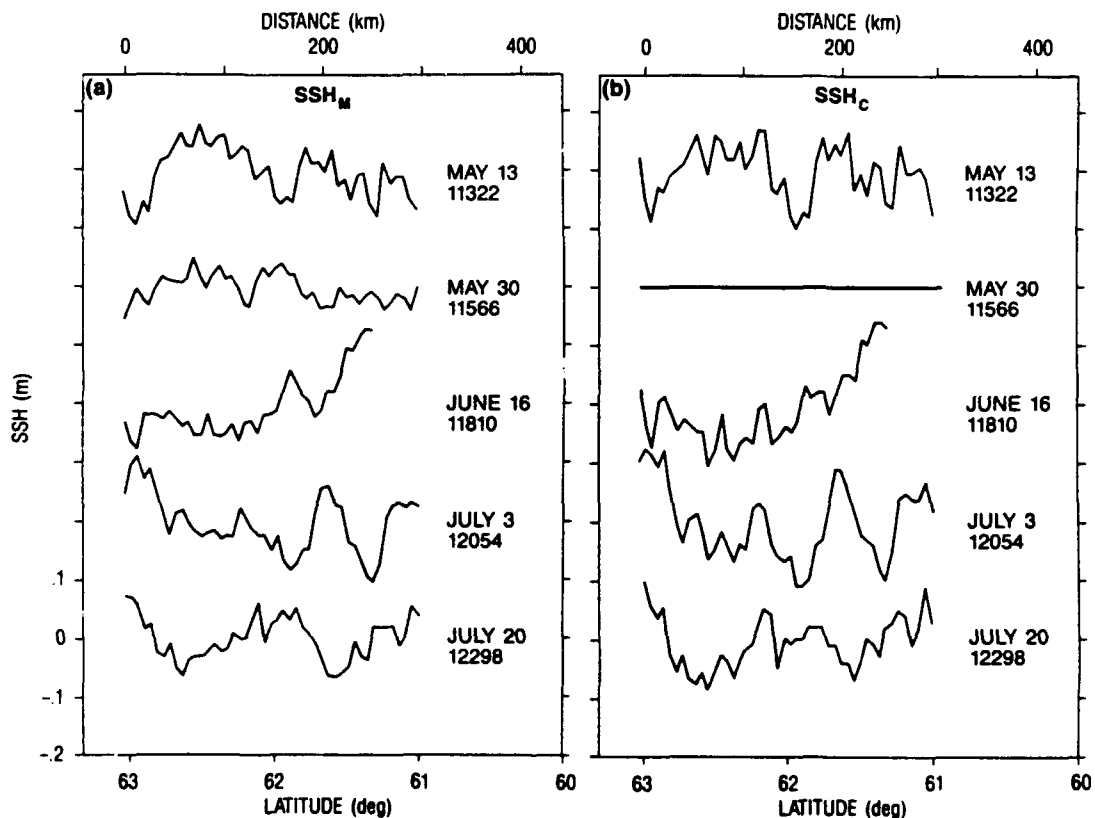


Figure 34. SSH residuals for five paths along the ground track A05. (a)  $SSH_M$  residuals created as a difference between the mean and particular pass as listed. The mean was created from five passes. (b)  $SSH_C$  residuals obtained as a difference between the May 30 (REV 11566) pass and particular pass as listed in figure. The straight line on May 30 represents dynamic height measurement obtained from CTD data.

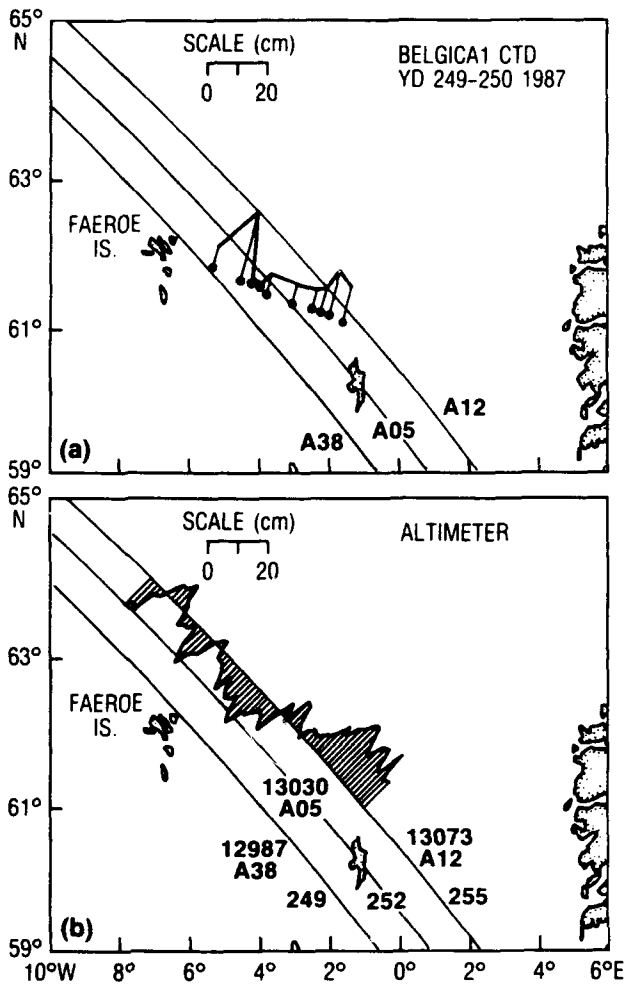


Figure 35. Dynamic height obtained from CTD across Færoe-Shetland Channel and  $SSH_M$ . (a) CTD data (from SACLANT) taken 6-7 September 1987. (b)  $SSH_M$  data, along A12 from 12 September 1987.

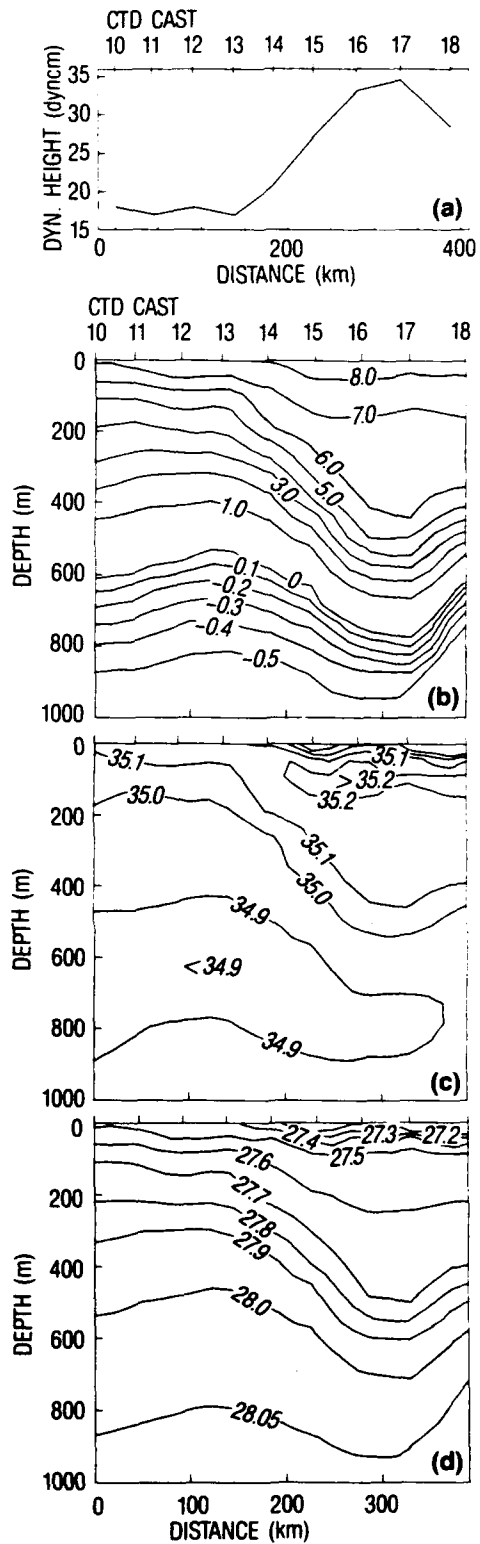


Figure 36. Cross section 1, across Norwegian Atlantic Current. Variables are (a) surface dynamic height, (b) potential temperature, (c) salinity, and (d) potential sigma, respectively. Section was taken 6-7 June 1987.

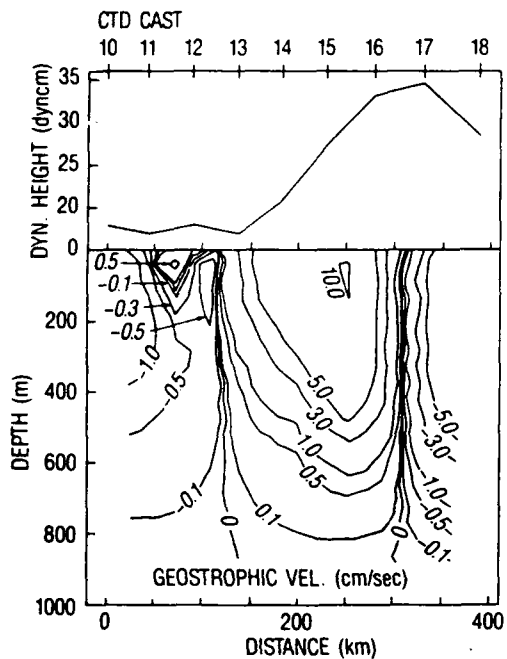


Figure 37. Cross section 1, across Norwegian Atlantic Current. Variables are surface dynamic height and geostrophic velocity. Velocity is positive in the northward direction.

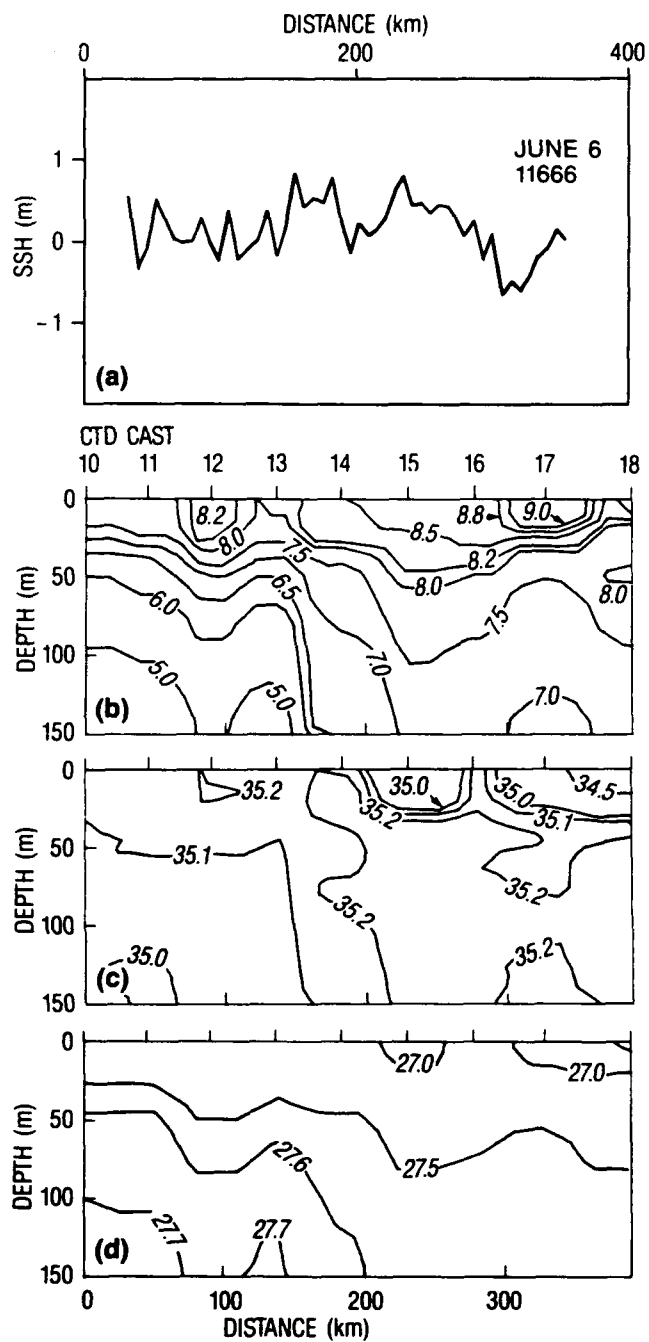


Figure 38. Cross section 1, surface layer (0-150 m) across Norwegian Atlantic Current. Variables are (a)  $SSH_M$ , (b) potential temperature, (c) salinity, and (d) potential sigma.  $SSH_M$  was taken along the ground track A21 on 6-7 June 1987.

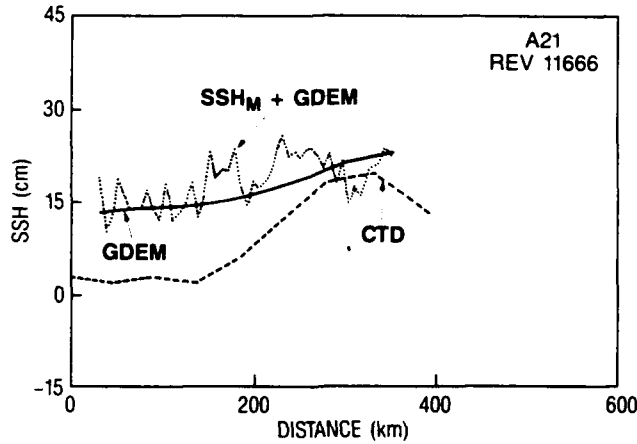


Figure 39. Comparison between the surface dynamic height obtained from CTD's, dynamic height computed from GDEM data and the "absolute" sea surface variation obtained by adding  $SSH_M$  and GDEM dynamic height. GDEM data correspond to the summer period.

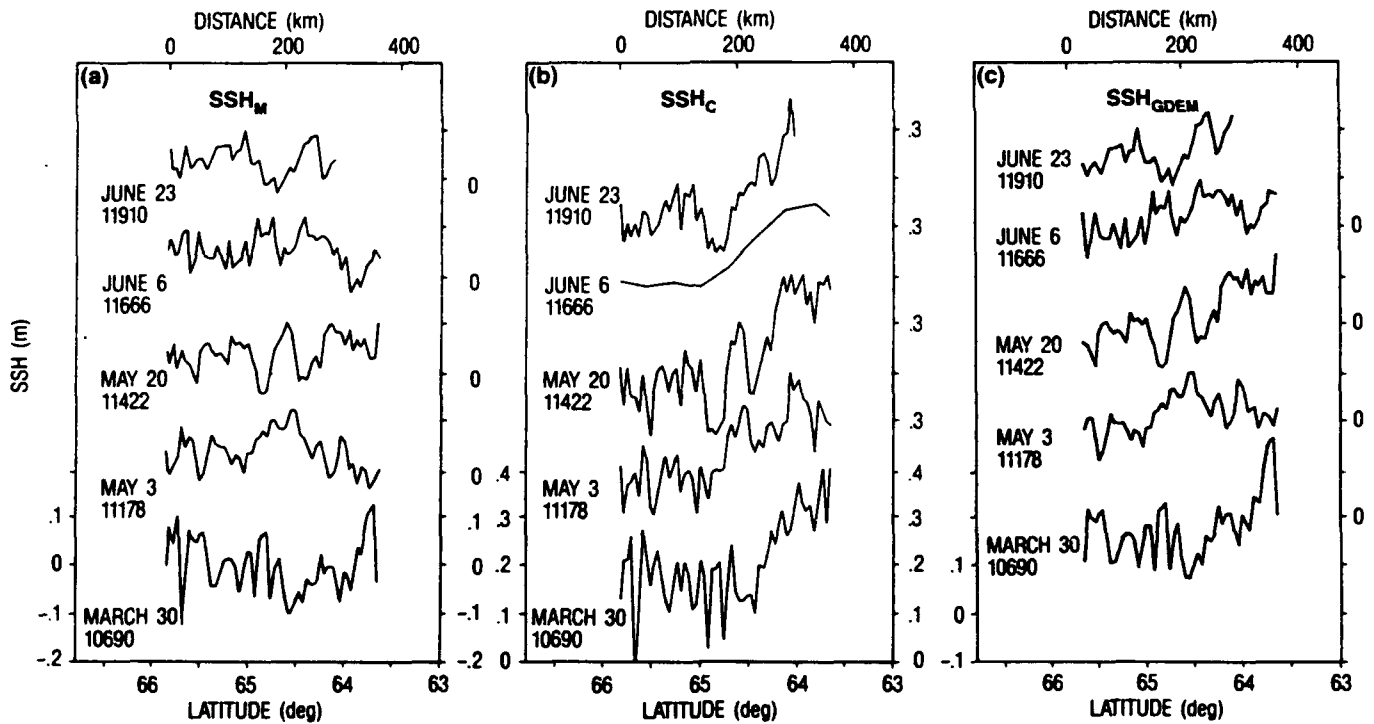


Figure 40. SSH residuals for several adjacent passes along ground track A21. (a)  $SSH_M$  residuals. (b) Corresponding  $SSH_C$  residuals, for which the geoid estimate was obtained from the 6 June altimeter data and the CTD dynamic height. (c)  $SSH_{GDEM}$  for the same data set.

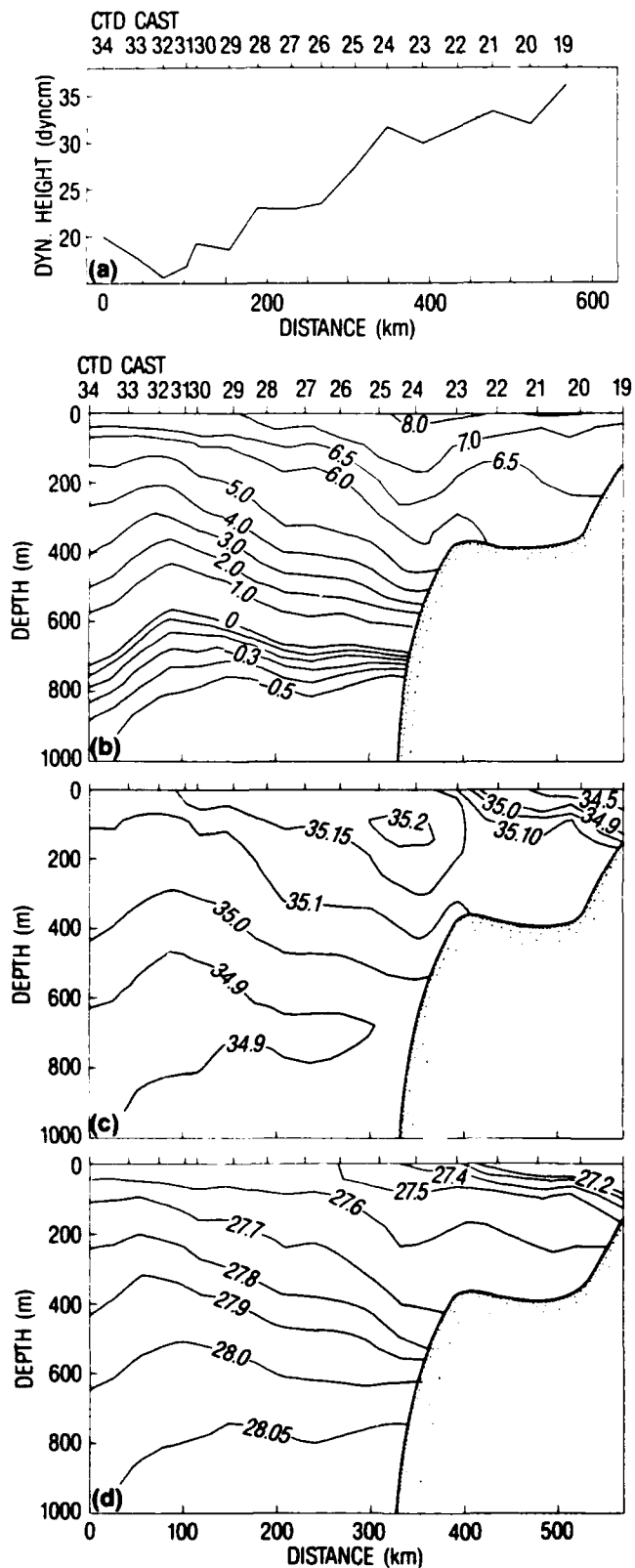


Figure 41. Cross section 2, across Norwegian Atlantic Current. Variables are (a) surface dynamic height, (b) potential temperature, (c) salinity, and (d) potential sigma. Section was taken 10–11 June 1987.

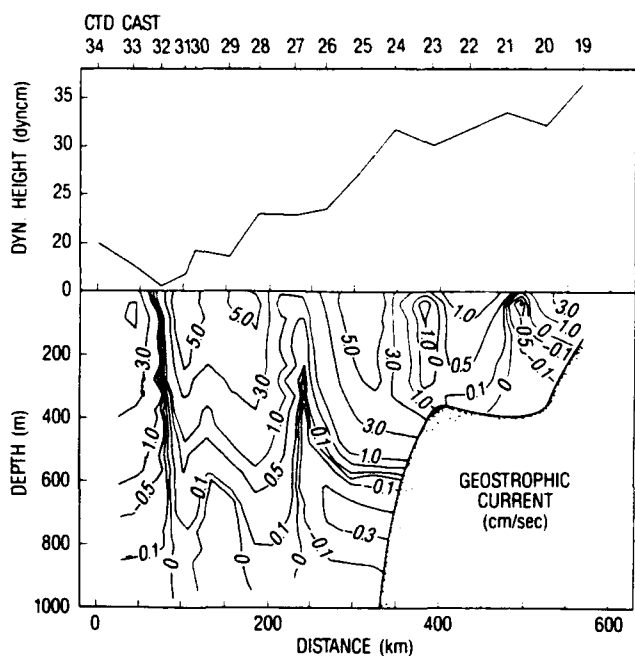


Figure 42. Cross section 2, across Norwegian Atlantic Current. Variables are surface dynamic height and geostrophic velocity. Velocity is positive in the northward direction.

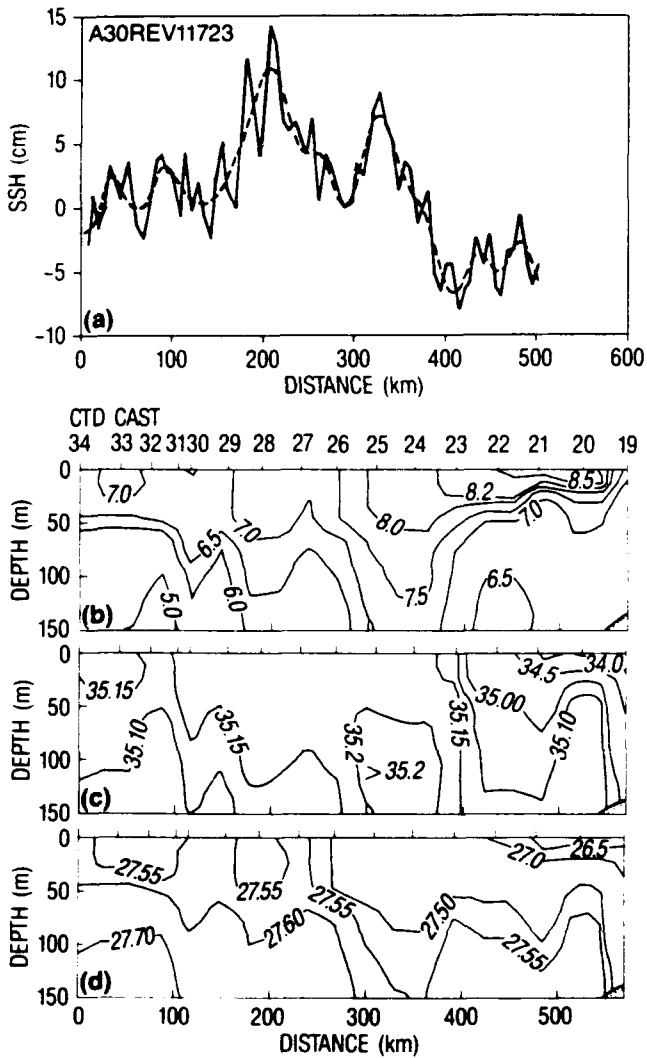


Figure 43. Cross section 2, surface layer (0–150 m) across Norwegian Atlantic Current. Variables are (a) SSH<sub>M</sub>, (b) potential temperature, (c) salinity, and (d) potential sigma. SSH<sub>M</sub> was taken along the ground track A30 on 10 June 1987.

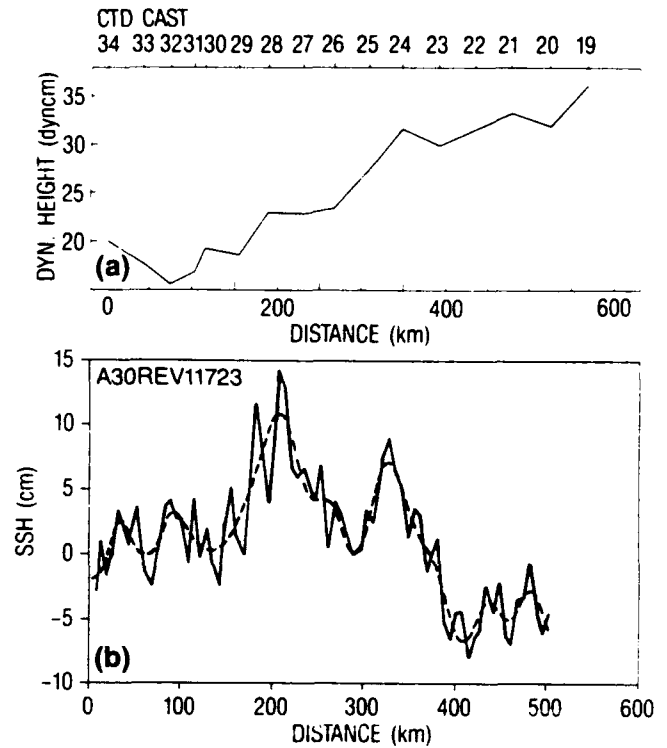


Figure 44. (a) Dynamic height obtained from CTD cross section 2 and (b) simultaneous SSH<sub>M</sub> along A30 coincident with the cross section 2. (Dashed line is the filtered version).

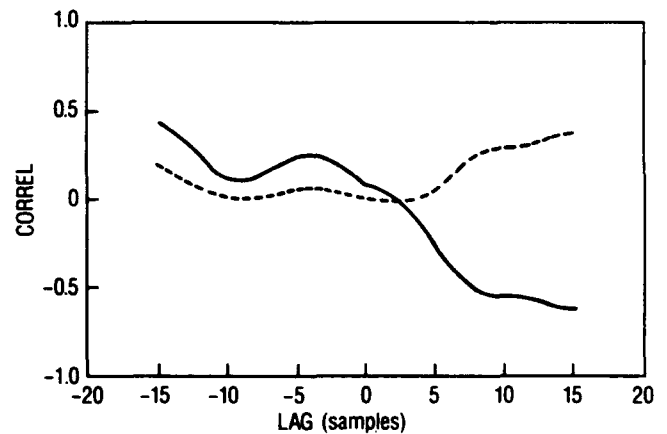


Figure 45. Cross correlation between the filtered version of SSH<sub>M</sub> and CTD dynamic height along section 2. Units of lag are given by altimeter sampling (1-second data, about 6.5 km). Positive lag signifies advancement of altimeter data. Dots represent the square of cross correlation.

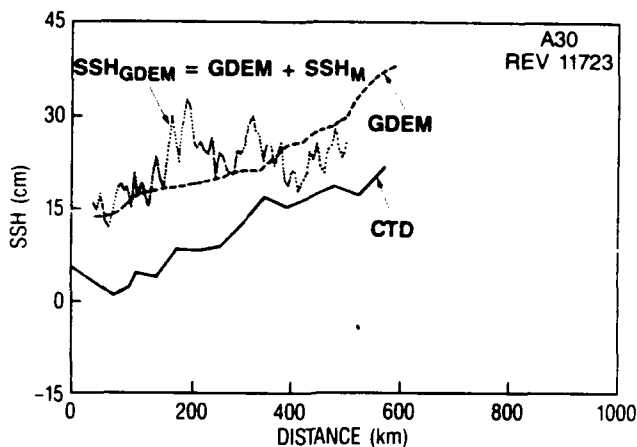


Figure 46. Comparison between the surface dynamic height obtained from CTD's, dynamic height computed from GDEM data and the absolute sea surface variation obtained by adding  $SSH_M$  and GDEM dynamic height. GDEM data correspond to the summer period.

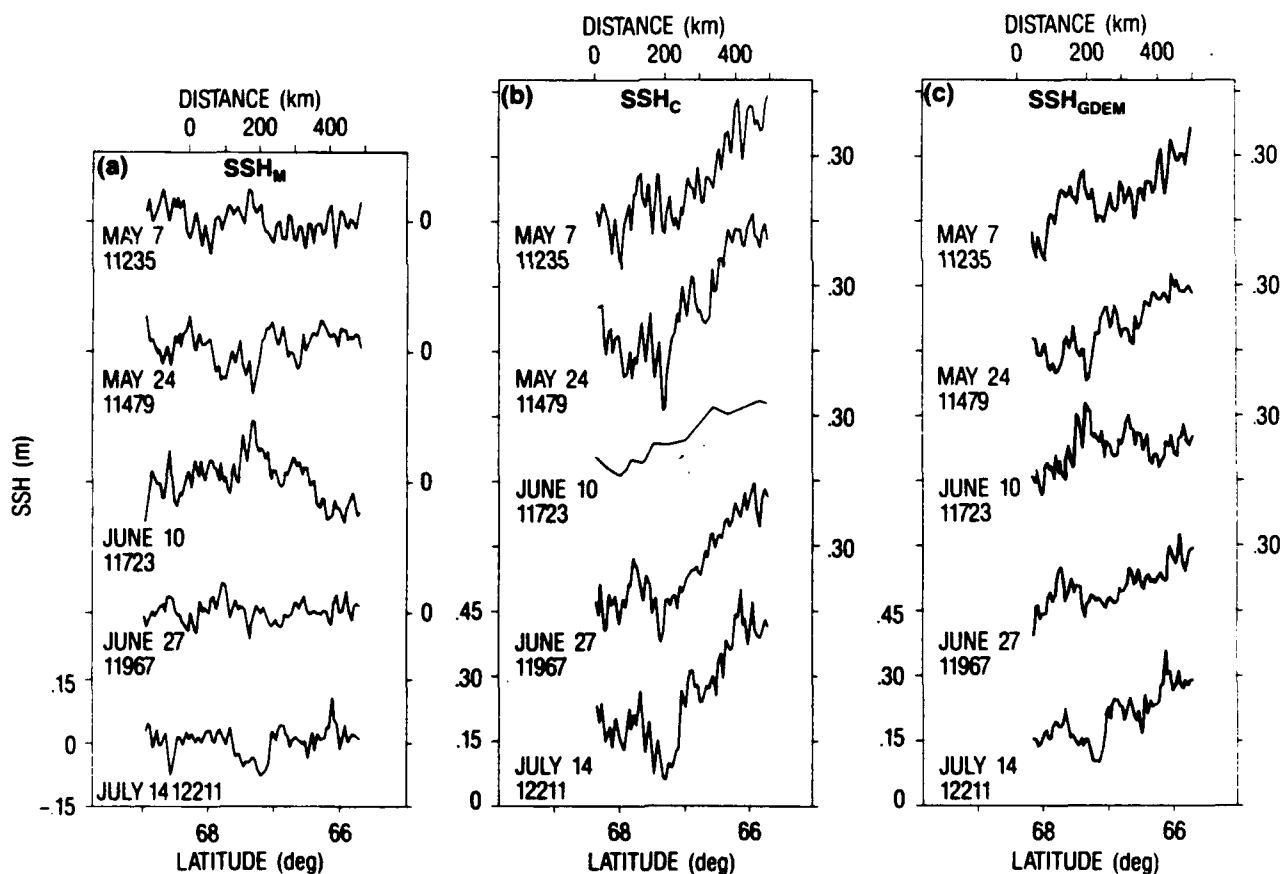


Figure 47.  $SSH_M$  residuals for several adjacent passes along the ground track A30. (a)  $SSH_C$  residuals. (b) Corresponding  $SSH_C$  residuals for which the geoid estimate was obtained from the 10 June altimeter data and the CTD-dynamic height. (c)  $SSH_{GDEM}$  for the same data set.

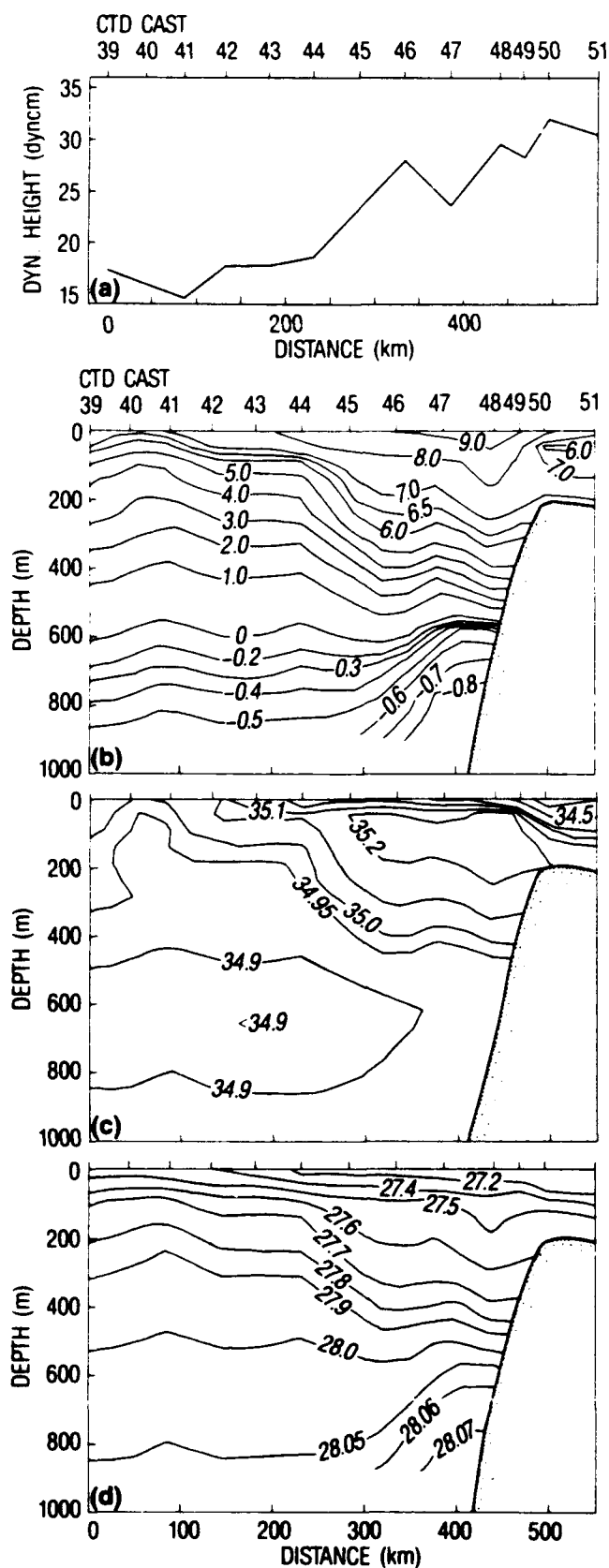


Figure 48. Cross section 3, across Norwegian Atlantic Current. Variables are (a) surface dynamic height, (b) potential temperature, (c) salinity, and (d) potential sigma. Section was taken 16-17 June 1987.

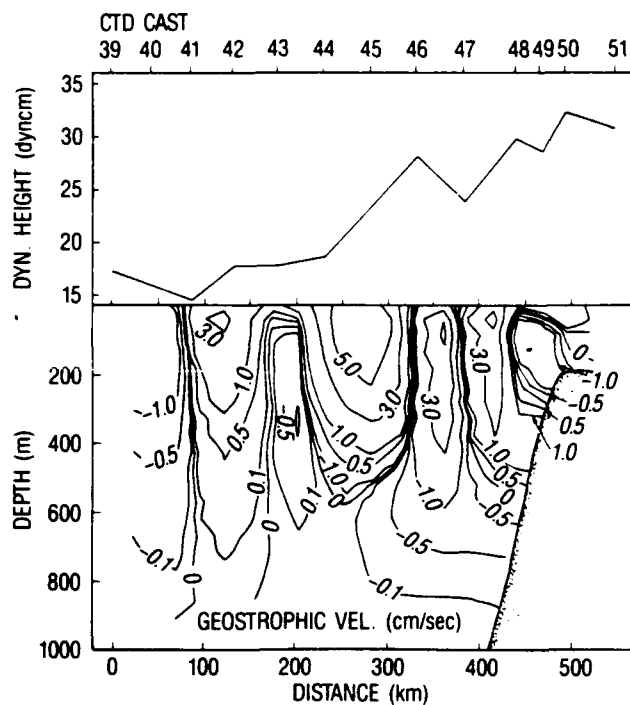


Figure 49. Cross section 3, across Norwegian Atlantic Current. Variables are surface dynamic height and geostrophic velocity. Velocity is positive in the northward direction.

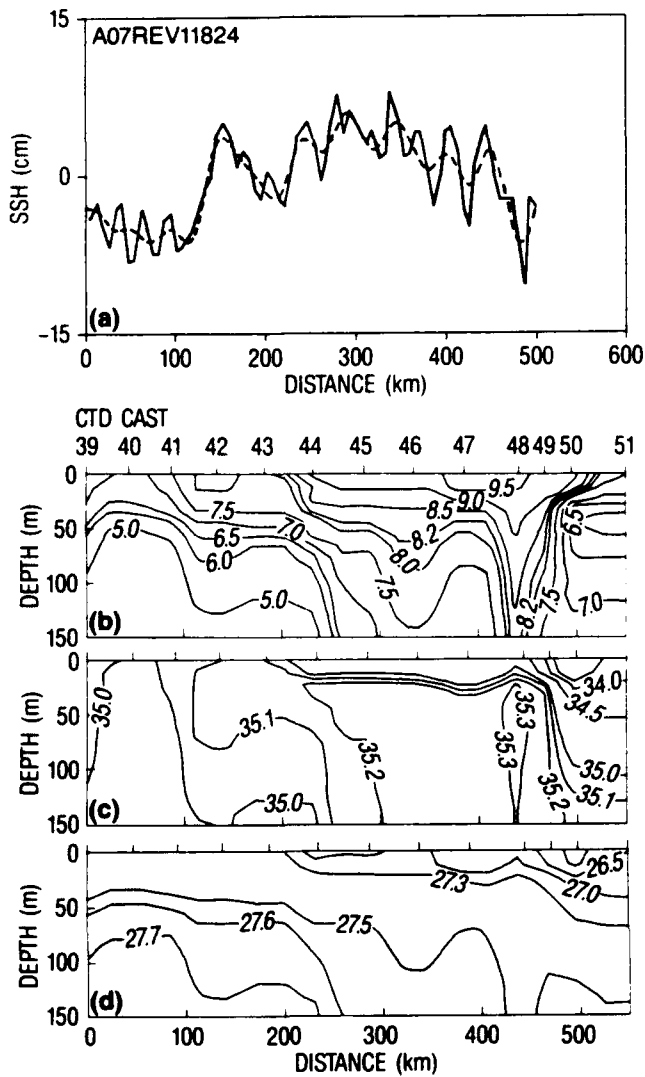


Figure 50. Cross section 3, surface layer (0–150 m) across Norwegian Atlantic Current. Variables are (a)  $SSH_M$ , (b) potential temperature, (c) salinity, and (d) potential sigma.  $SSH_M$  was taken along the ground track A07 on 17 June 1987.

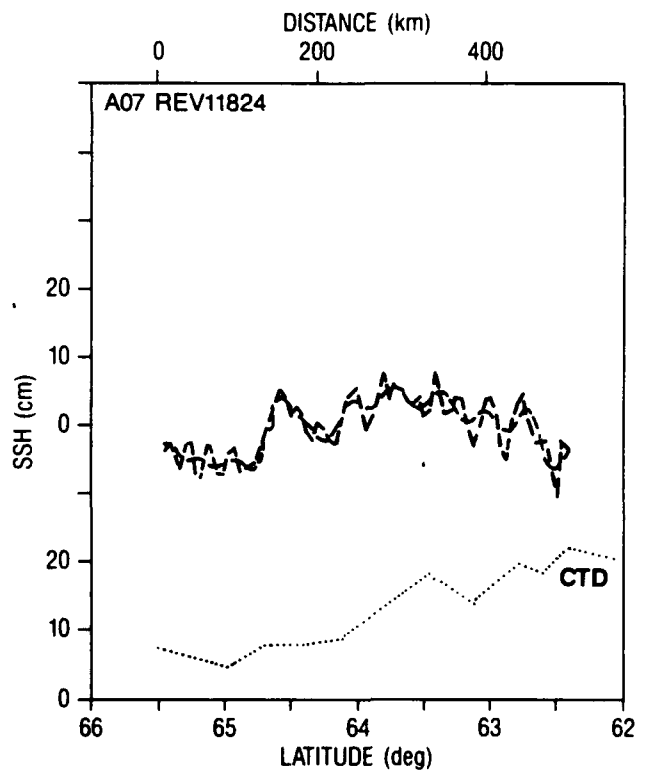


Figure 51.  $SSH_M$  along the track A07 and dynamic height obtained from CTD cross-section 3, simultaneously with the altimeter data.

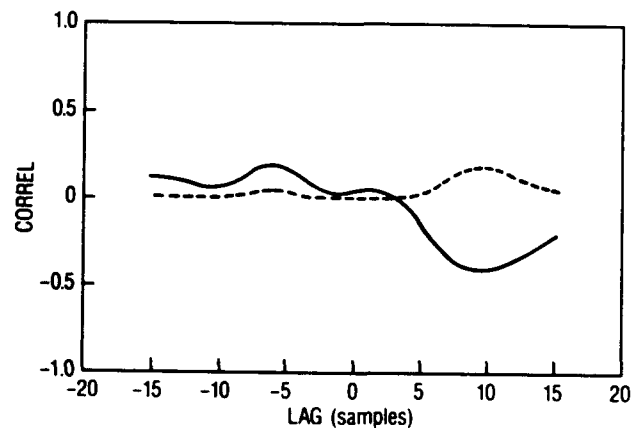


Figure 52. Cross correlation between the filtered version of  $SSH_M$  and CTD dynamic height along section 3. Units of lag are given by altimeter sampling (1-second data about 6.5 km). Positive lag signifies advancement of altimeter data. Dots represent the square of cross correlation.

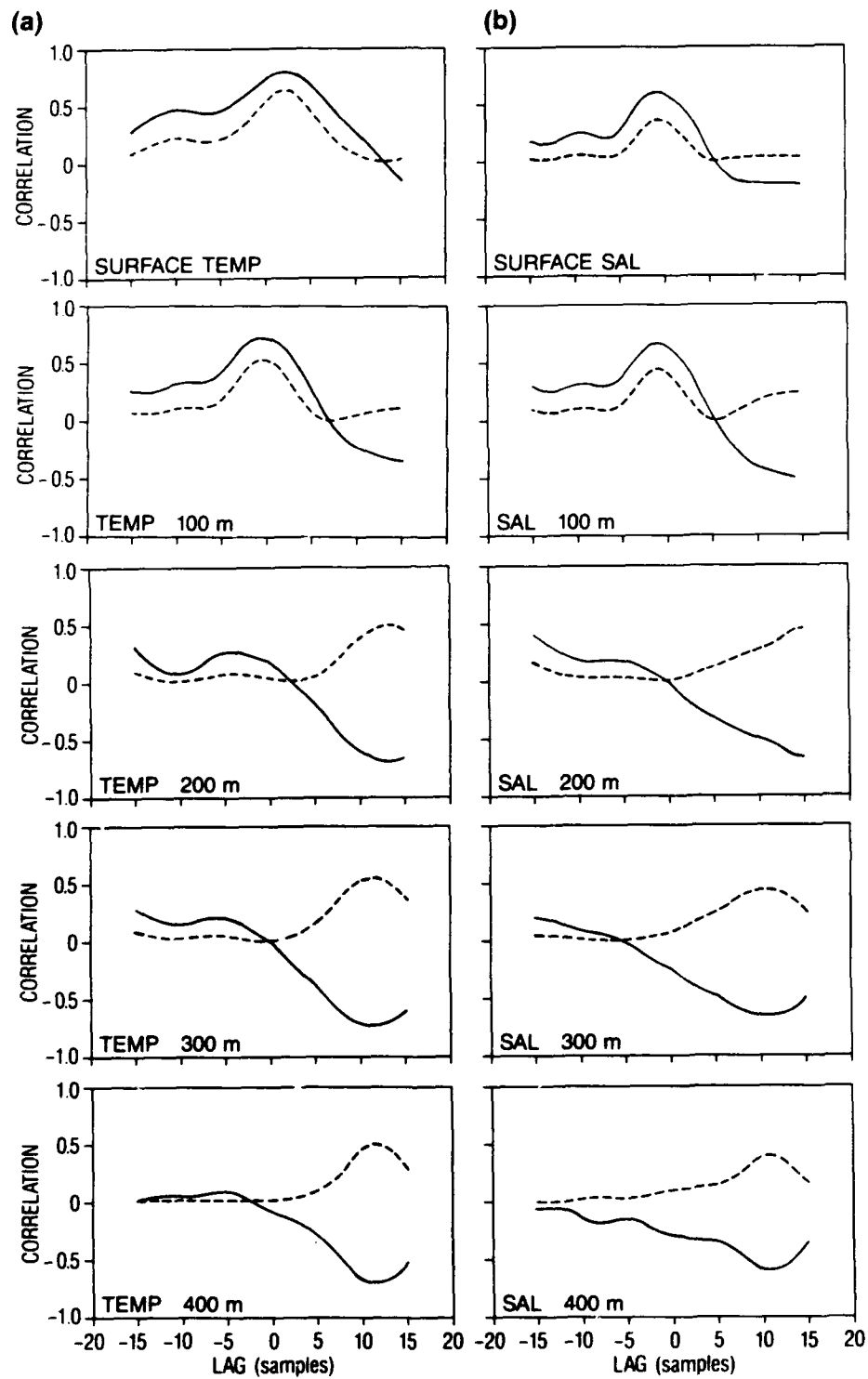
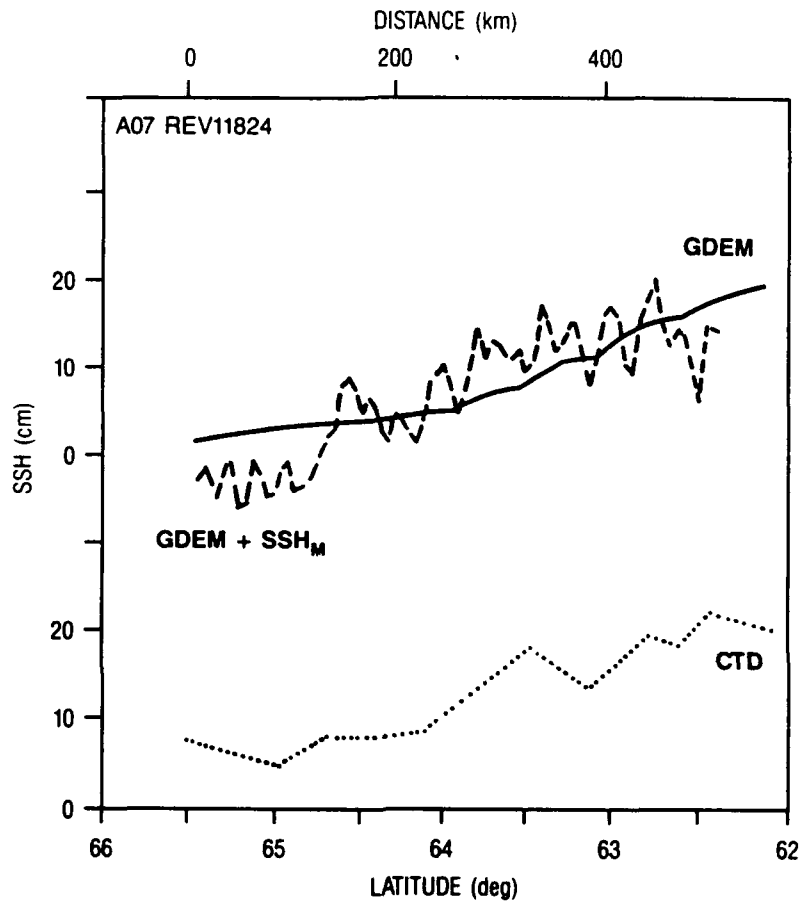


Figure 53. Cross correlations between the filtered version of  $SSH_M$  with potential (a) temperature and (b) salinity in various depths along the CTD cross section 3. Units of lag are given by altimeter sampling (1-second data, about 6.5 km). Positive lag signifies advancement of altimeter data. Dots represent the square of cross correlation.



*Figure 54. Comparison between the surface dynamic height obtained from CTD's. Dynamic height computed from GDEM data and the absolute sea surface variation obtained by adding  $SSH_M$  and GDEM dynamic height. GDEM data correspond to the summer period.*

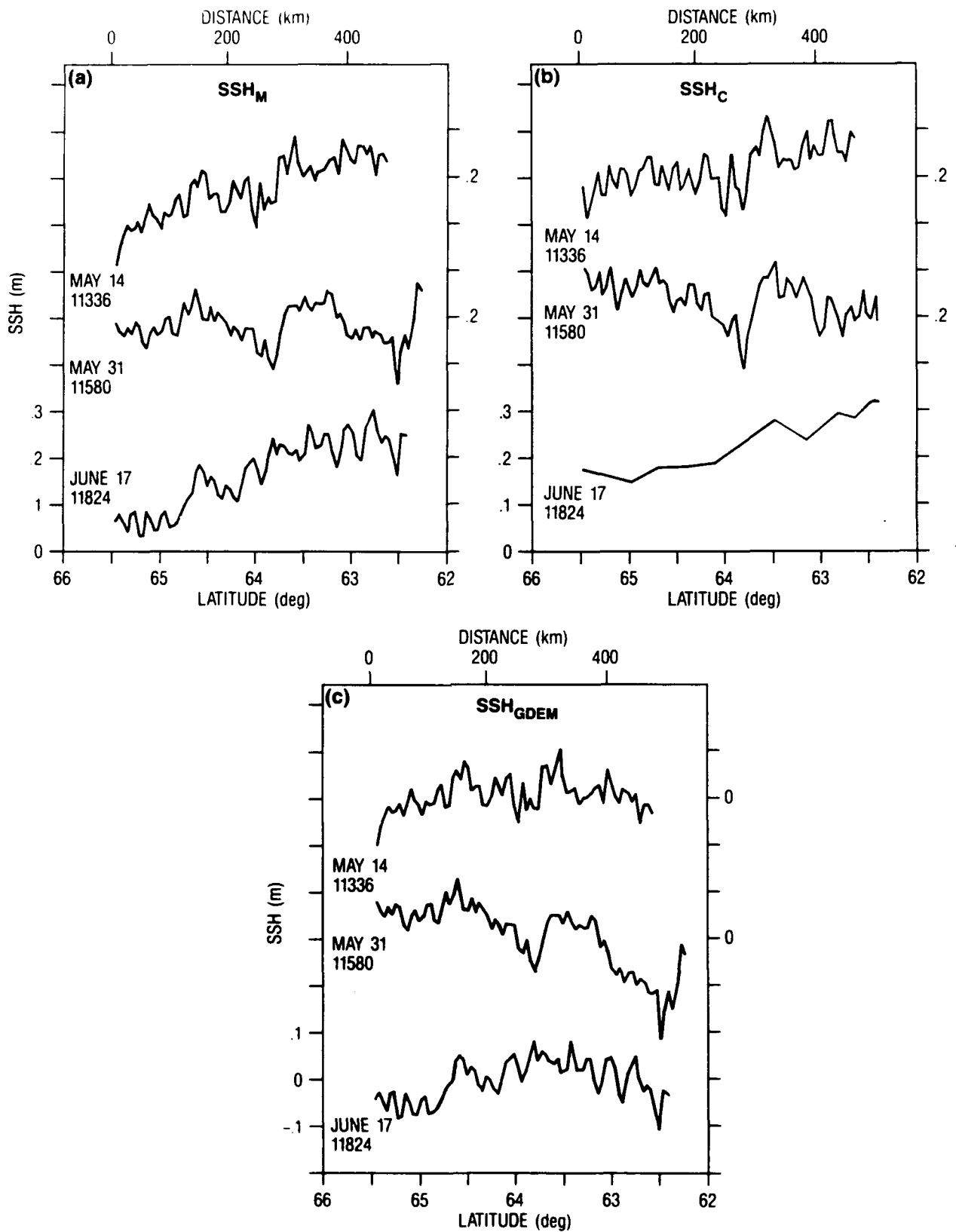


Figure 55. SSH residuals for several adjacent passes along the ground track A07. (a)  $SSH_M$  residuals. (b) Corresponding  $SSH_C$  residuals for which the geoid estimate was obtained from the 17 June altimeter data and the CTD-dynamic height. (c)  $SSH_{GDEM}$  for the same data set.

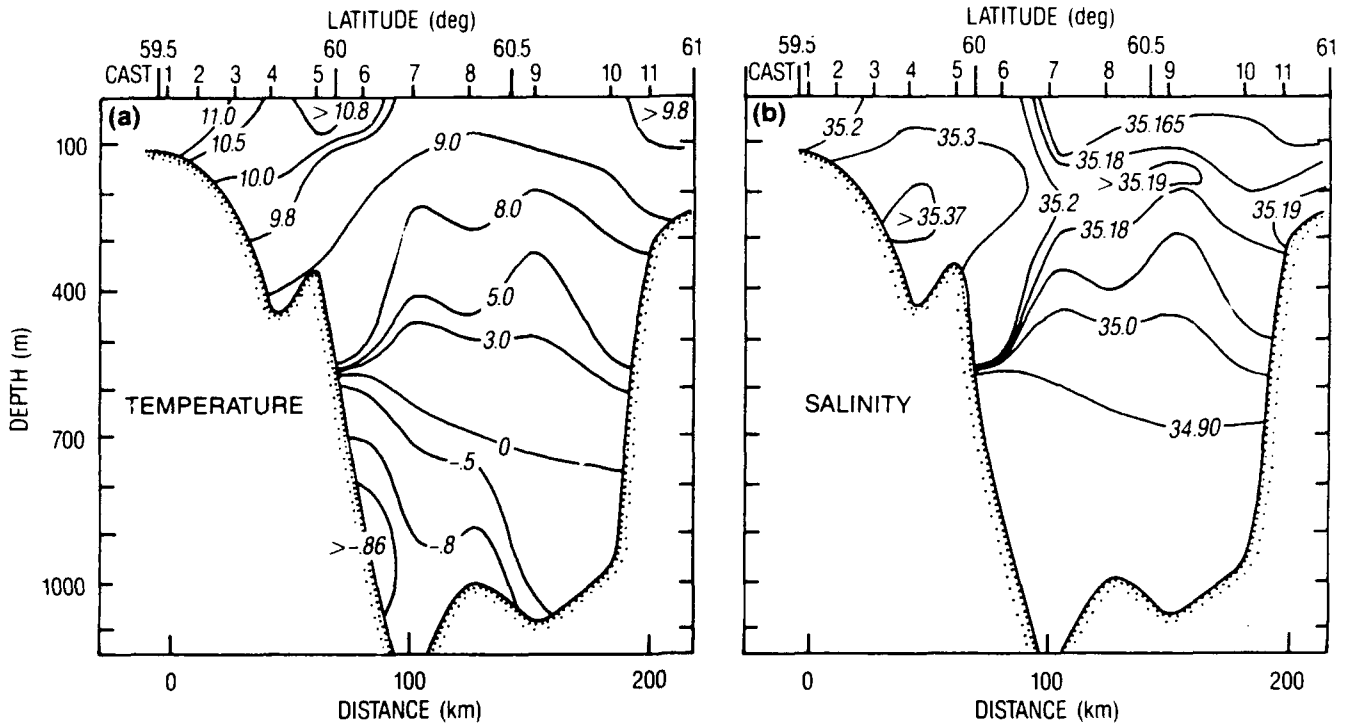


Figure 56. Cross section 4 across the North Atlantic Current. Variables are (a) potential temperature and (b) salinity. Section was taken 12 October 1988.

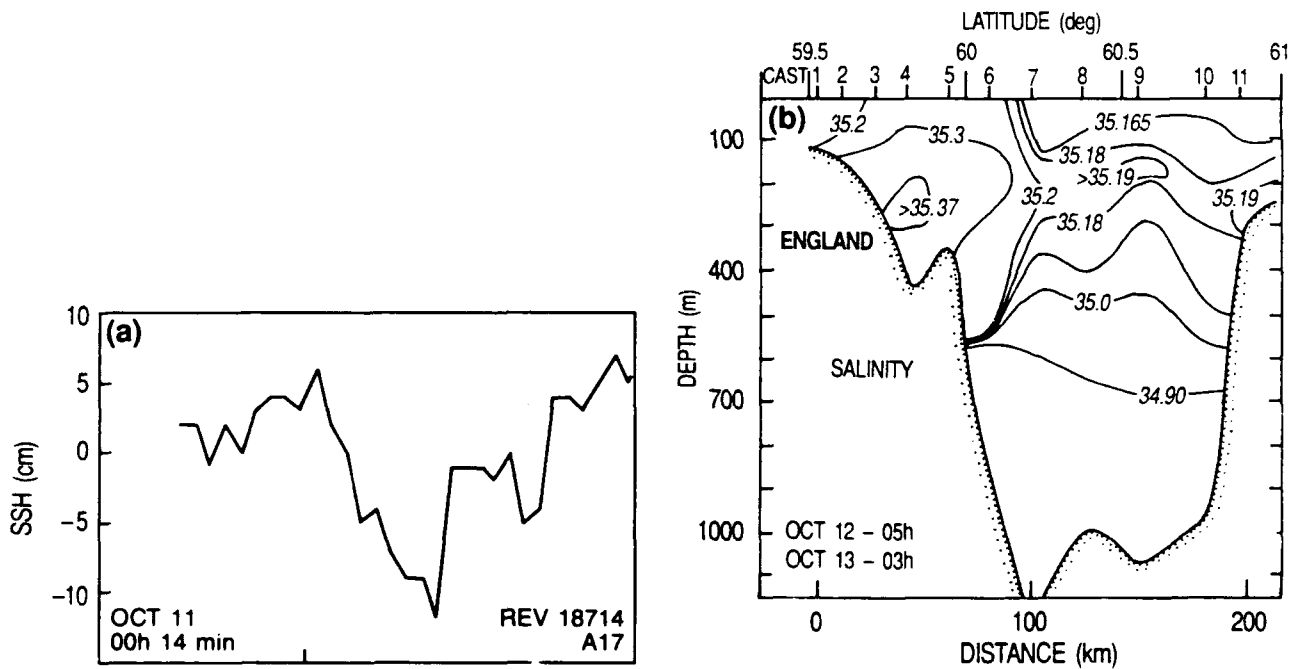


Figure 57. Comparison between (a) altimeter  $SSH_M$  taken along A17 on 11 October 1988 and (b) the CTD cross section 4 taken 1.5 days later along altimeter ground track.

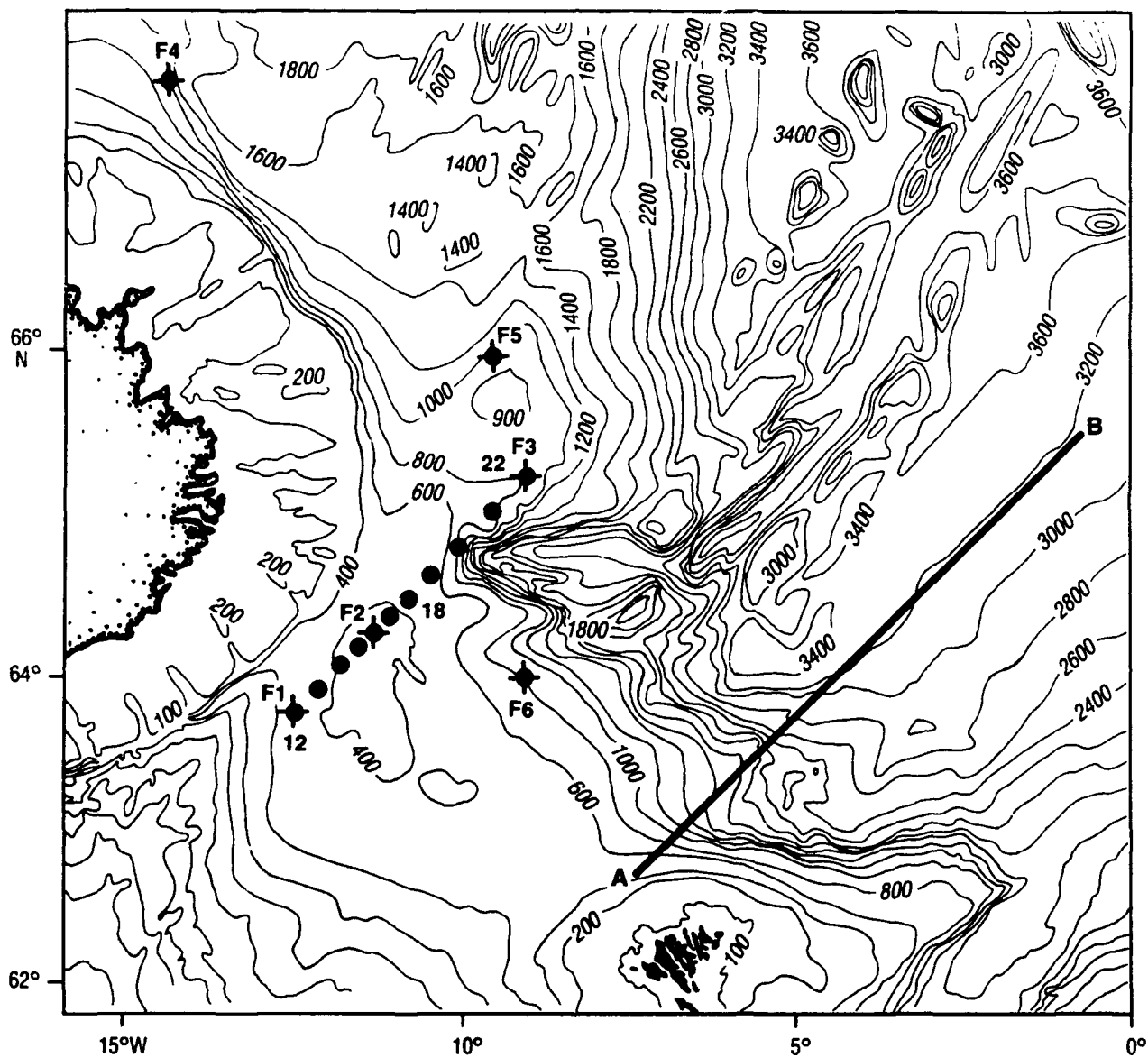


Figure 58. Bathymetric chart across Iceland-Færoe Ridge with the marked positions of oceanographic measurements. Thermistor chain tow from A to B. CTD casts marked from 12 to 22. Surface drifters deployment sites marked F1 to F6.

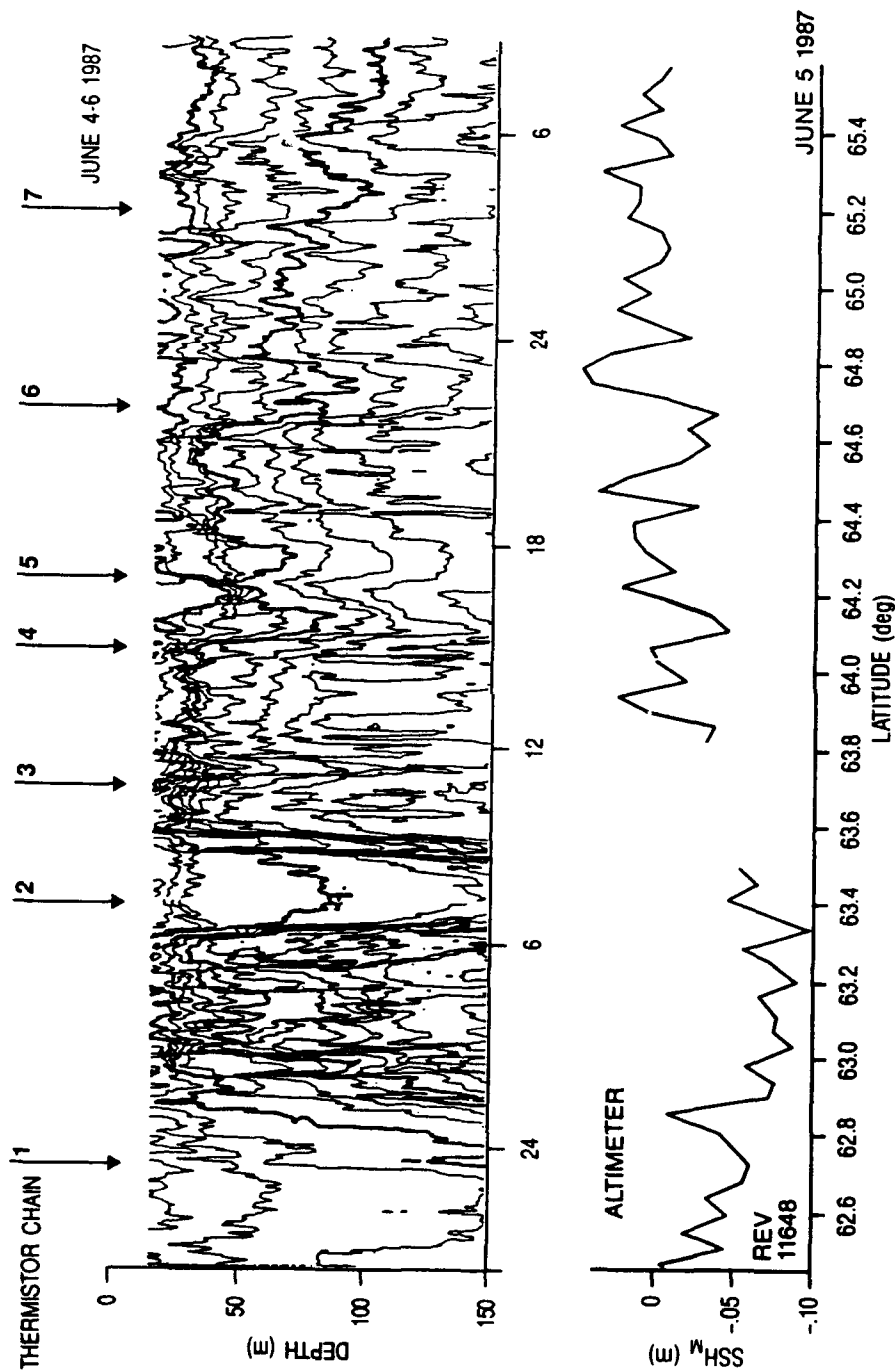


Figure 59. Comparison between thermistor chain temperature cross section and altimeter SSH<sub>M</sub>. Thermistor chain tow 4-6 June 1987. Altimeter overflight along D16 on 5 June 1987. Numbers above thermistor chain data identify the lenses of warm water. The 5 and 7°C isotherms are marked by the thicker lines.

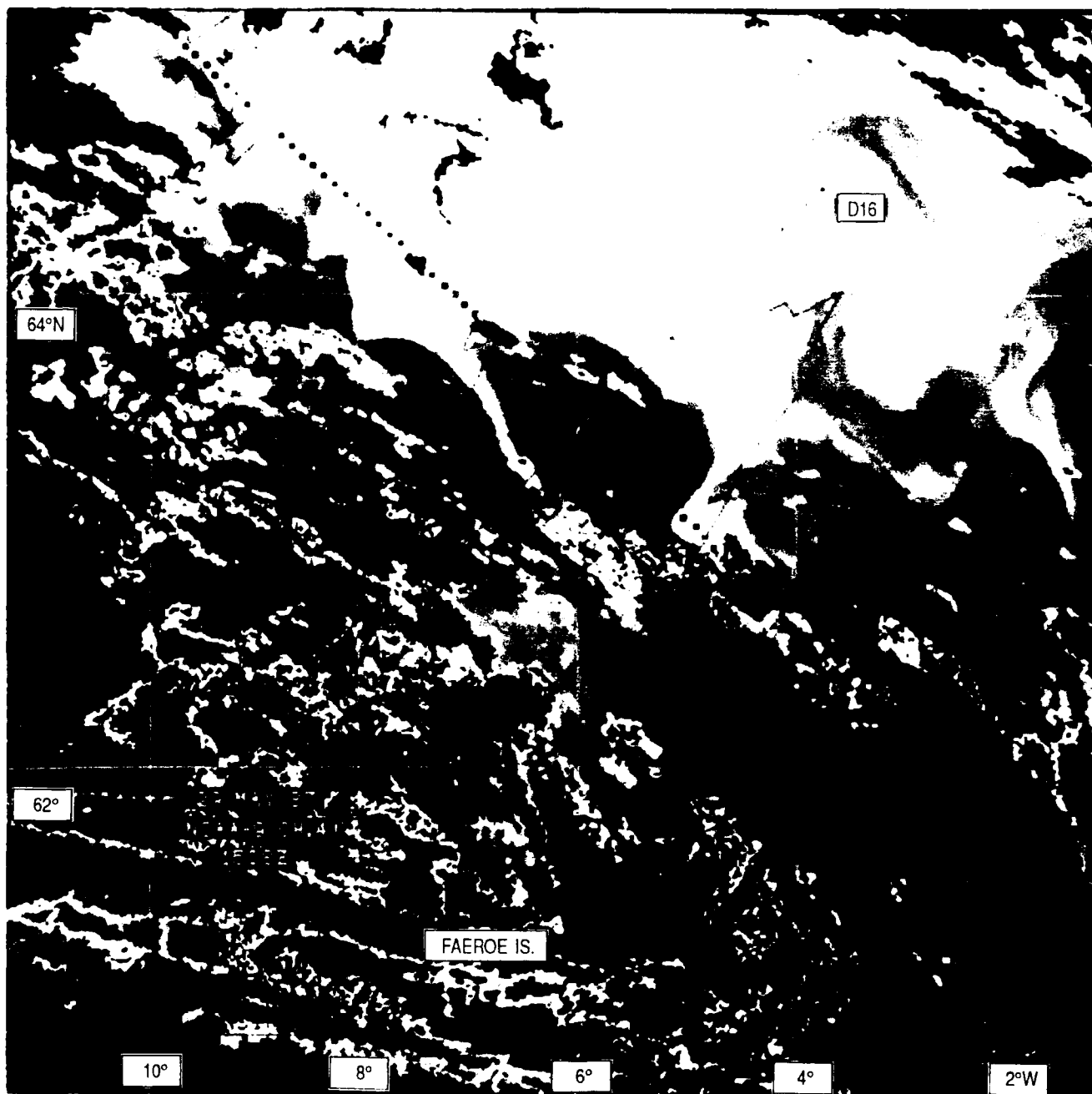


Figure 60. IR image with superimposed altimeter track with strong signal from the warm eddy in the middle. NOAA-9 ch #4 image is from 29 May 1987. Altimeter overflight along A12 on 2 June 1987. Line marked D16 indicates the direction of thermistor chain tow on 4-6 June 1987.

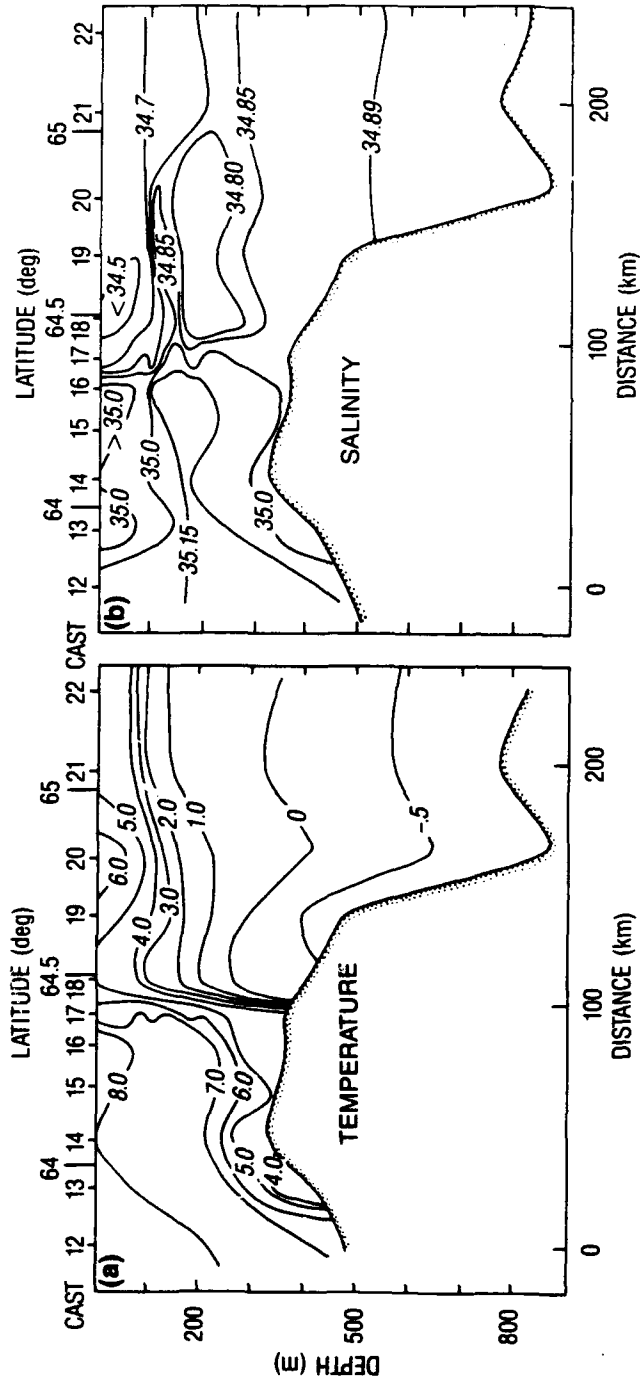


Figure 61. CTD cross section across Iceland-Færoe Front. Variables are (a) potential temperature and (b) salinity. Location of the cross section is shown in Figure 58. CTD casts were taken 13-14 October 1988.

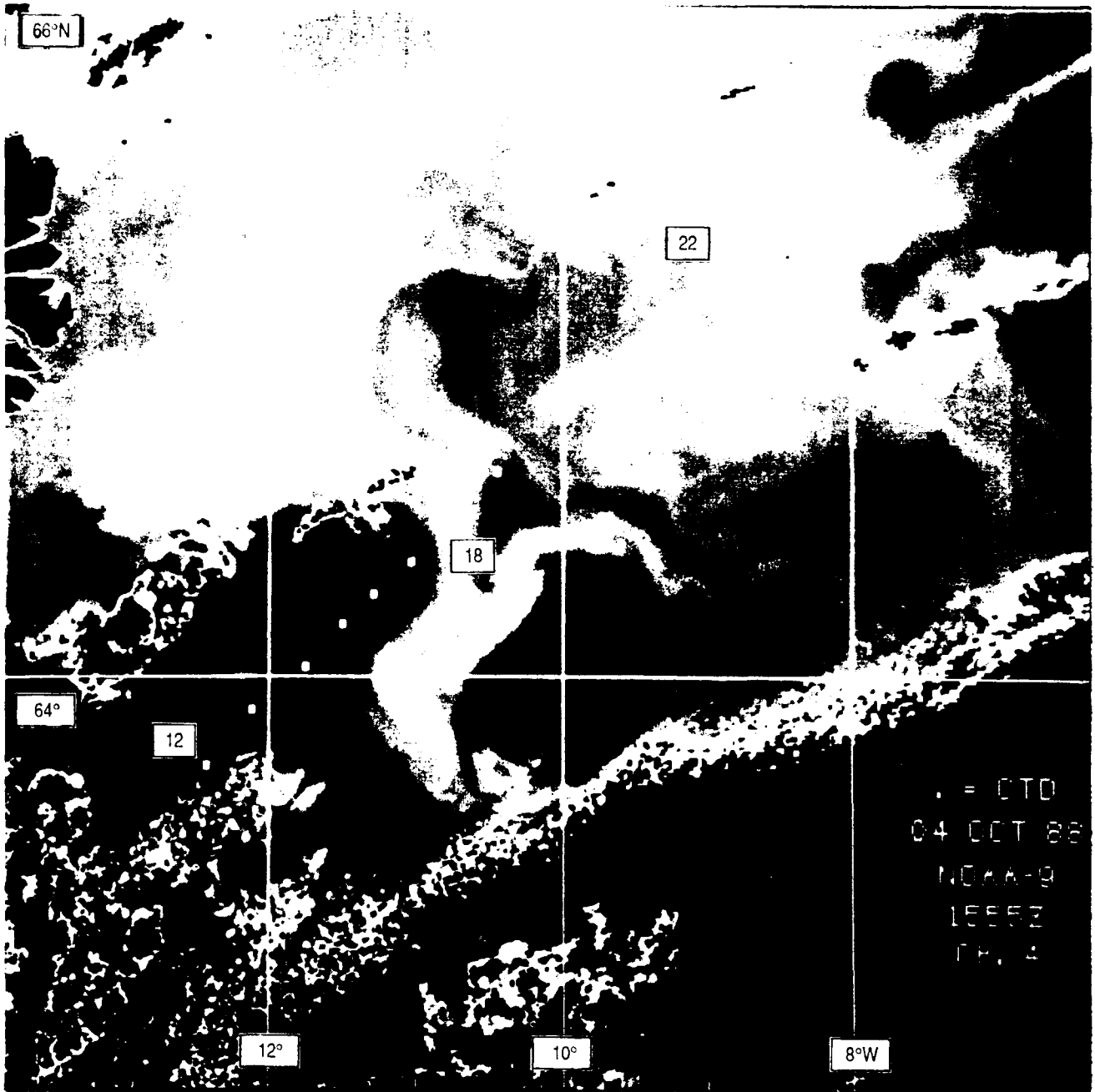


Figure 62. IR image showing the western part of Iceland-Færoe Front and position of CTD cross section. NOAA-9 ch #4 image is from 4 October 1988. CTD casts were taken 13-14 October 1988.

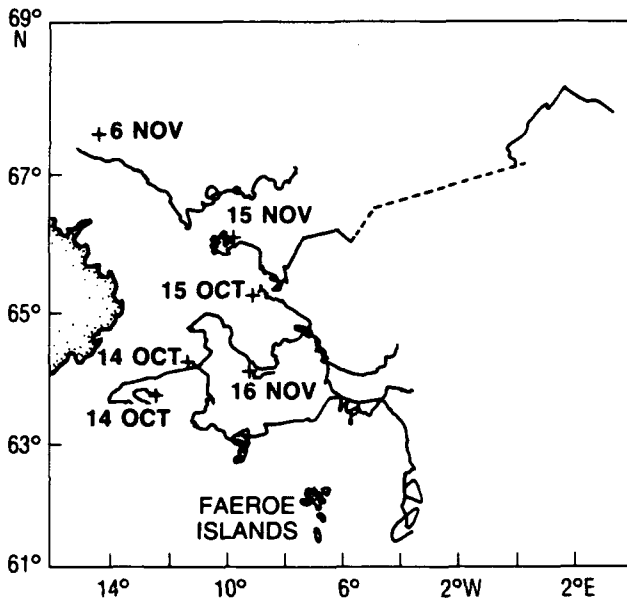


Figure 63. Chart of drifter tracks created from all position data received from Argos station. Deployment dates are marked in the beginning of each track. Drifter which was deployed on 15 November has part of track marked as dashed line because of very sparse localization in that area.

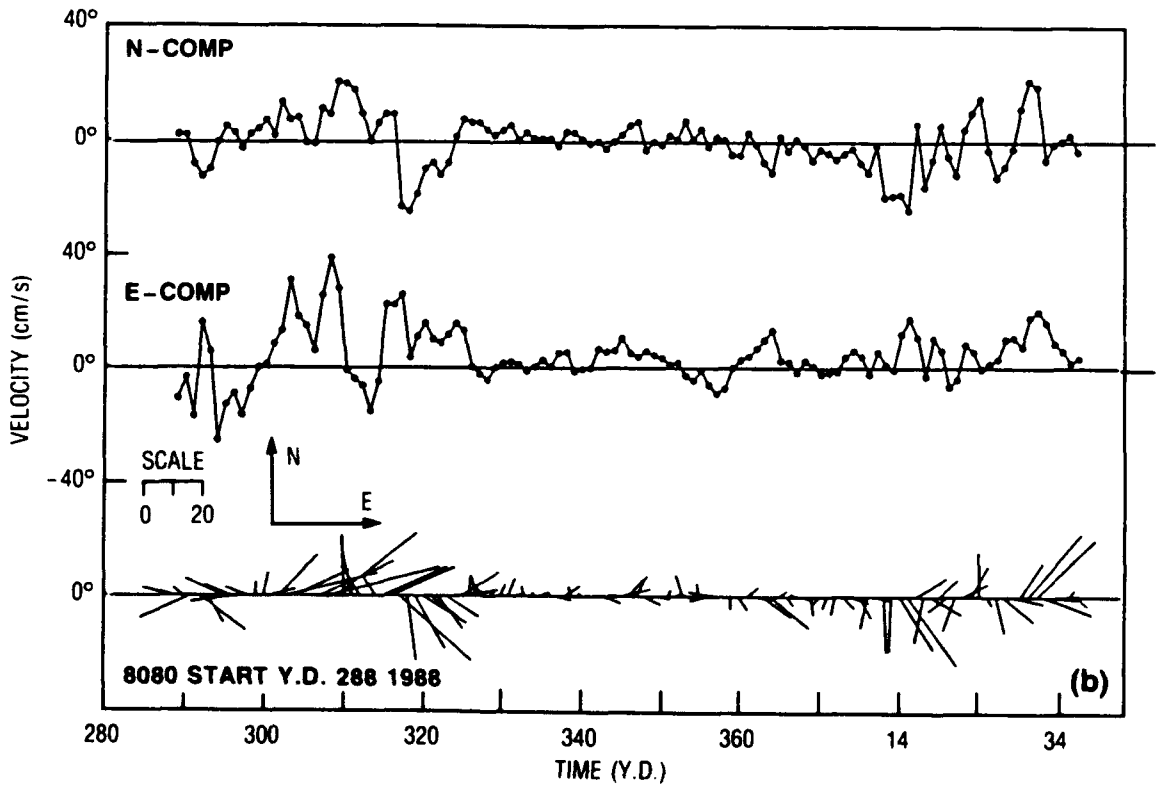
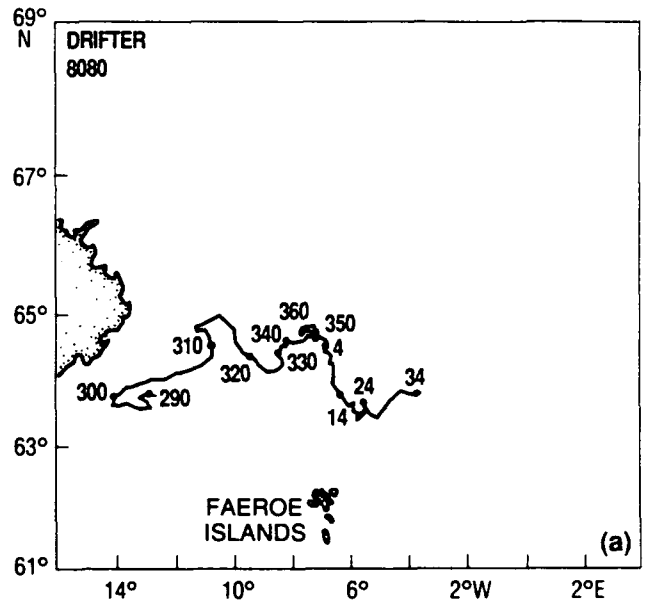


Figure 64. (a) Track of drifter F1 and (b) component and vector plots of velocity along the track. Numbers near the track represent the midday of 1988 and 1989 year-days. Data represent the daily averaged values.

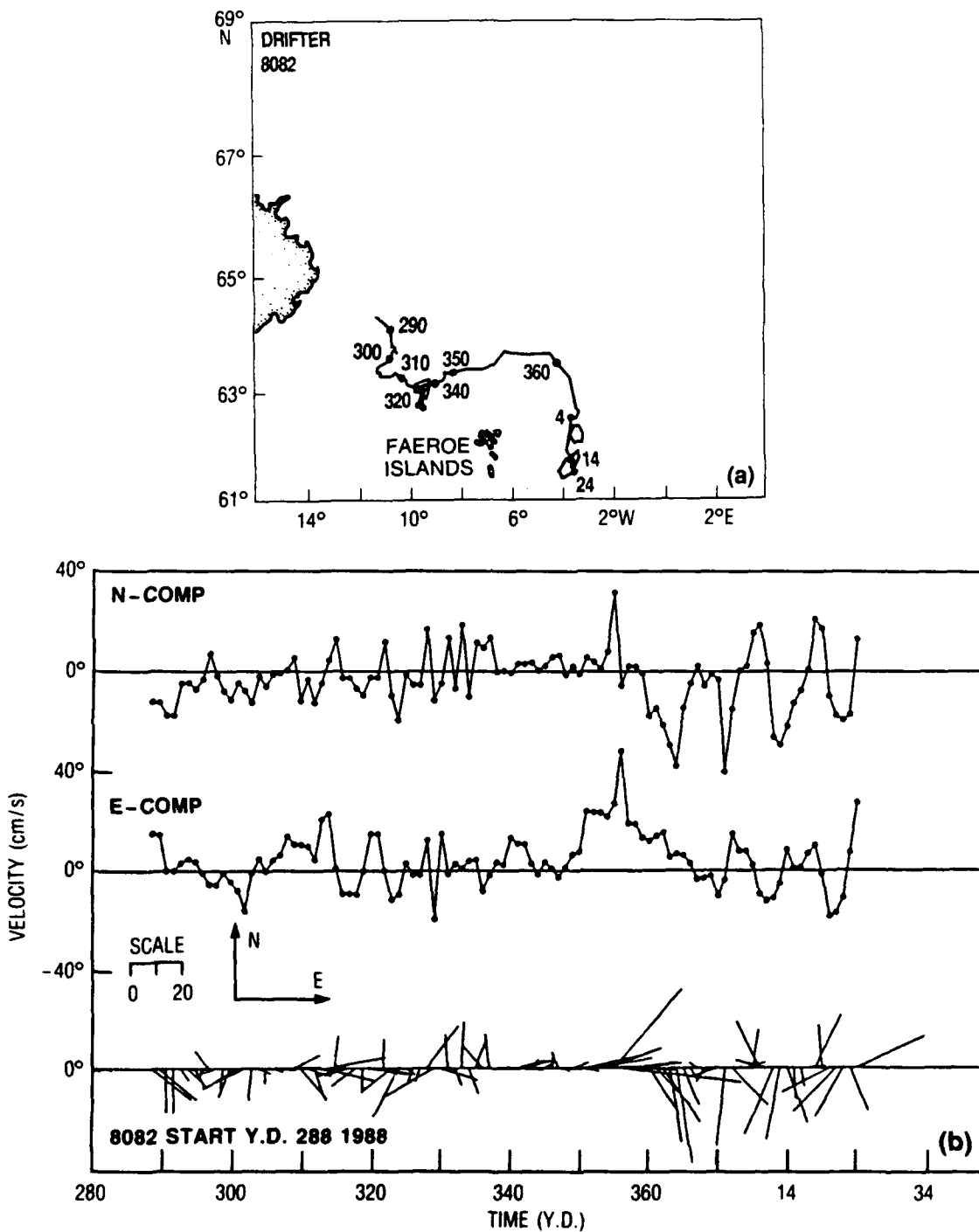


Figure 65. (a) Track of drifter F2 and (b) component and vector plots of velocity along the track. Numbers near the track represent the midday of 1988 and 1989 year-days. Data represent the daily averaged values.

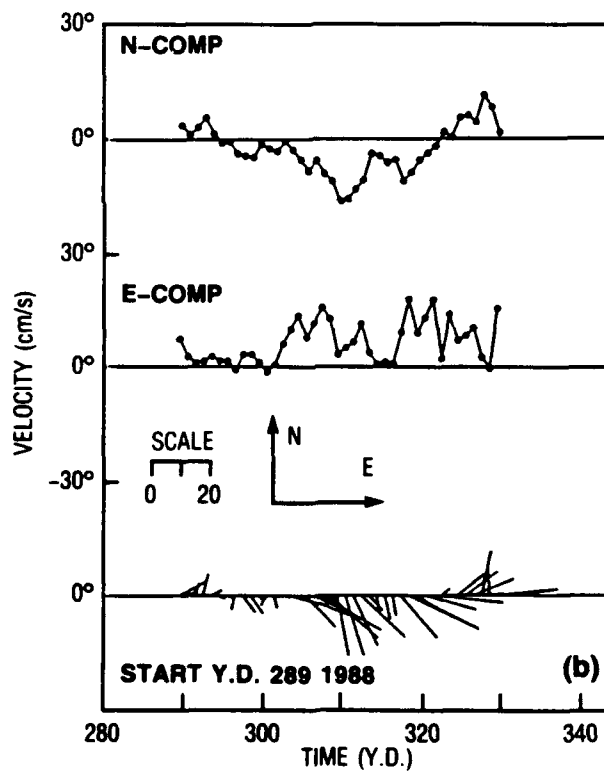
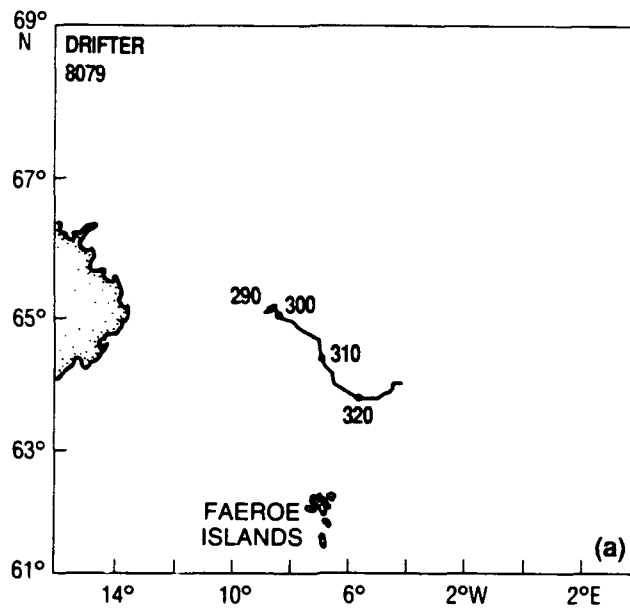


Figure 66. (a) Track of drifter F3 and (b) component and vector plots of velocity along the track. Numbers near the track represent the midday of 1988 and 1989 year-days. Data represent the daily averaged values.

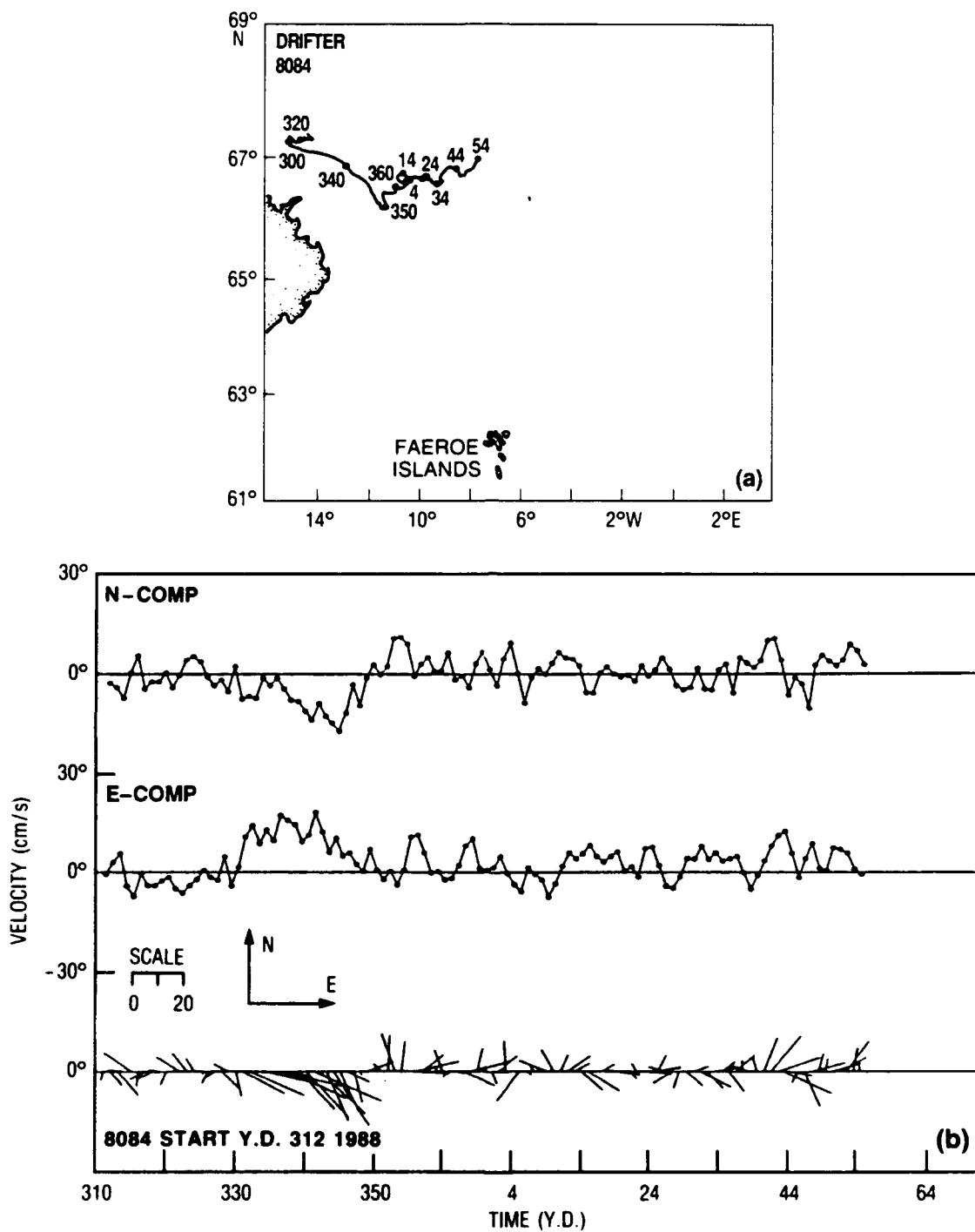


Figure 67. (a) Track of drifter F4 and (b) component and vector plots of velocity along the track. Numbers near the track represent the midday of 1988 and 1989 year-days. Data represent the daily averaged values.

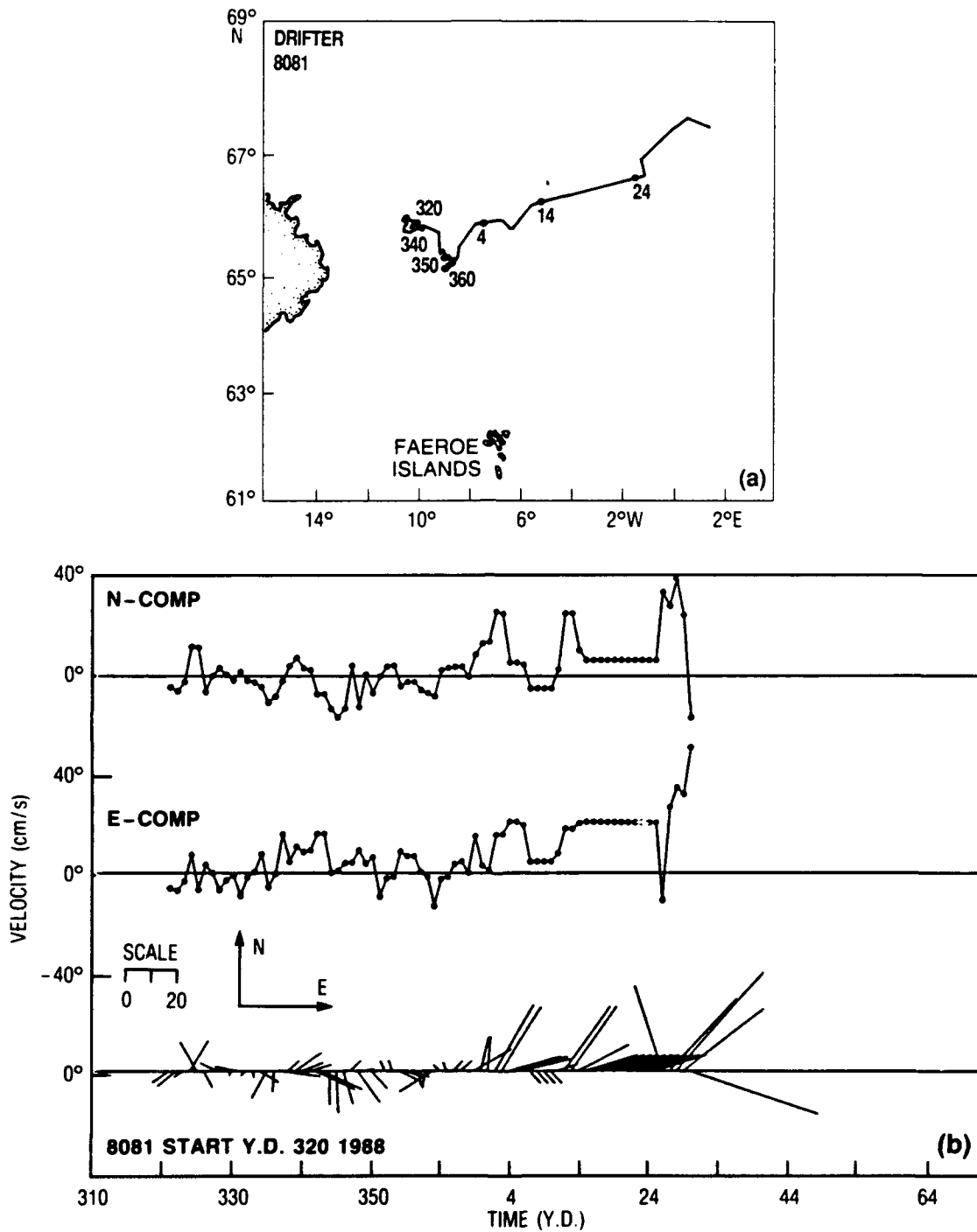


Figure 68. (a) Track of drifter F5 and (b) component and vector plots of velocity along the track. Numbers near the track represent the midday of 1988 and 1989 year-days. Data represent the daily averaged values. Data were linearly approximated during the missing days.

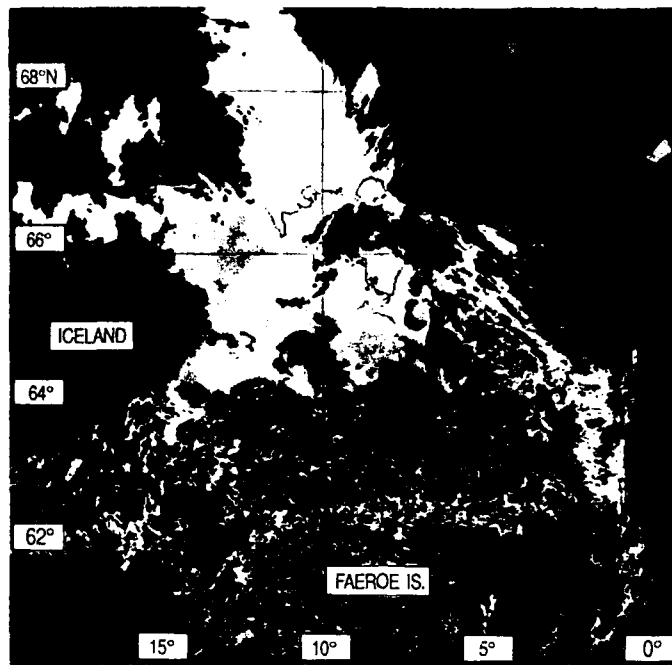


Figure 69. Tracks of drifters superimposed on the IR image. The yellow parts of tracks represent the paths of drifters during the period centered around the reception time of IR image (1–16 November 1988). NOAA-11 ch #4 IR image is a composite of 8 and 9 November 1988. Clouds are filtered and show up as a black background.

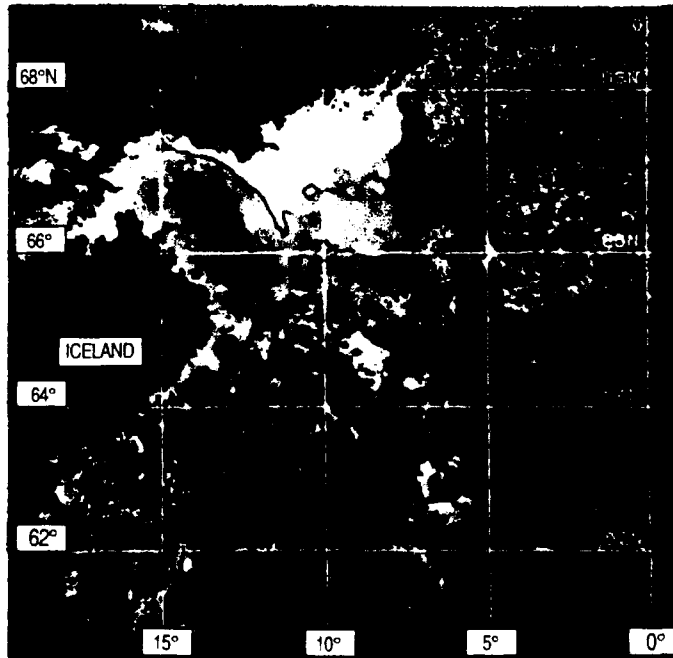


Figure 70. Tracks of drifters superimposed on the IR image. The yellow parts of tracks represent the paths of drifters during the period centered around the reception time of IR image (22 Dec.–6 January 1989). NOAA-11 ch #4 IR image is a 2-day composite of 29, and 30 December 1988. Clouds are filtered and show up as a black background.

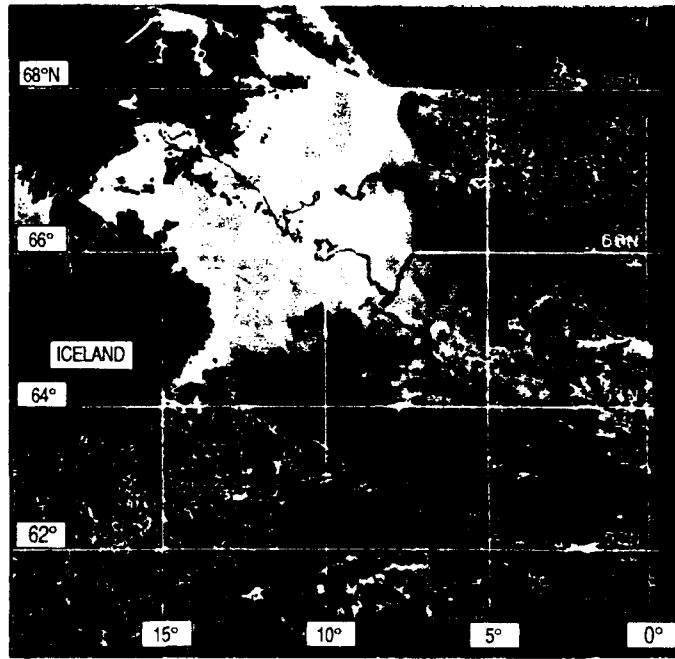


Figure 71. Tracks of drifters superimposed on the IR image. The yellow parts of tracks represent the paths of drifters during the period centered around the reception time of IR image (8–24 January 1989). NOAA-11 ch #4 IR image is a 3-day composite of 15, 16, and 17 January 1989. Clouds are filtered and show up as a black background.

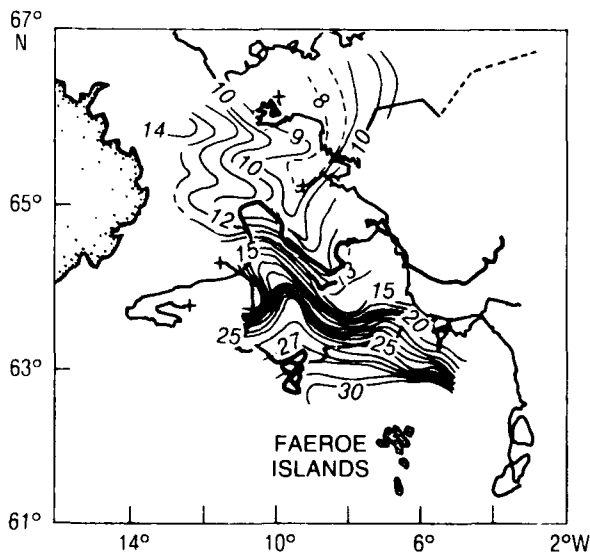


Figure 72. CTD dynamic height contour map superimposed on the tracks of drifters. CTD dynamic height contour map obtained by Hopkins (1988) from CTD measurements during 10–21 November 1988. The red parts of tracks represent the paths of drifters overlapping the CTD measurements (5–30 November 1988). Numbers near the contours represent the dynamic height value in dyn cm.

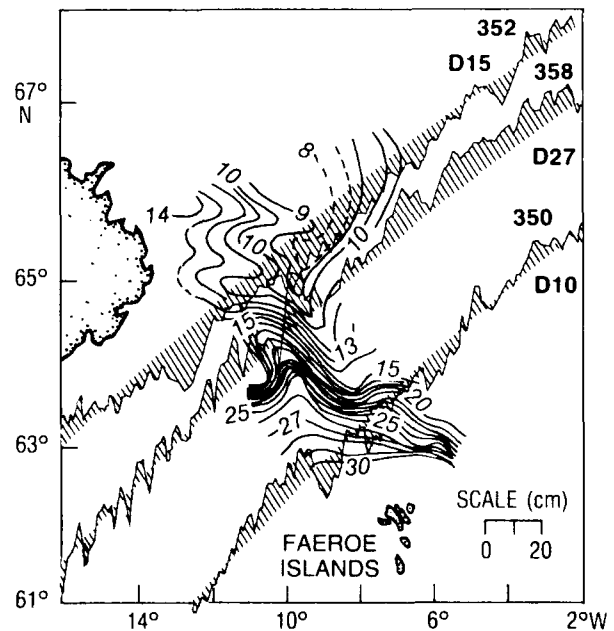


Figure 73. Altimeter  $SSH_M$  superimposed on CTD dynamic height topography. CTD dynamic height obtained from Hopkins (1988). CTD measurement was done during 10–21 November 1988. Altimeter data along tracks D15, D27, and D10 were obtained 17, 23, and 15 December 1988, respectively. Numbers near the contours of dynamic height mark the values in dyn cm. Scale calibrates the altimeter signal.

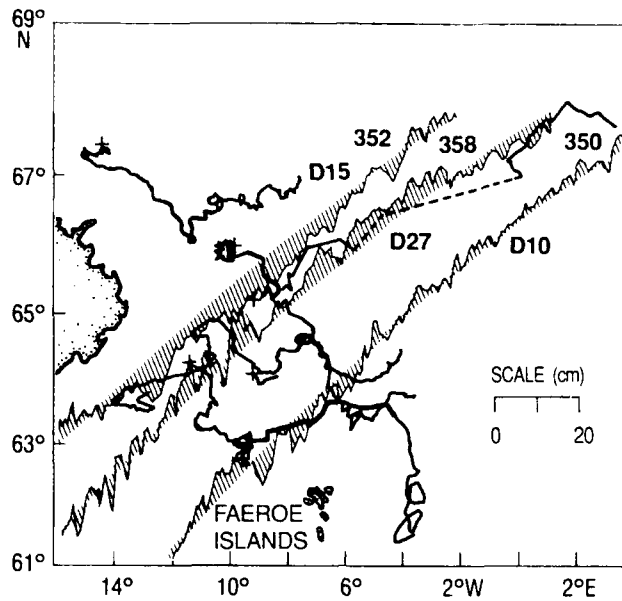


Figure 74. Altimeter  $SSH_M$  overlaid on the tracks of drifters. The red portion of tracks corresponds to the period (5–25 December 1988), which overlaps the time of altimeter passes. Altimeter data along tracks D15, D27, and D10 were obtained 17, 23, and 15 December 1988, respectively. Scale calibrates the altimeter data.

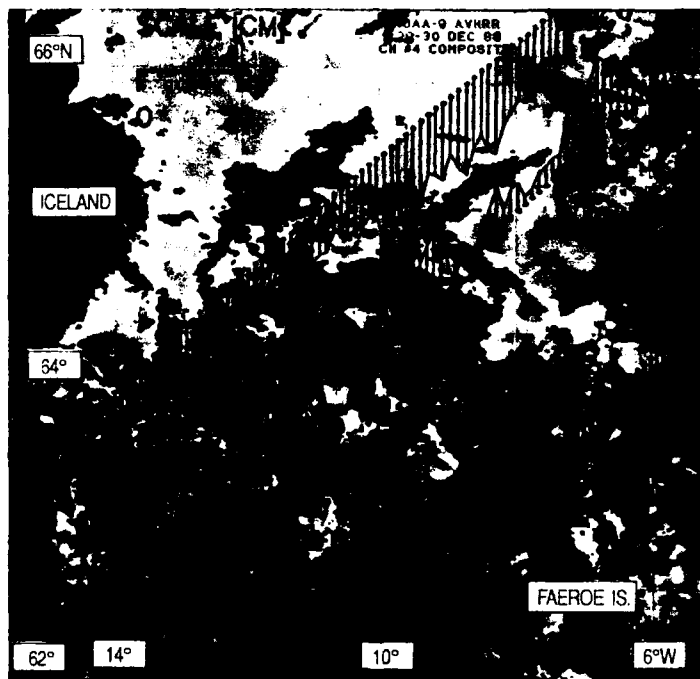


Figure 75. Altimeter  $SSH_M$  overlaid on IR image. Altimeter data along tracks D15, D27, and D10 were obtained 17, 23, and 15 December 1988, respectively. NOAA-11 ch #4 IR image is a composite of 2 days, 29 and 30 December 1988. Clouds are filtered and show up as a black background. Scale calibrates the altimeter data.

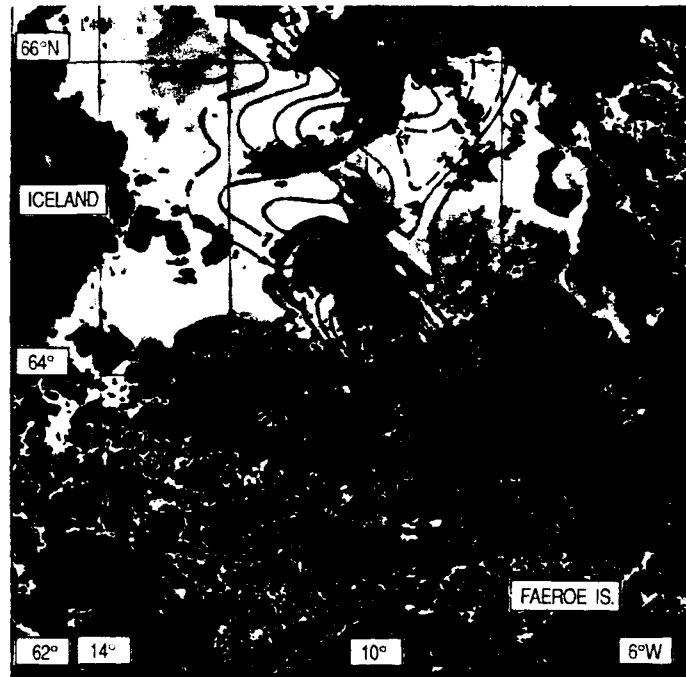


Figure 76. CTD dynamic height topography overlaid on IR image. CTD dynamic height contour map prepared by Hopkins (1988) from CTD measurements during 10–21 November 1988. NOAA-11 ch #4 IR image is a composite of 8 and 9 November 1988.

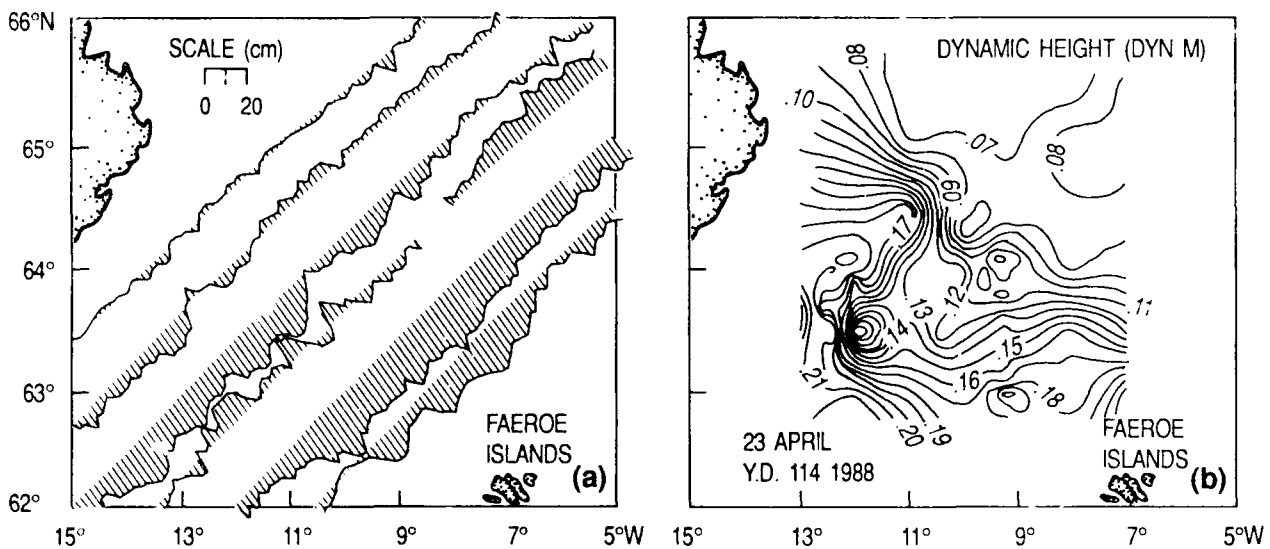


Figure 77. Comparison between (a) altimeter  $SSH_M$  data and (b) surface dynamic height topography derived from AXBT measurements. Altimeter data along tracks D15, D21, D27, D33, D04, and D10 were collected on days 24, 27, 13, 16, 19, and 22 April 1988, respectively. Dynamic height topography prepared by Boyd (1988) from AXBT data collected on 23 April 1988.

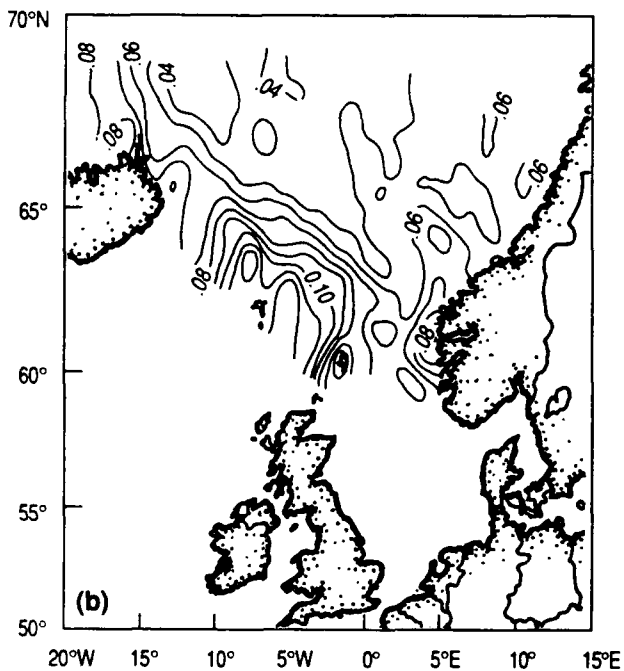
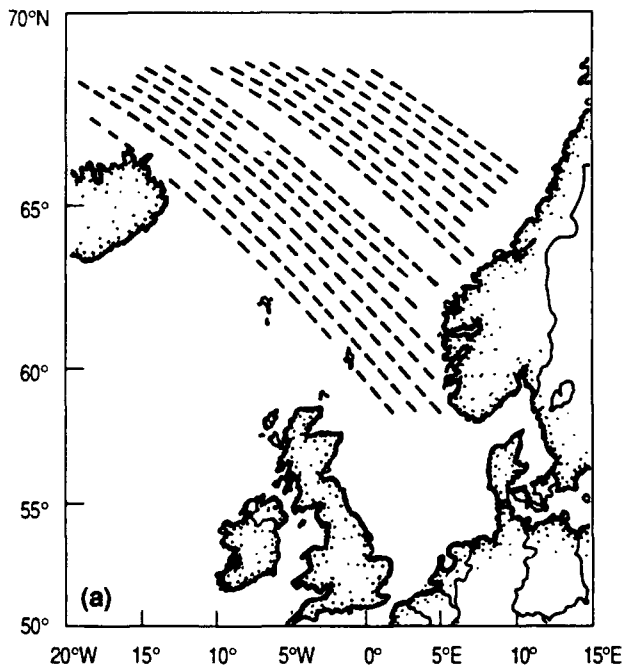


Figure 78. Altimeter surface variability obtained from the ascending passes. (a) Ascending tracks used in evaluation. (b) Surface variability in meters.

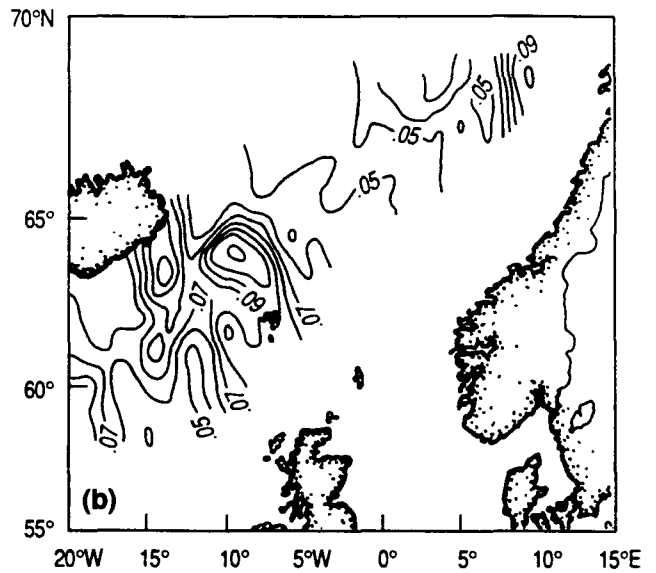
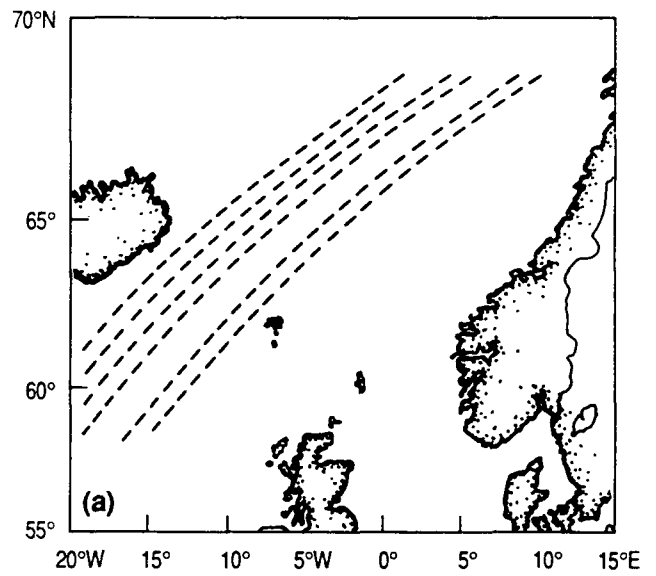


Figure 79. Altimeter surface variability obtained from the descending passes. (a) Descending tracks used in evaluation. (b) Contours of surface variability in meters.

## 5.0 Summary and Conclusions

Altimetric data were collected in the GIN Sea area during a 14-month period. Oceanographic measurements were taken simultaneously with altimetric measurements during several cruises and aircraft flights. These measurements consisted of data from CTD's, a thermistor chain, AXBT's, and surface drifters. The satellite AVHRR images were utilized during analysis. A set of these data served as a necessary means of verifying, understanding, and interpreting altimeter measurements.

The tidal correction used in altimeter processing was found to have significant error in the Iceland-Færoe-Shetland area. In addition to the large spatial scale error ( $>100$  km), tidal approximations along the altimetric path, obtained from coarse  $1^\circ \times 1^\circ$  grid tidal data, introduced short-scale error ( $<100$  km) of significant amplitude ( $>10$  cm), which masks mesoscale features.

The wet tropospheric correction was not applied to altimetric data, but the preliminary results obtained from the SSM/I show that the altimeter correction due to water vapor content and connected with atmospheric fronts can mask mesoscale features ( $>10$ -cm amplitude). Due to fast movement of the atmospheric fronts in the GIN Sea area ( $>35$  km/h), altimeter and water vapor data must be simultaneous to give proper results.

Altimeter data were sometimes observed as noisy. This noisiness is connected with the high seas. It appears if significant wave height is greater than 6 m.

Historic oceanographic data reveal that the GIN Sea area is an oceanographically complex area with large spatial and temporal variability. The frontal zones are complicated by the presence of mesoscale eddies and temporal variability of currents. Their presence imposes the spatial and temporal constraints on comparisons between the oceanographic and altimeter data. The quantitative comparisons between these data, gathered more than 2 days and 40 km apart, have to be carefully reasoned.

Dynamic height topography computed from CTD data shows 5 to 15 cm sea surface relief for fronts and mesoscale eddies. These values are on the verge of the altimeter detection capability. Nevertheless, good correlation was found between the temperature structure of the sea cross section and the altimetric signal along it, with *SSH* amplitudes of only 5–8 cm.

The main problem in interpretation of altimetry is the insufficient knowledge of precise geoid. Three

methods of its estimation were examined in this report: • the mean of many repeat passes; • subtraction of the surface dynamic height, obtained from the simultaneous CTD cross section taken along the altimeter ground track, from the corrected altimeter range data; • subtraction of the surface dynamic height, obtained from the historic (GDEM) CTD data along the altimeter ground track, from the mean of many repeat passes. The three types of *SSH* residuals ( $SSH_M$ ,  $SSH_C$ ,  $SSH_{GDEM}$ ) were then obtained by subtracting the corresponding estimated geoid from a particular pass.

The first method was used routinely, but because the time-steady component of oceanography was removed with the geoid, interpretation of the  $SSH_M$  in areas of steady currents was difficult. Correlations between  $SSH_M$  and oceanographic parameters obtained from cross sections suffered from this limitation.

The second method accumulates errors due to orbit tilt, due to the uncertainty and limitations of the geostrophic method of calculating dynamic height, and to the presence of a barotropic component in the dynamic height not detectable by CTD's. The presence of the barotropic component in the dynamic height (and current) is indicated by *SSH* data across the Iceland-Færoe Front where *SSH* is larger than dynamic height computed from CTD's.

The third method (in addition to the last two limitations of the second method) had an additional error introduced by averaging the data sets which are not obtained simultaneously (CTD's of GDEM were obtained in different times than altimeter *SSH*'s). This last error may be critical in the area of the Norwegian Atlantic Current where oceanographic measurements indicate that variations in the flux are comparable to the mean. The results obtained from cross sections 1 and 2 across the Norwegian Atlantic Current indicate that, in comparison with data obtained by the second method of geoid estimation, GDEM dynamic height underestimated the time-steady portion of Norwegian Atlantic Current while cross section 3 is in agreement with it.

Comparisons between *SSH* and the features indicated by IR images do not show complete agreement. Some IR features, interpreted as mesoscale variability may not be true features, or are too weak to be detected by altimeter. Features detected by oceanographic measurement had the equivalent expression in the *SSH*; as, for example, the detection of a warm-core eddy by thermistor chain, altimeter, and IR image. It should be noted

that simultaneity of data is important, namely, in areas of stronger currents where the 2 days' difference may cause the 15–20 km drift of the feature. Likewise, SST's obtained from IR data along the altimeter ground track were weakly correlated with  $SSH_M$ .

Five CTD cross sections and one AXBT cross section were taken across the North Atlantic Current and the Norwegian Atlantic Current along ground tracks and simultaneously with the altimetric data. Sections 0 and 4 were taken across the North Atlantic inflow. Section 4, taken north of the Wyville Thompson Ridge (~600 m deep), shows the very sharp boundary in about 600 m between Atlantic water in the upper layer and the water flowing from the north under it.  $SSH$  is well correlated with the ocean structure and shows the area of inflow with a surface relief of 15 cm. Section 0 was taken parallel to the Færoe-Shetland Channel but separated from the altimeter track by about 40 km to the south. The ensemble average for altimeter data was created only from five passes to avoid the large tidal error. The altimeter pass was 3 days in advance of CTD measurements. This time difference is generally too large (current meter measurements show spectral peak at 4 days—T. Hopkins, SACLANTCEN, personal communication), but good agreement between  $SSH$ 's obtained by different methods (1 and 2) justifies the assumption of simultaneity. Because the dynamic height obtained from CTD's did not show any relief, orbit-corrected altimeter range data were used as the geoid (method 2) for the other repeat passes. Only one of the five adjacent repeats showed substantial inflow of Atlantic water into the GIN Sea area. This result is strongly supported by agreement with the  $SSH$ 's obtained by method 1.

The rest of the cross sections are across the Norwegian Atlantic Current. They show that the core of Atlantic water is guided by the Norwegian Continental Slope and that the structure corresponds to elongated eddies to the east whose origins are not well understood. Altimeter data along corresponding ascending tracks were taken simultaneously with the oceanographic measurements. The Norwegian Coastal Current was not well covered by the altimeter because a delay in the adjustment of the automatic altimeter tracker caused a loss of data in about a 100-km-wide area seaward from the coast. High correlation between  $SSH$  and temperature structure is visible in the densely sampled AXBT cross section (casts 12 km apart).

Even the 5-cm variations in  $SSH_M$  have corresponding expressions in temperature structure, while a 35- to 40-km CTD sampling distance in CTD cross sections did not resolve all eddies. The cross correlation between  $SSH$  and the temperature averages, for different layers, showed the highest cross correlation where the layer was 200–350 m deep. This was true for the two northernmost cross sections, the AXBT and the CTD cross section 2. It may indicate the possibility of the unique determination of the subsurface structure from the surface altimetry data by the method similar to the solution known in the Gulf Stream area.

In the southern CTD cross section 3, the cross-correlation between  $SSH$  and the oceanic structure indicate the highest value for the upper 100-m-thick layer. This difference in the result may be partly due to interaction between the three current systems as they meet in this area (Icelandic, North Atlantic, and Norwegian Coastal Currents), and partly because of the limited validity of comparison between the absolute parameters obtained from oceanography and the residual  $SSH$  obtained by method 1.

Surface topography for several repeat passes along each cross section, obtained from CTD's by method 2, indicates a strong, steady component of northward flow in the northerly positioned sections (1, 2) and a rather variable flow with a small, steady component in cross-section 3. This behavior resembles variability of  $SSH$  in the Færoe-Shetland Channel. The explanation may be that cross-section 3 is in an area where different current systems change and are influenced strongly by Atlantic inflow from the Færoe-Shetland Channel, while the northern sections have more stability in flow because the Atlantic and Icelandic flows coalesce. This current is baroclinically unstable. The instability evolution plus advection of the eddies and meanders are the principal source of variability.

The Iceland-Færoe frontal zone is subjected to the same problems of spatial and temporal variability as the Norwegian Atlantic Current area. Historically, less oceanographic measurements were taken in this area than in the Norwegian Sea, and the knowledge of oceanography is still limited.

The frontal zone follows the northern-sloping bathymetry of the Færoe-Iceland Ridge. Its boundary is complicated by the presence of the warm- and cold-core eddies. The CTD cross section taken east of Iceland shows a very sharp boundary between Atlantic and Icelandic waters. This boundary extends almost vertically to the bottom, while cross sections

taken to the east of it (T. Hopkins and H. Perkins, SACLANTCEN, personal communication) show gradual sloping with Atlantic water overlaying the Icelandic water mass. The cross section passed across the tongue of warm water and was always visible in IR images around 64°–65°N and 10°W. This feature is situated in the convergence zone where the northeastward current associated with the strong thermal front between Atlantic and Icelandic waters near Iceland and the southeastward Icelandic current meet. The presence of Atlantic water in this feature is limited to the surface layer, which is less than 100 m thick. Nevertheless, it is dynamically important as shown in dynamic height calculations (T. Hopkins, SACLANTCEN, personal communication) and the drifter's track.

Six surface drifters tracked by Argos system were released in the frontal area. Drifters generally moved along the frontal zone. Transient speeds were sometimes as high as 50 cm/s. Dynamic height calculated from CTD data also shows a broad front (>100 km) with a total relief of 15 cm, but it was intensified in some areas so that the dynamic height changed 10 cm in less than 50 km. The two northernmost deployed surface drifters, after moving some time along the front, drifted to the northeast in the direction of the Norwegian Atlantic Current. This drift is the result of a general upward tilt of surface dynamic topography connected with the inflow of Atlantic water along the eastern boundary of the GIN Sea area (also demonstrated by Hopkins, 1988 measurements; surface dynamic height from CTD's). Temperature indicated that boundaries in IR images were in good agreement with the simultaneous motions of drifters and the CTD-derived surface dynamic height topography.

Descending ground tracks of the GEOSAT altimeter transected perpendicularly the Iceland-Færoe front. Data suffer from tidal error introduced mainly by approximations to the coarse  $1^\circ \times 1^\circ$  grid of the Schwiderski-Szeto model. The most severely influenced area is situated along the northern slope of the Iceland-Færoe Ridge, where the spatial tidal changes are largest and, unfortunately, are coincident with the frontal region. Ascending passes through the area have even more severe problems as they cross the shelves of the Iceland, the Færoe Islands, and the Shetland Islands where tide is not well determined. Smoothing of the tidal signal along the altimeter tracks (original tide was obtained by bilinear approximation of  $1^\circ \times 1^\circ$  data) removed the largest errors, but even the smaller residuals are detrimental to interpretation.

Several oceanographic measurements (NOARL's and SACLANTCEN's) were attempted simultaneously and along the altimeter ground tracks in the summer of 1988, but no altimetric data could be collected because of the GEOSAT's malfunction. From September to March 1988 only a few descending passes exist. Some are displayed together with drifters, dynamic height topography, and IR images. In general, there is good identification of altimetry with mesoscale eddies in this region. Some comparisons of altimetry, for example, with dynamic topography, are not simultaneous. They are compared because there is indication of the shift of features in IR images. The altimeter data compare the amplitude of their surface relief at a later time. There is indication that the amplitude of the altimeter  $SSH_M$  is larger than CTD-derived dynamic height topography, which would indicate the presence of a barotropic component. This result also agrees with the higher speeds of drifters than indicated by geostrophic currents computed from CTD's. It should be noted that the  $SSH$  residuals used in this comparison are only the deviations from the mean. Taking into account the unknown spatial variation of the front (and the mean), interpretation of  $SSH$  in terms of frontal position and amplitude is difficult. It is further complicated by the presence of eddies. It is a considerable advantage to use absolute  $SSH$  topography (method 2) obtained from CTD data in interpretation.

Finally, variation of the altimetric signal obtained from variances along ascending and descending tracks shows enhanced amplitude in the Iceland-Færoe frontal area and along the Norwegian Atlantic Current as would be expected from the oceanographic measurements. This result supports the evidence that the altimeter is a useful tool in the GIN Sea oceanographic investigation.

Results from the Norwegian Atlantic Current area related to the altimeter can be summarized as showing correlation between altimetry and oceanographic features even for small signal, (order of 5 cm) virtually buried in system noise. Correlation of  $SSH$  with the deeper ocean structure indicates the possibility of estimating this structure from the surface height data of the altimeter. This is also applicable for the area of the Iceland-Færoe front, where the two-layer assumption is a good approximation. The study of historical CTD cross sections would be needed to establish such a relationship. CTD cross sections or, as a first approximation, GDEM cross sections along altimeter ground tracks, are

important for establishing the absolute topography, which can be more easily interpreted. Several such cross sections across the Norwegian Atlantic Current or across the Færoe-Shetland Channel could monitor the inflow and variability of Atlantic water, a critical parameter for numerical modeling of GIN Sea circulation.

Altimeter data across the Iceland-Færoe Front have problems with tidal error. Altimeter data outside the tidal error range and data where the tide was

smoothed show that the frontal amplitude is larger than indicated by the surface dynamic topography obtained from CTD's. This CTD dynamic topography shows a frontal relief of 15 cm, in some places narrowed to 40-50 km width. This relief should be visible in altimetry. Improved tidal model or one with a denser grid than the Schwiderski model is needed. Likewise, simultaneous in situ CTD measurements are necessary to resolve this problem.

## 6.0 References

- Alekseev, A. P. and B. V. Istoshin (1956). *Scheme of Constant Currents in the Norwegian and Greenland Seas*. Trudy Poliamyi Nauchno-Issledovatel'skii Institut Morskogo Rybnogo Khoziaistva i Okeanografi, 9, 1956: 62-68. (Translation: US Fishery Wildlife Service, Special Scientific Report, 1956, pp. 69-76.)
- Bernstein, R. L., G. H. Born, and R. H. Whritner (1982). SEASAT altimeter determination of ocean current variability. *Journal of Geophysical Research* 87(C5):3261-3268.
- Born, G. H., M. A. Richards, and G. W. Rosborough (1982). An empirical determination of the effects of sea state bias on SEASAT altimetry. *Journal of Geophysical Research* 87:3221-3226.
- Boyd, J. D. (1986). *AXBT Measurements off the Northeast Coast of South America, Fall 1985*. Naval Ocean Research and Development Activity, Stennis Space Center, MS, NORDA Report 171, 352 p.
- Boyd, J. D. (1987). Improved depth and temperature conversion equations for Sippican AXBTs. *Journal of Atmospheric Oceanic Technology* 4:545-551.
- Boyd, J. D. (1988a). *AXBT Measurements in the Norwegian and Iceland Seas, May 1987*. Naval Ocean Research and Development Activity, Stennis Space Center, MS, NORDA Technical Note 399.
- Boyd, J. D. (1988b). *Aircraft Measurements in the Norwegian and Iceland Seas during Chair Helix, October 1987*. Naval Ocean Research and Development Activity, Stennis Space Center, MS, NORDA Technical Note 400.
- Boyd, J. D., P. W. May, and J. W. McCaffrey (1987). *Preliminary Report: Environmental Conditions in the Norwegian-Iceland Seas, May 1987*. Naval Ocean Research and Development Activity, Stennis Space Center, MS, NORDA Technical Note 341.
- Boyd, J. D., R. A. Brown, and R. T. Miles (1986). Evolution and Application of the NORDA AXBT Data Acquisition System, 1985. *Proceedings, 1986 Symposium, Marine Data Systems*, Marine Technology Society, pp. 30-309.
- Brundage, W. L., B. L. Lipphardt, Jr., and R. T. Miles (1985). An Evaluation of a Computer-Aided Air-Launched Expendable Bathythermograph Data Acquisition System. *Proceedings, 1985 Symposium, Ocean Data: Sensor-to-User*. Marine Technology Society, pp. 187-190.
- Cheney, R. E. (1982). Comparison data for SEASAT altimetry in the western North Atlantic. *Journal of Geophysical Research* 87:3247-3253.
- Cheney, R. E. and J. G. Marsh (1981). SEASAT altimeter observations of dynamic topography in the Gulf Stream region. *Journal of Geophysical Research* 86:473-483.
- Dickson, R. R. (1972). Variability and continuity within the Atlantic Current of the Norwegian Sea. *Rapport et Proces-Verbaux des Reunions, Conseil International pour l'Exploration de la Mer* 162:167-183.
- Dobson, E. B. (1988). Dynamic Topography as Measured by the GEOSAT Altimeter in Regions of Small Surface Height Signatures. *Proceedings of IGARSS '88 Symposium*, Edinburgh, Scotland, 13-16 September 1988. Ref. ESA SP-284 (IEEE 88CH2497-6). Published by ESA Publication Division, August 1988.
- Dooley, H. D., J. H. A. Martin, and R. Payne (1976). Flow across the continental slope off northern Scotland. *Deep-Sea Research* 23:875-880.
- Dooley, H. D. and J. Meincke (1981). J. circulation and water masses in the Færoese Channels during OVERFLOW'73. *Deutsche Hydrographische Zeitschrift* 34:41-55.
- Dorey, S. W. (1978). *Current-Meter Data Report for Observations Between Iceland and Norway During 1975 and 1976*. Naval Oceanographic Office, Stennis Space Center, MS, NAVOCEANO TN-3431-01-78.
- Gotthardt, G. A. (1974). *Observed Variations of the UK-Iceland GAP Front*. Naval Oceanographic Office, Stennis Space Center, MS, NAVOCEANO TN-6150-20-74.
- Hansen, B. and J. Meincke (1979). Eddies and meanders in the Iceland-Færoe Ridge Area. *Deep-Sea Research* 26:1067-1082.
- Harvey, J. G. (1982). T-S relations and water masses in the eastern-North Atlantic. *Deep-Sea Research* 29:1021-1033.
- Helland-Hansen, B. (1934). The Sognefjord Section. Oceanographic Observations in the Northernmost Part of the North Sea and the Southern Part of the Norwegian Sea. In *James Johnstone Memorial Volume*, Liverpool, University Press, pp. 257-274.
- Helland-Hansen, B. and F. Nansen (1909). *The Norwegian Sea, Its Physical Oceanography. Based on the Norwegian Researches 1900-1904*. Report on Norwegian Fishery and Marine Investigations, Bergen, 2 (2).

- Hermann, F. and H. Thomsen (1946). Drift-bottle experiments in the northern North Atlantic. *Medd. Komm. Havunders., Hydrografi* 3(4).
- Holland, C. R., R. T. Miles, and R. A. Brown (1982). *Operation and Maintenance Manual for the Expendable Probes Data Acquisition System*. Naval Ocean Research and Development Activity, Stennis Space Center, MS, NORDA Technical Note 127, 33 pp.
- Hollinger, J. P. (1980). SEASAT Altimeter Atmospheric Range Correction, Memorandum 4342, Naval Research Laboratory, Washington, D.C.
- Hopkins, T. S. (1988a). *Cruise Report, R/V ALLIANCE 4-88, 31 October to 23 November, 1988*. The Iceland-Færoe Ridge Area, AOG, DED December 14.
- Hopkins, T. S. (1988b). *The GINSEA, Review of Physical Oceanography and Literature from 1972*. SACLANTCEN Report, serial no. SR-124, La Spezia, Italy, SACLANT Undersea Research Centre.
- Johannessen, J. A. (1984). Can Eddies in the Norwegian-Greenland and Barents Seas be Detected with Radar Altimeter? *Proceedings of Workshop on ERS-1 Radar Altimeter Data Products*, Frascati, Italy, 8-11 May, 1984 (ESA SP-221, August 1984).
- Kao, T. W. and R. E. Cheney (1982). The Gulf Stream Front: A comparison between SEASAT altimeter observations and theory. *Journal of Geophysical Research* 87(C1):539-545.
- Kilgus, C. C. (1989). Gulf Stream dynamic topography measured from space (meeting report), EOS Trans., *American Geophysical Union* 70:709.
- Kislyakov, A. G. (1960). Fluctuations in the Regime of the Spitsbergen Current. In *Soviet Fisheries Investigations in the Northern European Seas*. Moscow, The Polar Research Institute of Marine Fisheries and Oceanography (PINRO), pp. 39-49. (In Russian).
- Kvinge, T., A. J. Lee, and R. Sætre (1968). *Report on Study of Variability in the Norwegian Sea, April-May 1967*. Bergen, Geophysical Institute, University of Bergen.
- Lybanon, M. and R. L. Crout (1987). The NORDA GEOSAT ocean applications program, *Johns Hopkins APL Tech. Dig.* 8:212-218.
- Lybanon, M., R. L. Crout, C. H. Johnson, and P. Pistek (1989). Operational altimeter-derived oceanographic information: The NORDA GEOSAT ocean application program. *Journal of Atmospheric and Oceanic Technology* (in press).
- MacArthur, J. L., P. C. Marth, Jr., and J. G. Wall (1987). The GEOSAT Radar Altimeter, *Johns Hopkins APL Tech. Dig.* 8:176-181.
- Meincke, J. (1983). The Modern Current Regime across the Greenland Scotland Ridge. In Bott, M. H. P., Saxov, S., Talwani, M. and Thiede, J. (eds.), *Structure and Development of the Greenland Scotland Ridge, New Methods and Concepts, Proceedings of a NATO Advanced Research Institute*, Padua University, 11-15 May, 1981. New York, NY, Plenum Press.
- Meincke, J. and T. Kvinge (1978). On the Atmospheric Forcing of Overflow Events. ICES. C.M. C:9 (unpublished document).
- Mitchell, J. L. (1989). The estimation of geoid profiles in the NW Atlantic from simultaneous satellite altimetry and AXBT sections, *Journal of Geophysical Research*, to be published.
- Perry, R. K. and H. S. Fleming et al. (1980). *Bathymetry of the Norwegian-Greenland and Western Barents Seas*. Naval Research Laboratory, Acoustic Division, Environmental Sciences Branch.
- Reid, J. L. (1979). On the contribution of the Mediterranean Sea outflow to the Norwegian-Greenland Sea. *Deep-Sea Research* 26:1199-1223.
- Robinson, A., L. Walstad, J. Calman, E. Dobson, D. Denbo, S. Glenn, D. Porter, and J. Goldhirsh (1988). Frontal signals east of Iceland from the GEOSAT altimeter. Submitted to *JGR Letters*.
- Ross, C. K. and J. Meincke (1979). *Near Bottom Current Vectors Observed during ICES OVERFLOW'73 Experiment, August-September 1973, B1-79-8*. Bedford Institute of Oceanography.
- Saelen, O. H. (1959). Studies in the Norwegian Atlantic Current. Part I: The Sognefjord section. *Geophysica Norwegica* 20(13):1-28.
- Saelen, O. H. (1963). Studies in the Norwegian Atlantic Current. Part II: Investigations during the years of 1954-1959 in an area west of Stad. *Geophysica Norwegica* 23(6):1-82.
- Saunders, K. D. and D. A. Burns (1985). *Atlas of Sognefjord Sections 1900-1970*. Naval Ocean Research and Development Activity, Stennis Space Center, MS, NORDA Report 92.
- Schwiderski, E. W. (1986). Tides. In Hurdle, B. G. (ed.), *The Nordic Seas*. New York, NY, Springer, pp. 191-209.
- Schwiderski, E. W. and L. T. Szeto (1981). *The NSWC Global Ocean Tide Data Tape (GOTD), Its Features and Application, Random-Point Tide Program*. Naval Surface Weapons Center, Dahlgren, VA, Technical Report TR81-254, 43 pp.

Sellschopp, T. (1987). Towed thermistor chain data collected during the cruise "NORDMEER 87", FWG-Bericht 1987-4. *Forschungsanstalt der Bundeswehr für Wasserschall und Geophysik*, Kiel, Federal Republic of Germany.

Stefansson, U. (1962). North Icelandic water. *Rit Fiskideildar* 3.

Stefansson, U. (1972). Near-shore fluctuation of the frontal zone southeast of Iceland. *Rapport et Proces-Verbaux des Reunions, Conseil International pour l'Exploration de la Mer* 162:201-205.

Swift, J. H. (1986). The Arctic Waters. In Hurdle, B. G. (ed.), *The Nordic Seas*. New York, NY, Springer, pp. 124-153.

Tait, J. B. (1957). Recent Oceanographical Investigations in the Færoe-Shetland Channel. *Proceedings of the Royal Society of Edinburgh*, 64 (A), pp. 239-289.

Tait, J. B. and J. H. A. Martin (1961). The Atlantic Current and water masses in the Færoe-Shetland Channel and over the Iceland-Færoe Ridge during the I. G. Y. *Rapport et Proces-Verbaux des Reunions, Conseil International pour l'Exploration de la Mer* 149:60-83.

Tapley, B. D., R. S. Nerem, C. K. Shum, J. C. Ries, and D. N. Yuan (1988). Circulation from a

joint gravity field solution determination of the general ocean. *Geophysical Research Letters* 15:1109-1112.

Trangeled, S. (1973). *Oceanography of the Norwegian and Greenland Seas and Adjacent Areas*. Volume 1. Bibliography. SACLANTCEN SM-4. La Spezia, Italy, SACLANT Undersea Research Centre.

Trangeled, S. (1974). *Oceanography of the Norwegian and Greenland Seas and Adjacent Areas*. Volume 2. Survey of 1870-1970 Literature. SACLANTCEN SM-4, La Spezia, Italy, SACLANT Undersea Research Centre.

UNESCO (1983). Algorithms for computation of fundamental properties of sea water. *Unesco Technical Paper in Marine Science* 44:53.

Wiesenburg, D. A., G. F. Krebs, and P. Pistek (1987). *CTD Measurements from the Norwegian Sea during NORDMEER '87, June 1987, WFS Planet*. Naval Ocean Research and Development Activity, Stennis Space Center, MS, NORDA Technical Note 356.

Willebrand, J. and J. Meinke (1980). Statistical analysis of fluctuations in the Iceland-Scotland frontal zone. *Deep-Sea Research* 27:1047-1066.

### Distribution List

Applied Physics Laboratory  
Johns Hopkins University  
Johns Hopkins Road  
Laurel MD 20707

Applied Physics Laboratory  
University of Washington  
1013 NE 40th St.  
Seattle WA 98105

Applied Research Laboratory  
Pennsylvania State University  
P.O. Box 30  
State College PA 16801-0030

Applied Research Laboratory  
University of Texas at Austin  
P.O. Box 8029  
Austin TX 78713-8029

Assistant Secretary of the Navy  
Research, Development & Acquisition  
Navy Department  
Washington DC 20350-1000

Chief of Naval Operations  
Department of the Navy  
Washington DC 20350-2000  
Attn: OP-71  
OP-987

Chief of Naval Operations  
Oceanographer of the Navy  
U.S. Naval Observatory  
34th & Massachusetts Ave. NW  
Washington DC 20392-1800  
Attn: OP-096  
OP-096B

Defense Mapping Agency  
8613 Lee Hwy.  
Fairfax VA 22031-2138  
Attn: Code PRN, Mailstop A-13  
Director

Fleet Antisub Warfare Tng Ctr-Atl  
Naval Station  
Norfolk VA 23511-6495  
Attn: Commanding Officer

Fleet Numerical Oceanography Center  
Monterey CA 93943-5005  
Attn: Commanding Officer

National Ocean Data Center  
1825 Connecticut Ave., NW  
Universal Bldg. South, Rm. 206  
Washington DC 20235

Naval Air Systems Command HQ  
Washington DC 20361-0001  
Attn: Commander

Naval Air Warfare Center  
Aircraft Division Warminster  
Warminster PA 18974-5000  
Attn: Commander

Naval Civil Engineering Laboratory  
Port Hueneme CA 93043  
Attn: Commanding Officer

Naval Command Control and Ocean  
Surveillance Center  
RDT&E Division  
San Diego CA 92152-5000  
Attn: Commander

Naval Facilities Engineering Command  
200 Stovall St.  
Alexandria VA 22332-2300  
Attn: Commander

Naval Oceanographic Office  
Stennis Space Center MS 39522-5001  
Attn: Commanding Officer  
Code TD  
Library (2)

Naval Oceanography Command  
Stennis Space Center MS 39529-5000  
Attn: Commander

Naval Postgraduate School  
Monterey CA 93943  
Attn: Superintendent

Naval Research Laboratory  
Atmospheric Directorate  
Monterey CA 93943-5006  
Attn: Director  
Code 400

Naval Research Laboratory  
Stennis Space Center MS 39529-5004  
Attn: Code 115  
Code 125L (10)  
Code 125P  
Code 200  
Code 300

Naval Research Laboratory  
Washington DC 20375  
Attn: Commanding Officer  
Library (2)

Naval Sea Systems Command HQ  
Washington DC 20362-5101  
Attn: Commander

Naval Surface Warfare Center  
Dahlgren Division  
Detachment White Oak  
10901 New Hampshire Ave.  
Silver Spring MD 20903-5000  
Attn: Officer in Charge  
Library

Naval Surface Warfare Center  
Dahlgren Division  
Dahlgren VA 22448-5000  
Attn: Commander

Naval Surface Warfare Center  
Coastal Systems Station  
Dahlgren Division  
Panama City FL 32407-5000  
Attn: Commanding Officer

Naval Surface Warfare Center  
Carderock Division  
Bethesda MD 20084-5000  
Attn: Commander

Naval Undersea Warfare Center  
Division  
Newport RI 02841-5047  
Attn: Commander

Naval Undersea Warfare Center Det  
New London CT 06320  
Attn: Officer in Charge

Office of Naval Research  
800 N. Quincy St.  
Arlington VA 22217-5000  
Attn: Code 10D/10P, E. Silva  
Code 112, E. Hartwig  
Code 12  
Code 10

Office of Naval Research  
ONR European Office  
PSC 802 Box 39  
FPO AE 09499-0700  
Attn: Commanding Officer

Office of Naval Technology  
800 N. Quincy St.  
Arlington VA 22217-5000  
Attn: Code 20, P. Selwyn  
Code 228, M. Briscoe  
Code 228, CDR L. Bounds  
Code 22, T. Warfield

Scripps Institution of Oceanography  
University of California  
291 Rosecrans St.  
San Diego CA 92106-3505

Scripps Institution of Oceanography  
P.O. Box 6049  
San Diego CA 92166-6049

Space & Naval Warfare Sys Com  
Director of Navy Laboratories  
SPAWAR 005  
Washington DC 20363-5100  
Attn: Commander

Woods Hole Oceanographic Institution  
P.O. Box 32  
Woods Hole MA 02543  
Attn: Director

# REPORT DOCUMENTATION PAGE

*Form Approved*  
OMB No. 0704-0188

Public reporting burden for this collection of information is estimated to average 1 hour per response, including the time for reviewing instructions, searching existing data sources, gathering and maintaining the data needed, and completing and reviewing the collection of information. Send comments regarding this burden estimate or any other aspect of this collection of information, including suggestions for reducing this burden, to Washington Headquarters Services, Directorate for Information Operations and Reports, 1215 Jefferson Davis Highway, Suite 1204, Arlington, VA 22202-4302, and to the Office of Management and Budget, Paperwork Reduction Project (0704-0188), Washington, DC 20503

<b>1. Agency Use Only (Leave blank).</b>	<b>2. Report Date.</b> June 1992	<b>3. Report Type and Dates Covered.</b> Final	
<b>4. Title and Subtitle.</b> Altimeter and Oceanographic In Situ Measurements in the Area of the Greenland-Iceland-Norwegian Sea, 1987-1988		<b>5. Funding Numbers.</b>  <i>Program Element No.</i>  <i>Project No.</i>  <i>Task No.</i>  <i>Accession No.</i> DN257097	
<b>6. Author(s).</b>  Pavel Pistek		<b>8. Performing Organization Report Number.</b>  NOARL Report 14	
<b>7. Performing Organization Name(s) and Address(es).</b>  Naval Oceanographic and Atmospheric Research Laboratory Ocean Science Directorate Stennis Space Center, Mississippi 39529-5004		<b>10. Sponsoring/Monitoring Agency Report Number.</b>	
<b>9. Sponsoring/Monitoring Agency Name(s) and Address(es).</b>		<b>11. Supplementary Notes.</b>	
<b>12a. Distribution/Availability Statement.</b>  Approved for public release; distribution is unlimited. Naval Oceanographic and Atmospheric Research Laboratory, Stennis Space Center, Mississippi 39529-5004.		<b>12b. Distribution Code.</b>	
<b>13. Abstract (Maximum 200 words).</b>  A multidisciplinary oceanographic study was performed in the area of the Greenland-Iceland-Norwegian Sea (GIN Sea). To assess the usefulness and the potential of altimetry in this region, the GEOSAT data, the satellite infrared images, and simultaneous in situ measurements of (a) airborne expendable bathythermographs deployed from P-3 aircraft, and (b) ship measurements of conductivity-temperature-depth (CTD) and thermistor chain data along the altimeter tracks were collected. In addition, the historical CTD data base, Generalized Digital Environmental Model (GDEM), was studied and used with altimetry. It was found that the variation in the signal amplitude of altimetric residuals corresponding to mesoscale variability is between 5 and 15 cm. In spite of this small amplitude, the signal is correlated with the oceanographic structure. Dynamic heights computed from CTD cross sections taken along the altimeter ground tracks were used to improve the empirical geoid. The altimetric signal results, namely, across the Norwegian current and the Færoe-Shetland inflow, indicate the possibility of monitoring the inflow by altimeter. In analogy to the CTD method discussed, dynamic height was computed from GDEM data and was used for correcting the altimeter data. This method can be useful in some areas as a first approximation in the improvement of the geoid. In spite of the detection by altimeter of the stronger and larger mesoscale features south of the Iceland-Færoe front, the front itself was not easily detected because of tidal contamination. Statistical results (namely variance) derived from altimetry indicate the larger variability to be near the frontal regions.			
<b>14. Subject Terms.</b>  oceanography, digital image analysis, satellite altimeter, satellites, remote sensing			<b>15. Number of Pages.</b>  74
			<b>16. Price Code.</b>
<b>17. Security Classification of Report.</b>  Unclassified	<b>18. Security Classification of This Page.</b>  Unclassified	<b>19. Security Classification of Abstract.</b>  Unclassified	<b>20. Limitation of Abstract.</b>  Same as report